Development of a Bed-Based Nighttime Monitoring Toolset

by

Charles Carlson

B.S., Fort Hays State University, 2013
B.S., Kansas State University, 2013
M.S., Kansas State University, 2015

AN ABSTRACT OF A DISSERTATION

submitted in partial fulfillment of the requirements for the degree

DOCTOR OF PHILOSOPHY

Department of Electrical and Computer Engineering
College of Engineering

KANSAS STATE UNIVERSITY
Manhattan, Kansas

2019

Abstract

A movement is occurring within the healthcare field towards evidence-based or preventative care-based medicine, which requires personalized monitoring solutions. For medical technologies to fit within this framework, they need to adapt. Reduced cost of operation, ease-of-use, durability, and acceptance will be critical design considerations that will determine their success. Wearable technologies have shown the capability to monitor physiological signals at a reduced cost, but they require consistent effort from the user. Innovative unobtrusive and autonomous monitoring technologies will be needed to make personalized healthcare a reality.

Ballistocardiography, a nearly forgotten field, has reemerged as a promising alternative for unobtrusive physiological monitoring. Heart rate, heart rate variability, respiration rate, movement, and additional hemodynamic features can be estimated from the ballistocardiogram (BCG). This dissertation presents a bed-based nighttime monitoring toolset designed to monitor BCG, respiration, and movement data motivated by the need to quantify the sleep of children with severe disabilities and autism – a capability currently unmet by commercial systems.

A review of ballistocardiography instrumentation techniques (Chapter 2) is presented to 1) build an understanding of how the forces generated by the heart are coupled to the measurement apparatus and 2) provide a background of the field. The choice of sensing modalities and acquisition hardware and software for developing the unobtrusive bed-based nighttime monitoring platform is outlined in Chapters 3 and 4. Preliminary results illustrating the system's ability to track physiological signals are presented in Chapter 5. Analyses were conducted on overnight data acquired from three lower-functioning children with autism (Chapters 6 and 9) who reside at Heartspring, Wichita, KS, where results justified the platform's multi-sensor architecture and demonstrated the system's ability to track physiological signals from this sensitive population over many months. Further, this dissertation presents novel BCG signal processing techniques – a signal quality index (Chapter 7) and a preprocessing inverse filter (Chapter 8) that are applicable to any ballistocardiograph. The bed-based nighttime monitoring toolset outlined in this dissertation presents an unobtrusive, autonomous, robust physiological monitoring system that could be used in hospital-based or personalized, home-based medical applications that consist of short or long-term monitoring scenarios.

Development of a Bed-Based Nighttime Monitoring Toolset

by

Charles Carlson

B.S., Fort Hays State University, 2013
B.S., Kansas State University, 2013
M.S., Kansas State University, 2015

A DISSERTATION

submitted in partial fulfillment of the requirements for the degree

DOCTOR OF PHILOSOPHY

Department of Electrical and Computer Engineering
College of Engineering

KANSAS STATE UNIVERSITY
Manhattan, Kansas

2019

Approved by:

Major Professor
Steve Warren

Copyright

Abstract

A movement is occurring within the healthcare field towards evidence-based or preventative care-based medicine, which requires personalized monitoring solutions. For medical technologies to fit within this framework, they need to adapt. Reduced cost of operation, ease-of-use, durability, and acceptance will be critical design considerations that will determine their success. Wearable technologies have shown the capability to monitor physiological signals at a reduced cost, but they require consistent effort from the user. Innovative unobtrusive and autonomous monitoring technologies will be needed to make personalized healthcare a reality.

Ballistocardiography, a nearly forgotten field, has reemerged as a promising alternative for unobtrusive physiological monitoring. Heart rate, heart rate variability, respiration rate, movement, and additional hemodynamic features can be estimated from the ballistocardiogram (BCG). This dissertation presents a bed-based nighttime monitoring toolset designed to monitor BCG, respiration, and movement data motivated by the need to quantify the sleep of children with severe disabilities and autism – a capability currently unmet by commercial systems.

A review of ballistocardiography instrumentation techniques (Chapter 2) is presented to 1) build an understanding of how the forces generated by the heart are coupled to the measurement apparatus and 2) provide a background of the field. The choice of sensing modalities and acquisition hardware and software for developing the unobtrusive bed-based nighttime monitoring platform is outlined in Chapters 3 and 4. Preliminary results illustrating the system's ability to track physiological signals are presented in Chapter 5. Analyses were conducted on overnight data acquired from three lower-functioning children with autism (Chapters 6 and 9) who reside at Heartspring, Wichita, KS, where results justified the platform's multi-sensor architecture and demonstrated the system's ability to track physiological signals from this sensitive population over many months. Further, this dissertation presents novel BCG signal processing techniques – a signal quality index (Chapter 7) and a preprocessing inverse filter (Chapter 8) that are applicable to any ballistocardiograph. The bed-based nighttime monitoring toolset outlined in this dissertation presents an unobtrusive, autonomous, robust physiological monitoring system that could be used in hospital-based or personalized, home-based medical applications that consist of short or long-term monitoring scenarios.

Table of Contents

List of Figures

List of Tables

Acknowledgements

I am extremely grateful for all the advice and mentorship I have received from Dr. Steve Warren and the rest of my committee. I would also like to thank all of the staff at Heartspring, Wichita, KS for their efforts. Without their flexibility, patience and willingness to work with a group of students from Kansas State University, none of the invaluable data collected from the children would have been possible. I would especially like to thank Dr. Wayne Piersel, Megan Swett, Hannah Harvey, Karime Castillo, and the Heartspring group home 3 staff who were tremendously helpful.

Dedication

I dedicate this dissertation to my parents, Doug and Cathy Carlson. Without their support and encouragement, I never would have pursued a Ph.D.

Chapter 1 - Introduction

There is a growing need for accurate, flexible, and robust physiological monitoring devices and platforms to meet the demands of numerous industries and services. For example, consider the improvements that are needed within home-based healthcare technologies to reduce the large percentage of preventable deaths that occur in the United States due to heart disease and other chronic diseases [1]. Further, many standard medical health monitoring technologies (e.g., electrocardiographs, pulse oximeters) are unsuitable for residential care facilities that house sensitive populations. E.g., children with severe disabilities and/or low-functioning autism who are always accompanied by care assistants (paraeducators), babies born prematurely that require constant monitoring in neonatal care facilities, and older adults who may suffer from an array of conditions like dementia. For such populations, at-home care can provide the best option for an improved quality of life.

Other major obstacles faced by modern healthcare technologies are cost and acceptance. Wearable sensors can affordably monitor the health of someone in the comfort of their own home, but such sensors may be impractical for long-term use – especially for older adults who tend to be less enthusiastic about technology – and statistics reveal that our nation is getting older. In 2000, people 65 and older accounted for 12.4% of the population; in 2016, people 65 and older accounted for 15.2% of the population [2]. As the population ages, a greater percentage of people will face medical conditions and chronic diseases [3]. As a result, medical costs will continue to rise in the United States. By 2050, inpatient care will need to grow by 18% to meet the demands of the growing, aging population [4]. These rising medical costs put tremendous financial burdens on families. In 2012, one in four families faced financial hardships due to medical care expenses [5]. There is a clear need for affordable, at-home based medical devices to reduce the financial burden that this aging population will have on care facilities and families [6].

Further, the healthcare industry realizes that the one-cure-for-all approach is an unsuitable framework for modern medicine [7], and the healthcare system is moving away from simply treating diseases (an illness-based perspective) to a more preventative-based approach [8]–[10]. Part of this newer approach involves personalized solutions designed to meet individual needs on a case-by-case basis [11]–[13]. Such solutions will not only improve overall quality of life but will also be cost effective, reducing the financial burden placed on care facilities and individuals. Such systems require near continuous, reliable, and accurate data streams of

personalized information (e.g., physiological metrics such as heart rate and respiration rate). Again, wearable medical technologies offer a solution but are not ideal, as specific populations that arguably have the greatest monitoring need would not tolerate wearing intrusive or even minimally intrusive devices. These populations include the elderly and hypersensitive individuals such as children with low-functioning autism – a population that will be discussed further later in the chapter. Unobtrusive sensing modalities are needed to make this movement a reality.

Improvements in sensor technology along with advancements in digital signal processing have propelled medical technologies forward – making unobtrusive and ubiquitous platforms possible which offer a promising alternative to wearable technologies [14]–[16]. When it comes to unobtrusive nighttime monitoring technologies, some options are currently available on the market. The company EMFit [17] offers the EMFit QS+ACTIVE^{TM}, a contactless sleep tracker system [18]. Beddit sells its Beddit Sleep Monitor [19], which is also designed to track sleep unobtrusively. Each system employs a single flat sensor strip that is recommended to be placed under or on the mattress directly beneath the chest area. This sensor placement has been shown to acquire signals from individuals when they sleep in a supine or prone position, keeping their chest positioned above the sensor. However, such systems fall short when it comes to monitoring the sleep of autistic children with severe disabilities as these children tend to sleep in a wide variety of positions (see Chapter 6). Having only a single sensor strip reduces a system's chances of capturing quality signals for every possible sleeping orientation. Even for neurotypical individuals who also may not sleep in standard positions, these systems available on the market might not always provide reliable signals.

Further, depending on the mattress used by the individual, significant distortion can occur in a recorded ballistocardiogram (BCG). The basis for this distortion is discussed in Chapter 2, with a remedy discussed in Chapter 8. As mentioned earlier, children with low-functioning autism and severe disabilities are one of the populations that can benefit from a nighttime monitoring toolset. This dissertation details a bed-based system created to meet this need – a design that can (a) help to quantify the general nighttime wellbeing of children with severe disabilities and autism and (b) also be utilized for a variety of other sensitive populations (e.g., the elderly).

Review of Ballistocardiography Instrumentation

The body's recoil forces due to each heartbeat (the ballistocardiogram) were investigated in the late 19th century (1877) by J.W. Gordon [20], but the field of ballistocardiography did not become popular until the late 1940s [21]–[23]. In 1967, Isaac Starr and Abraham Noordergraaf (pioneers in the field) published a book detailing the history, instrumentation techniques, and other aspects of ballistocardiography [24] – a must read for understanding the history and advancements made during the golden age of ballistocardiography. However, due to a lack of reliability and accuracy needed for clinical applications, the wide variety of recording devices and variations in signal morphology reported in the literature, and the rise of new medical technologies (e.g., echocardiography), interest within the research community (mostly comprised of medical doctors) faded. Most people today have not heard of the BCG, as it was not cemented as a standard clinical waveform despite advances made in the field's prime years [25].

In [26], the authors outline advances in the fields of ballistocardiography and seismocardiography that occurred in the early 2000s. This revival most likely occurred due to advances in sensor technology, the miniaturization and advancement of electronic instrumentation, and improved digital signal processing techniques – all of which were much more primitive in the early days of both fields. The revival was driven by the need for unobtrusive physiological monitoring technologies (e.g., noninvasive, continuous blood pressure monitoring and noncontact pulse rate estimation).

Ballistocardiogram acquisition is a key function of the bed system detailed in this dissertation. Thus, an in-depth review of ballistocardiograph instrumentation is provided in Chapter 2, which also seeks to explain how the forces generated by each heartbeat are manifested in the signals acquired by the recording system. An overview of the original ballistocardiograph systems (the ultralow-, low-, high-frequency, and direct-body ballistocardiographs) is provided along with a model for explaining why the recorded waveforms differed for each of the popular techniques employed during the golden age of ballistocardiography. The same model is applied to the popular modern measurement techniques (standing, chair- and bed-based, wearable, and noncontact systems, plus systems deployed in low gravity), making it possible to 1) compare the newer systems and any future ballistocardiographs to the original devices and 2) understand how BCG morphology can be affected by the measurement device.

Quantifying the Sleep of Children with Severe Disabilities and Autism

Heartspring

Cerebral palsy, autism, and other severe developmental disabilities make it difficult for children to function, especially in learning environments. The traditional classroom is simply not suited for children faced with these disabilities. Thankfully, alternative facilities and institutions exist that can provide services for these children. Heartspring, located in Wichita, Kansas, offers a collection of such facilities. Heartspring [27], founded in 1934 as a not-for-profit institution, began serving children with speech defects and has now grown into a therapeutic residential and day school program that provides services and therapies for children with a wide range of developmental disabilities. Heartspring currently provides year-round residential services for approximately 62 children plus outpatient services for hundreds of children each year. Nearly all of these residential children have an ASD (autism spectrum disorder), and a number of them experience seizures. These children often require specialized care to the point that their parents can no longer meet their needs. Heartspring offers residential group homes where each child gets their own room, and each on-campus group home houses up to eight children.

Heartspring seeks innovative solutions that help to improve the quality of life for children that stay at their facilities. To this end, Heartspring collaborates with researchers at Kansas State University to create new technologies to address an array of needs. Specific areas of interest are 1) detecting/predicting seizures, 2) detecting bed-wetting or enuresis events, and 3) understanding how the sleep quality of these children relates to their daytime behaviors. The bed-system platform outlined in this thesis was motivated by the need for an innovative solution to monitor the nighttime well-being of these children since, as detailed in the following sections, standard sleep quality metrics and measurement technologies are not an option.

Quantifying Sleep

Nighttime Data Acquisition and Autistic Children. There is a known connection between poor sleep quality and reduced daytime cognitive ability in neurotypical individuals [28]. However, this relationship in children with autism and severe disabilities is not as clear [29], [30]. Sleep quality and daytime functionality metrics are typically measured objectively (e.g., through sleep studies [31]) or subjectively (e.g., via surveys [32], [33]). The issue is that neither of these approaches are suitably utilized with children with low-functioning autism.

Polysomnography is typically used to objectively quantify sleep quality, but a polysomnograph involves a multitude of sensing equipment that includes uncomfortable and distracting wires and electrodes. Such systems have been successfully utilized with higher-functioning autistic children [34], but lower-functioning autistic children tend to be hypersensitive and unable to tolerate such a disruptive monitoring environment [35], [36].

Some less intrusive approaches have been developed (e.g., actigraphy [37]) that work well with higher functioning children with autism. Still, such a system requires the subject to wear the device, and a low-functioning, sensitive child can be too distracted by even a simple wristwatch [38]. Although wrist-based devices are capable of monitoring pulse rate and pulse rate variability, actigraphy devices only track movement and do not provide other physiological information (e.g., Actigraph's CentrePoint Insight Watch [39] or the Phillips Actiwatch 2 [40]). Many of these children are also nonverbal, making it impossible to use subjective measures such as surveys to quantify their sleep or to determine how they feel the next day. Because of these difficulties, the relationship between sleep quality and daytime functionality for this population remains to be fully developed. Currently, the primary means to quantify the sleep of this population is periodic, manual bed checks [41]. Cleary, an unobtrusive and autonomous solution is needed.

Ballistocardiography as a Response. Ballistocardiography has re-emerged as a means to unobtrusively monitor physiological signals that can be used to quantify sleep quality. The ballistocardiogram (BCG) can be viewed as the body's recoil response due to each heart beat [26]. Several different unobtrusive sensing modalities have shown the capability to record a BCG: contact systems that measure force [42] and acceleration [43], plus noncontact systems that use camera images [44].

Three cycles of a typical BCG are displayed in Figure 1-1. Each pair of vertical dashed lines represents the rise and fall of a time-aligned electrocardiogram R wave that indicates the initiation of the electrical heart activity for that heart cycle. The prominent peaks (H, I, J, and K) are labeled, where the H feature is generated by an isovolumetric contraction that occurs at the beginning of the heartbeat cycle, and the remaining features are generated by the blood flow/pressure waves moving through the aorta [45].

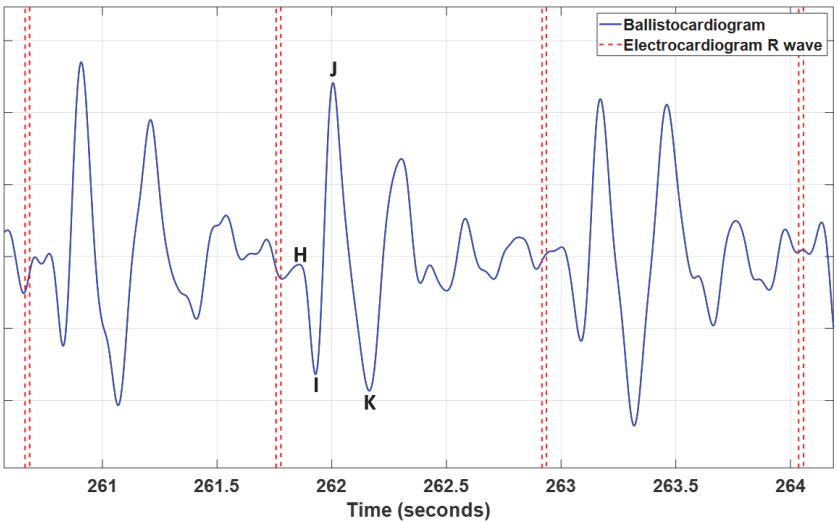

Figure 1-1. Three ballistocardiogram cycles that demonstrate prominent waveform features. Each pair of dashed lines represents the rise and fall of the respective time-aligned electrocardiogram R wave – a visual reference for the beginning of each cycle of electrical heart activity.

Heartbeat interval, respiratory rate, and movement information can be extracted with bed-based BCG systems [46]. Although these parameters are only a subset of the information typically recorded with a full polysomnograph, some investigators have used cardiorespiratory analysis [47]–[49] and movement to estimate sleep quality [50]–[52].

Ballistocardiogram Signal Processing

In Chapter 2, a model is presented for how the body and the BCG instrumentation can cause distortion in the recorded waveform. Even without distortion, a BCG is challenging to analyze, and complex algorithms are needed to extract heartbeat interval information [53], [54]. Further, multi-sensor systems that record similar waveforms complicate parameter estimation. E.g., when eight sensors all record slightly different forms of a BCG generated by the same heart activity, which sensor's data stream should be used for parameter estimation? Would a fusion approach provide results that are more accurate? Responses to such questions are investigated in Chapters 7 and 8.

For example, in the context of instantaneous heart rate estimation and the identification of individual heartbeat intervals (HBIs), a signal quality index is useful to quantify the quality of the estimate. Typically, simultaneously acquired ECG R peaks are used to partition individual BCG cycles, and these cycles are then analyzed to determine the BCG signal quality [55]. However, in most cases, especially longer-term monitoring scenarios, ECG data will not be

available. Further, both the ballistocardiograph instrumentation and the subject's posture affect a BCGs morphology. Thus, in real-world applications, BCG morphology will vary greatly from person to person and from instrument to instrument – meaning that non-ECG-based BCG signal quality metrics are needed that are applicable in a broad range of application scenarios.

To that end, this dissertation presents a novel, BCG-specific signal quality index in Chapter 7. The relationships between the index and performance metrics (e.g., sum squared error, false alarm rate, and false negative rate) are investigated using a linear regression model. With the signal quality index defined, Chapter 8 outlines a novel digital signal processing technique to robustly estimate HBIs. The algorithm is robust in the sense that regardless of the mattress type (a firm and plush mattress were analyzed) or sleeping position (five positions were considered), the HBI estimates were consistently accurate with few false alarms (extra intervals) and few false negatives (missed intervals).

Chapter 2 - Review of Ballistocardiograph Instrumentation

A ballistocardiogram (BCG) represents the body's recoil response due to the ejection of blood from the heart [56]. This signal is similar to other cardiopulmonary signals (e.g., an electrocardiogram or photoplethysmogram) in that the waveform occurs at a pseudo-periodic rate driven by the cardiac cycle. Several BCG and electrocardiogram (ECG) cycles are depicted in Figure 2-1, where the prominent BCG features (H, I, J, and K) are labeled for one cycle and time-aligned with the corresponding ECG R peak. Ballistocardiography was investigated in the late 19th and early 20th centuries by J.W. Gordan and Y. Henderson [20], [57]. It became quite popular in the 1940s through the late 1960s after one of the pioneers in the field, Isaac Starr, created a scientific and reproducible recording system [22]. However, due to limited clinical acceptance, accuracy and repeatability concerns, and the invention of newer medical technologies (e.g., echocardiography), the research community's BCG interests faded [25]. The BCG was not therefore established as a standard clinical waveform despite the advances made in the "golden age" of ballistocardiography. In the early 2000s, ballistocardiography experienced a revival as people were drawn back to study this now "outdated" technique.

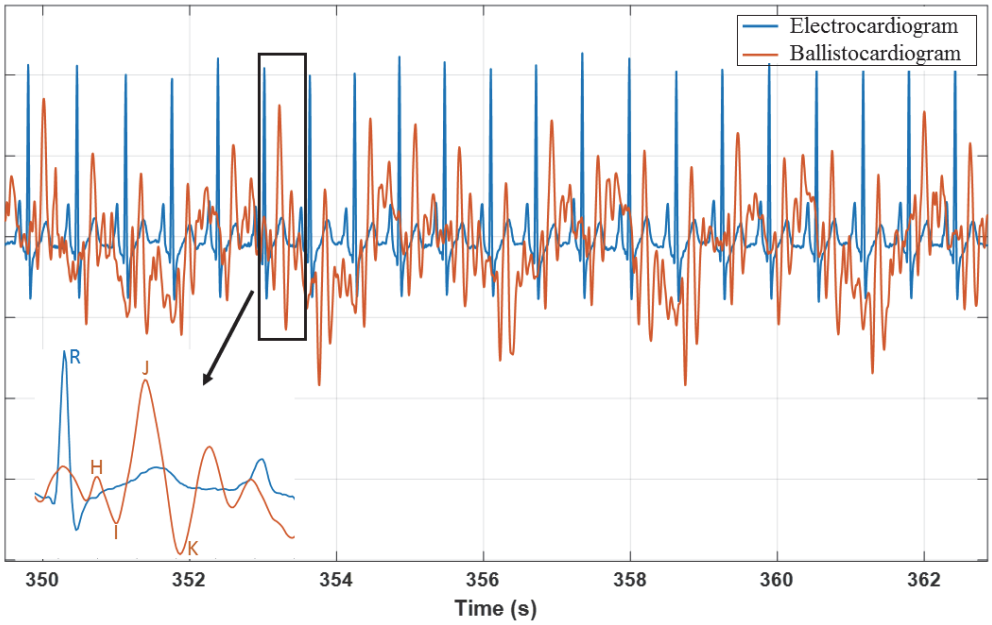

Figure 2-1. Several ECG and BCG cycles (top). One BCG cycle with labeled features (lower left).

BCGs are currently being investigated in numerous research contexts: unobtrusive heart rate monitoring [42], sleep staging [49], blood pressure monitoring [58], biometric applications

including continuous authentication systems [59], and quantifying cardiovascular health (e.g., contractility, and cardiac output) [60], to name a few. Since a BCG can be measured unobtrusively and monitored continuously, it is also a promising modality for personalized healthcare systems [61].

Force [62], displacement [63], velocity, and acceleration sensors are all capable of recording BCGs [64]. Even a sensing modality that has no coupling to the body, such as a radar or camera-based system, can record a BCG as long as it has a direct line of sight [44], [65]. A coupling mechanism can be direct (e.g., an accelerometer attached to a subject) or indirect (e.g., coupling through a medium such as a mattress in a bed-based system [66], [67]). Modern measurement setups involve subjects that stand on weighing scales or force plates, signals recorded from bed-based systems, wearable devices that utilize accelerometers and gyroscopes, and chair-based systems with sensors integrated into seat cushions or backrests [62], [68]–[74]. Regardless of how a BCG is recorded, it is important to understand the effects the system or setup might have on the recorded waveform.

The high-frequency ballistocardiograph system used by Starr (abbreviated as HF-BCG) was just one of several measurement modalities that researchers used during the early days of ballistocardiography (the 1940s through the early 1980s) [25]. The very first systems used by Gordan and Henderson were based on modified scales that utilized spring systems to capture BCGs when the subjects stood on, or lied down on, the recording devices. Later BCG measurement systems required subjects to lie down, as investigators soon realized it was difficult for sick subjects to stand motionless for a prolonged period of time [24]. Four main acquisition systems became popular: the HF-BCG system used by Starr, the low-frequency ballistocardiograph (LF-BCG), the ultralow-frequency or aperiodic ballistocardiograph (ULF BCG), and the direct-body ballistocardiograph (DB-BCG) [75].

This chapter presents an overview of the instrumentation techniques first used in the field of ballistocardiography in comparison to modern techniques, plus how these systems relate to a model that describes the interactions between the heart, body, and measurement platform. The goal is to provide researchers with an understanding of how the old and new techniques are related to better understand the differences/similarities between the recorded waveforms. One truth that will become clear is that, although the waveforms recorded from different systems are presented as BCGs, the morphologies of these signals can vary drastically.

Overview of Early Measurement Devices

Some of the earliest BCG recordings can be found in J.W. Gordon's article, "On Certain Molar Movements of the Human Body Produced by the Circulation of the Blood" in the *Journal of Anatomy*, 1877 [20]. Two figures from that article are shown below in Figure 2-2. The left figure contains a recording from a subject standing on the apparatus, while the right figure contains a recording from a subject lying supine on the apparatus. At the time of Mr. Gordon's article, a naming convention for BCG waveforms had not been defined; hence, the waveform features identified in Figure 2-2 do not match the features in Figure 2-1.

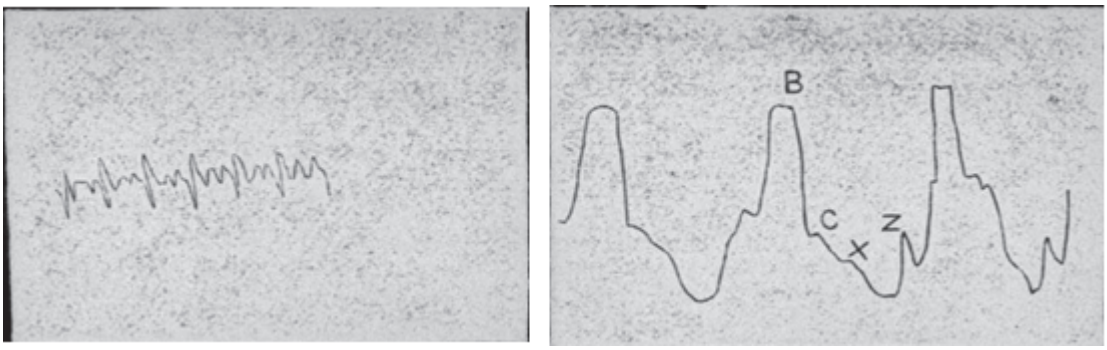

Figure 2-2. BCG waveforms recorded by J.W. Gordon: standing (left) and lying (right). Adapted from [20].

During the mid-20th century, several types of BCG acquisition systems became popular after Starr provided a detailed description of his team's acquisition system [22]. Each recording setup was named based on its frequency characteristics in relation to the normal heart rate, typically 60 beats/min or 1 Hz. As mentioned previously, the instrumentation techniques that were becoming popular were grouped into four categories: HF-BCGs (resonant frequency ≈ 10 Hz), LF-BCGs (resonant frequency ≈ 1.5 Hz), ULF-BCGs (resonant frequency ≈ 0.5 Hz), and DB-BCGs (resonant frequency ≈ 6 Hz) [26]. The researchers at the time soon discovered that the design of an instrumentation device greatly affected the shape of the commensurate BCG. In order to understand the differences between the instrumentation techniques and to create guidelines and conventions for the various acquisition systems, an American Heart Association Committee was formed, *The Committee on Ballistocardiographic Terminology*, which released two reports in the 1950s [75], [76]. The second, extended report, which was published in 1959, detailed a spatial axis and standard conventions for determining polarity. The three axial definitions, along with their relationship to the human body, which served as the frame of reference, were defined positive-to-negative as the longitudinal axis (head to foot), the transverse

axis (side to side, and right to left), and the dorsoventral axis (back to belly). Furthermore, a three-part series was published that addressed a dynamic comparison of the four popular BCG-acquisition methods, or base systems [77]–[79].

To understand the different systems that were available (as well as modern systems), the following analysis considers the forces acting in the head-to-foot direction. The heart, body, and recording mechanism can be modeled as masses coupled by spring/dashpot interconnects (see Figure 2-3 and refer to the variable definitions in Table 2-1). The dynamic positioning of the heart mass (m_H), the subject mass (m_S), and the platform mass (m_P) are tracked along an *x* axis, which represents the head-to-foot axis [80]. In order to simplify the problem, the body can be modeled as a single mass, which is pushed by the internal forces generated by the heart, see Figure 2-4. A similar model was discussed in [26], where a further simplification was made – the BCG recording system or platform was assumed to move freely (D_{PG} and β_{PG} = 0), which is a good starting approximation to understand the differences between the original three popular techniques: the ULF-BCG, LF-BCG, and HF-BCG systems. However, the coupling between the supporting platform and the ground is important to understand the DB-BCG system and modern-day techniques. Such an analysis (the summation of forces and the resulting ideal types of ballistocardiographs) helps to quantify the relationships between the recorded metrics and the center of mass' displacement, velocity, and/or acceleration. For further insight into the modeling characteristics, the reader is directed towards the analysis provided in 'Chapter 3: Instrumentation' in Starr and Noordergraaf's book, *Ballistocardiography in cardiovascular research: Physical aspects of the circulation in health and disease,* which was published in 1967, or the three-part series discussed earlier [24].

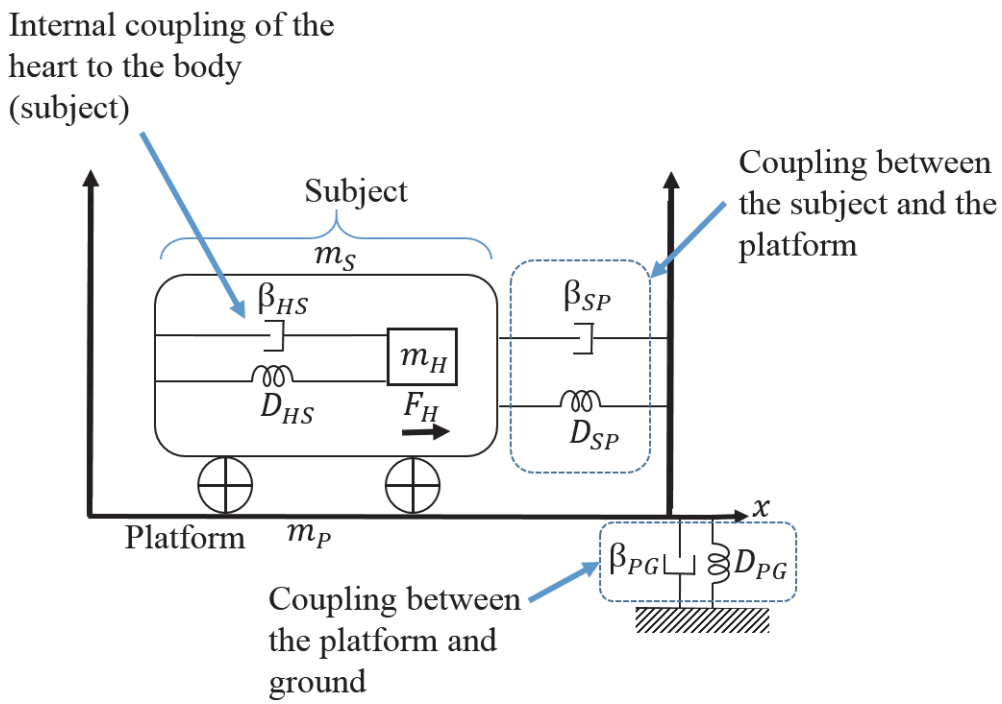

Figure 2-3. Model for the interconnections between the forces generated between the heart, the subject/body, the recording device/platform, and 'ground' during each cardiac cycle. Adapted from [80].

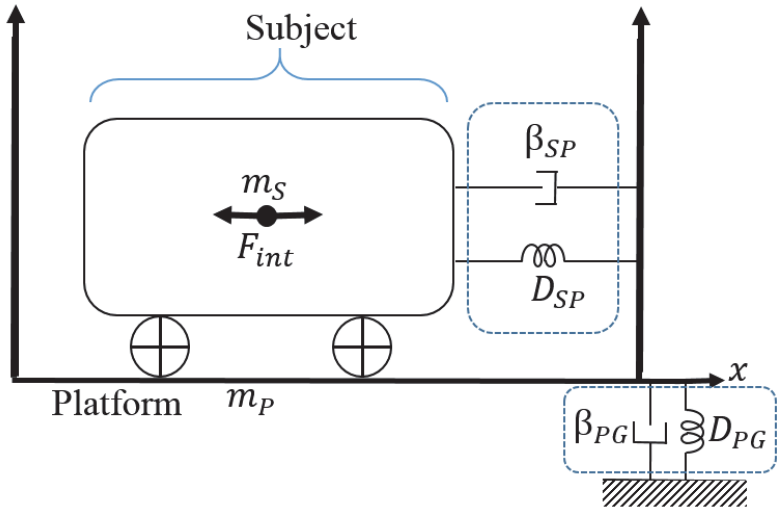

Figure 2-4. Simplified model, assuming the body moves as a single mass. Adapted from [24].

Table 2-1. Variable Definitions.

Variable	Definition
m_H	Mass of the heart
m_S	Mass of the subject
m_P	Mass of the platform
β_{HS}	Dashpot constant, heart to subject
D_{HS}	Spring constant, heart to subject
β_{SP}	Dashpot constant, subject to platform
D_{SP}	Spring constant, subject to platform
β_{PG}	Dashpot constant, platform to ground
D_{PG}	Spring constant, platform to ground
F_H	Force generated by the heart
F_{int}	Internal force
x_S	Displacement of the subject
x_C	Displacement of the body's center of mass due to internal forces

Regarding the forces in the head-to-foot direction (x axis), the two equations of motion considering Figure 2-4 are

$$F_{int} = m_S\ddot{x}_S + \beta_{SP}(\dot{x}_S - \dot{x}_P) + D_{SP}(x_s - x_P) \tag{1}$$

and

$$0 = m_P\ddot{x}_P + \beta_{PG}\dot{x}_P + D_{PG}x_P + \beta_{SP}(\dot{x}_P - \dot{x}_S) + D_{SP}(x_P - x_S) \tag{2}$$

Assuming the platform can move freely in its environment, i.e., D_{PG} and β_{PG} are zero, and that the platform is fixed to the reference frame, i.e., $x_P = 0$, equation 1 can be written as

$$F_{int} = m_S\ddot{x}_S + \beta_{SP}\dot{x}_S + D_{SP}x_s \tag{3}$$

After substituting for $F_{int} = m_S\ddot{x}_C$,

$$m_S\ddot{x}_S + \beta_{SP}\dot{x}_S + D_{SP}x_s = m_S\ddot{x}_C \tag{4}$$

From equation 4, three types of ballistocardiographic systems, which closely resemble three of the popular systems at the time (ULF-BCG, LF-BCG, and HF-BCG), can be addressed by considering which parameter dominates the left side of equation 4.

The Ultralow-Frequency Ballistocardiograph

First, consider the situation in which the body and platform move together in unison (i.e., there is no damping or restoring force coupling the body to the platform, meaning β_{SP} and D_{SP} are zero). Equation 4 can then be simplified to

$$m_S\ddot{x}_S = m_S\ddot{x}_C \tag{5}$$

Solving for x_S yields

$$x_S = x_C + k_1 t + k_2 \tag{6}$$

This scenario is straightforward and is simply a conservation of momentum problem. In this ideal scenario, the recorded quantity, whether it is displacement, velocity, or acceleration, will be equal to the corresponding quantity for the body's center of mass given that the constants, k_1 and k_2 due to integration, are zero. This special case (β_{SP} = D_{SP} = zero) can be approximated when the body and platform move together, and the platform has a weak coupling to its environment. Of the three original ballistocardiograph devices, this approximation most closely resembles the ULF-BCG system, or aperiodic ballistocardiograph.

A ULF-BCG system was created by suspending a platform from a ceiling using rope, floating a platform on mercury, or using pressurized air to create a floating platform (see Figure 2-5) [20], [81], [82]. The ULF system was commonly seen as the gold standard at the time given its limited distortion of the "true" BCG at higher frequencies [83].

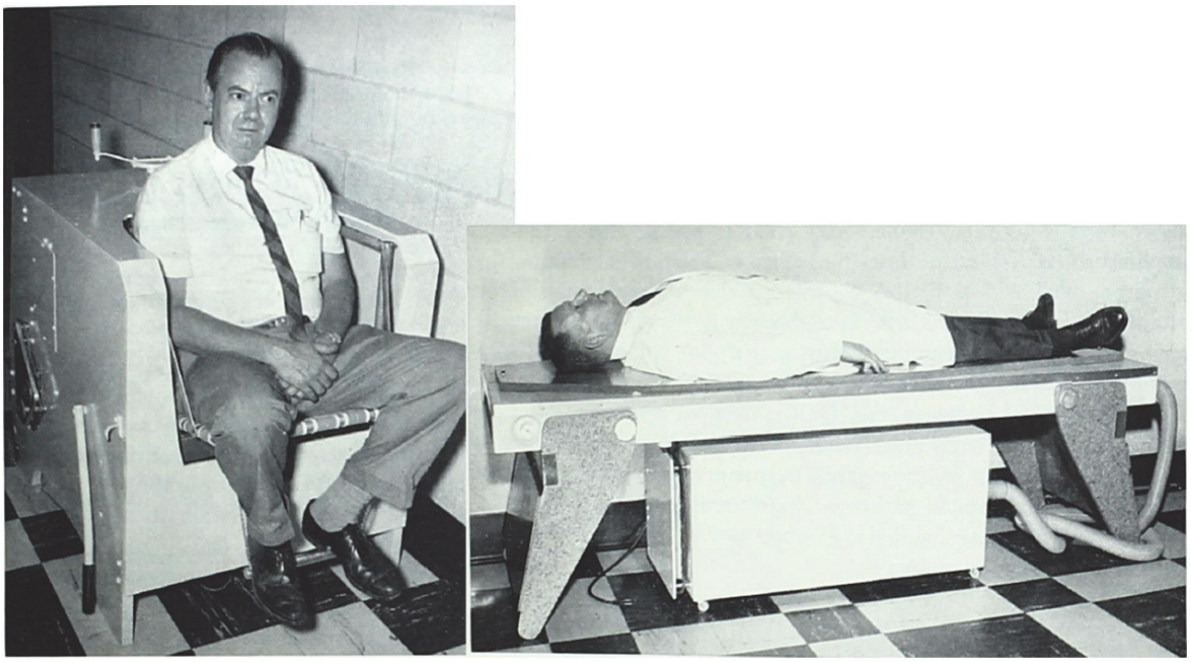

Figure 2-5. Two examples of "new" ultralow-frequency ballistocardiographs: a chair-based system that can adjust for patients with different weights (left), and a pressurized air-based table (right) [82]. Reprinted with permission from S. Karger AG, Basel.

The Low-Frequency Ballistocardiograph

For the second special case, consider β_{SP} to be the dominating term in equation 4, resulting in

$$\beta_{SP}\dot{x}_S = m_S\ddot{x}_C \tag{7}$$

Again, solving for x_S yields

$$x_s = \frac{m_s}{\beta_{SP}}\dot{x}_C + k_3 \tag{8}$$

Here, the recorded displacement will be proportional to the center of mass' velocity. Thus, the recorded velocity will be proportional to the center of mass' acceleration. The closest system to this approximation was the LF-BCG system used by Nickerson, where the external damping between the subject and the platform was high compared to the damping of the coupling springs between the system and ground. An LF-BCG system was typically critically damped by adding weight to the platform equivalent to the subject's weight, resulting in a platform resonance around 1.5 Hz [75].

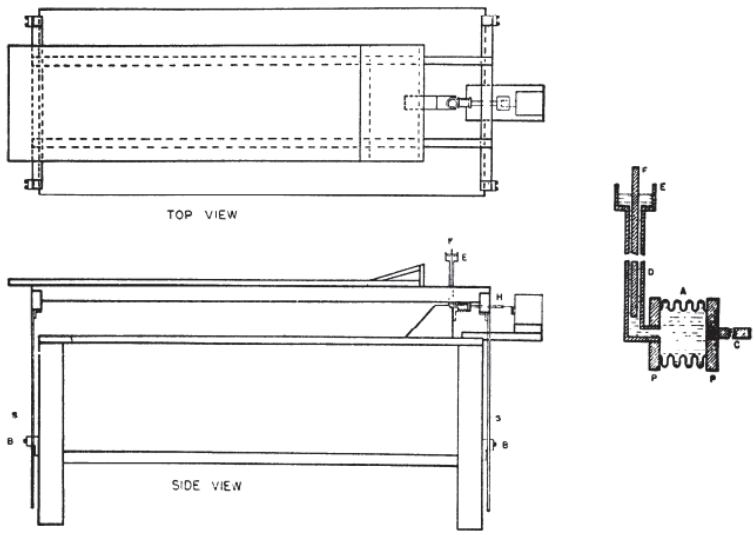

Figure 2-6. Diagram of Nickerson's low-frequency ballistocardiograph (left) and damping device (right) [84]. Reprinted with permission from ©The American Physiological Society.

The High-Frequency Ballistocardiograph

For the last case, the damping factor, D_{SP}, between the subject and the platform is considered the dominating term in equation 4. This leads to

$$x_S = \frac{m_S}{D_{SP}} \ddot{x}_C \tag{9}$$

This case most closely relates to the HF-BCG system popularized by Starr. It is interesting to note that, for this system, recorded displacement is proportional to the center of mass' acceleration, which should (in theory) be the closest measurement to the internal forces. HF-BCG systems typically had a natural resonance of 8-14 Hz when occupied by a subject [75] – a much higher resonance frequency relative to the heart pulse frequency when compared to the previously mentioned systems. Figure 2-7 illustrates an example HF-BCG system used by Starr, which had vibration frequencies ranging from 9.5 to 12.5 Hz when the table was weighted down with iron bars weighing from 50 to 100 lbs [22].

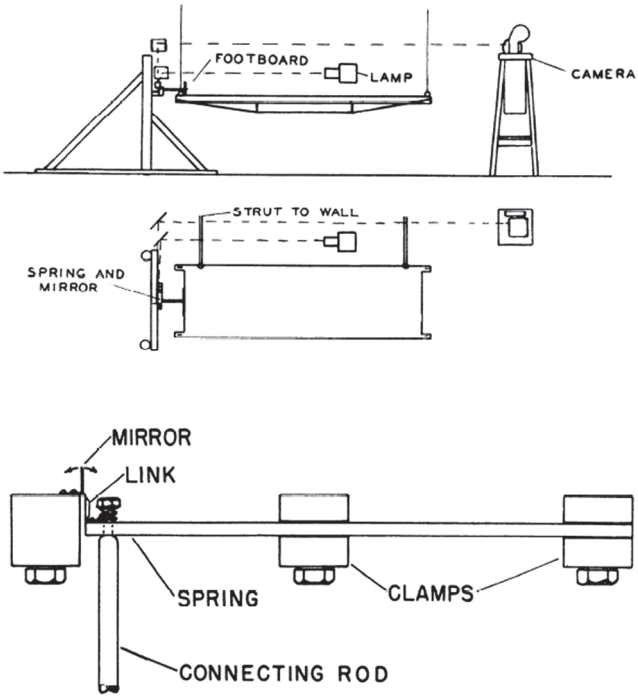

Figure 2-7. High-frequency ballistocardiograph proposed by Starr [22]. Reprinted with permission from © The American Physiological Society.

The Direct-Body Ballistocardiograph

The above analysis, which assumes the body and platform can both move, leaves out the other popular measurement framework – the direct-body ballistocardiograph system (DB-BCG). The DB-BCG system was based on the fact that the body will still move on the platform even when the platform is held stationary. In reality, a ULF-BCG, LF-BCG, or HF-BCG system would also have a similar coupling between the body and the platform, just to a much lesser degree. With the platform held stationary, the model can be viewed as in Figure 2-8.

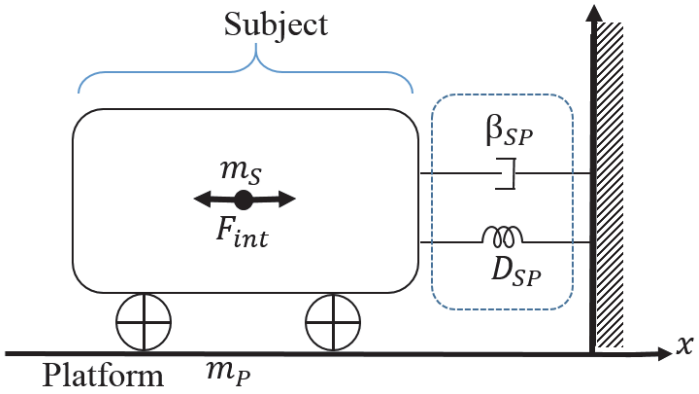

Figure 2-8. System model with the platform held stationary.

Summing the forces in the *x* direction results in

$$F_{int} - \beta_{SP}\dot{x}_S - D_{SP}x_S = 0 \tag{10}$$

Again, substituting $F_{int} = m_S\ddot{x}_C$, gives

$$m_S\ddot{x}_S + \beta_{SP}\dot{x}_S + D_{SP}x_s = m_S\ddot{x}_C \tag{11}$$

Equation 11 and equation 4 are essentially identical, but there is an important difference. To move from equation 1 to 4, a frame of reference adjustment was made to simplify the problem, since the platform could move. For the DB-BCG, the platform is held stationary, so the coupling between the subject and platform will always be present. I.e., the damping and spring constant terms cannot be assumed to be zero for special cases. Both of these terms must be considered, and they are determined by how the body is coupled to the platform. Damping techniques were commonly used with the DB-BCG systems (e.g., footplates or shin-bars) in order to approximate the HF-BCGs, but the stronger damping led to greater BCG distortion – an aspect that was debated, as researchers did not fully understand what BCG frequency characteristics were the most important [85]. An example of a shin-bar ballistocardiograph system is pictured in Figure 2-9 [86].

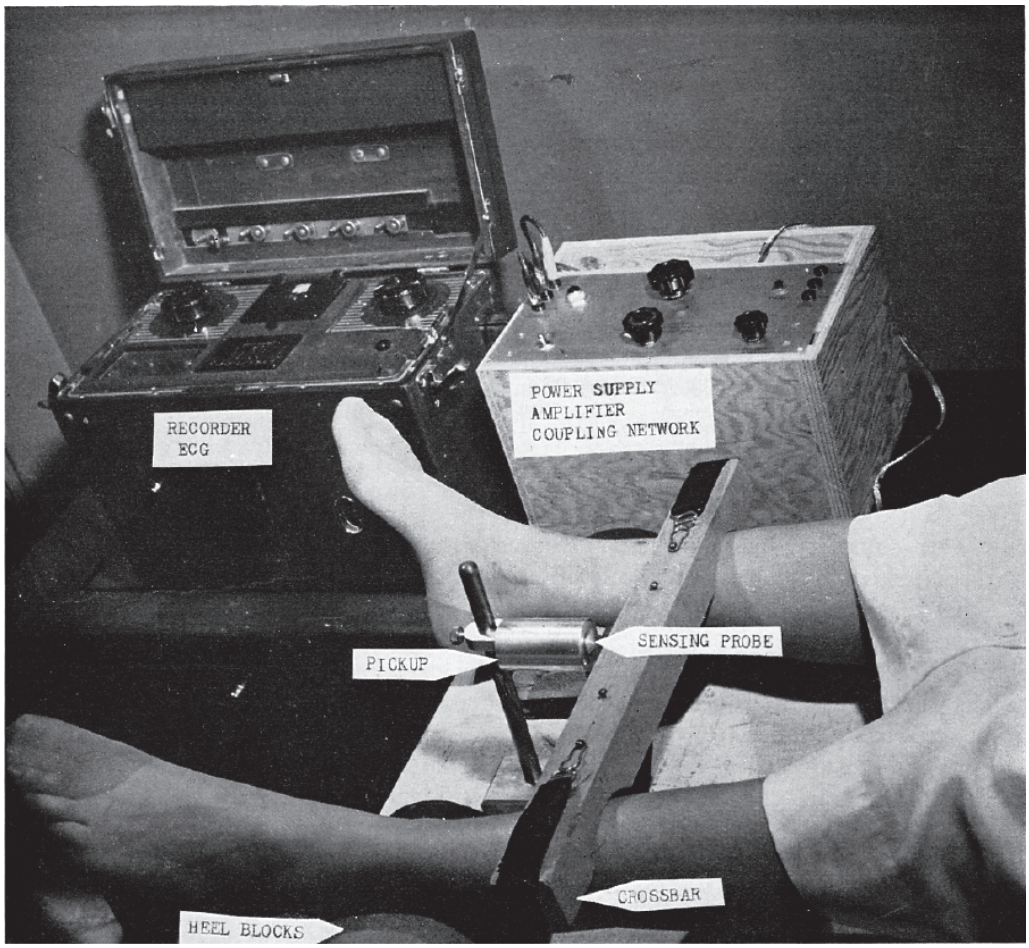

Figure 2-9. Example shin or crossbar ballistocardiograph [86]. Reprinted with permission from Elsevier.

Comparison of ULF, LF, HF, and DB Ballistocardiographs

The ULF-BCG system was considered the gold standard, as the recorded metrics were closest to those belonging to the center of mass. When measuring displacement, the LF-BCG system captures the center of mass' velocity, while the HF-BCG system records its acceleration. With DB-BCG systems, the relationship is not as clear. If significant external damping is applied (e.g., holding the subject firmly in place with either a footboard or a shin bar as depicted in Figure 2-9) then the DB-BCG system recordings approach those acquired by the HF system, but as was noted earlier, heavily damping the system can cause considerable distortion. Comparisons between the recorded quantities for the ideal BCGs are contained in Table 2-2.

Table 2-2. Recorded quantities for the ideal ballistocardiographs.

Ideal Ballistocardiograph	Recorded Quantity		
	x	$\dot{x}$	$\ddot{x}$
Case I – close to ULF-BCG	x_c	$\dot{x}_c$	$\ddot{x}_c$
Case II – close to LF-BCG	$\dot{x}_c$	$\ddot{x}_c$	
Case III – close to HF-BCG	$\ddot{x}_c$		

With the special cases now defined, another view of equation 4 can be constructed by deciding which term to consider on the right side of the equation. For the HF-BCG, we can rewrite equation 4 in another familiar, frequency-dependent form:

$$m_S\ddot{x}_S + 2\zeta\omega\dot{x}_S + \omega^2 x_s = m_S\ddot{x}_C \tag{12}$$

Using operational notion

$$(m_S s^2 + 2\zeta\omega s + \omega^2)Y(s) = (m_S s^2)X(s) \tag{13}$$

Finally, the transfer function can be written as

$$\frac{Y(s)}{X(s)} = \frac{s^2}{s^2 + \frac{2\zeta}{m_S}\omega s + \frac{\omega^2}{m_S}} \tag{14}$$

The takeaway is to recognize that this is a *highpass* transfer function, which approximately characterizes the ULF-BCG system. For the LF-BCG system, knowing that displacement will be proportional to velocity, a slight adjustment is made to equation 12:

$$m_S\ddot{x}_S + 2\zeta\omega\dot{x}_S + \omega^2 x_s = m_S\dot{v}_c \tag{15}$$

Again, following the same analysis above leads to the following transfer function:

$$\frac{Y(s)}{X(s)} = \frac{s}{s^2 + \frac{2\zeta}{m_S}\omega s + \frac{\omega^2}{m_S}} \tag{16}$$

Therefore, the LF-BCG system has a *bandpass* filtering effect. Lastly, the transfer function for the HF-BCG system, where displacement is proportional to force, becomes

$$\frac{Y(s)}{X(s)} = \frac{1}{s^2 + \frac{2\zeta}{m_s}\omega s + \frac{\omega^2}{m_s}} \tag{17}$$

meaning that the HF-BCG system will have a *lowpass* filtering effect on the recorded signal. Ideal frequency responses using typical resonant frequencies and damping ratios for the three setups are depicted in Figure 2-10 [77].

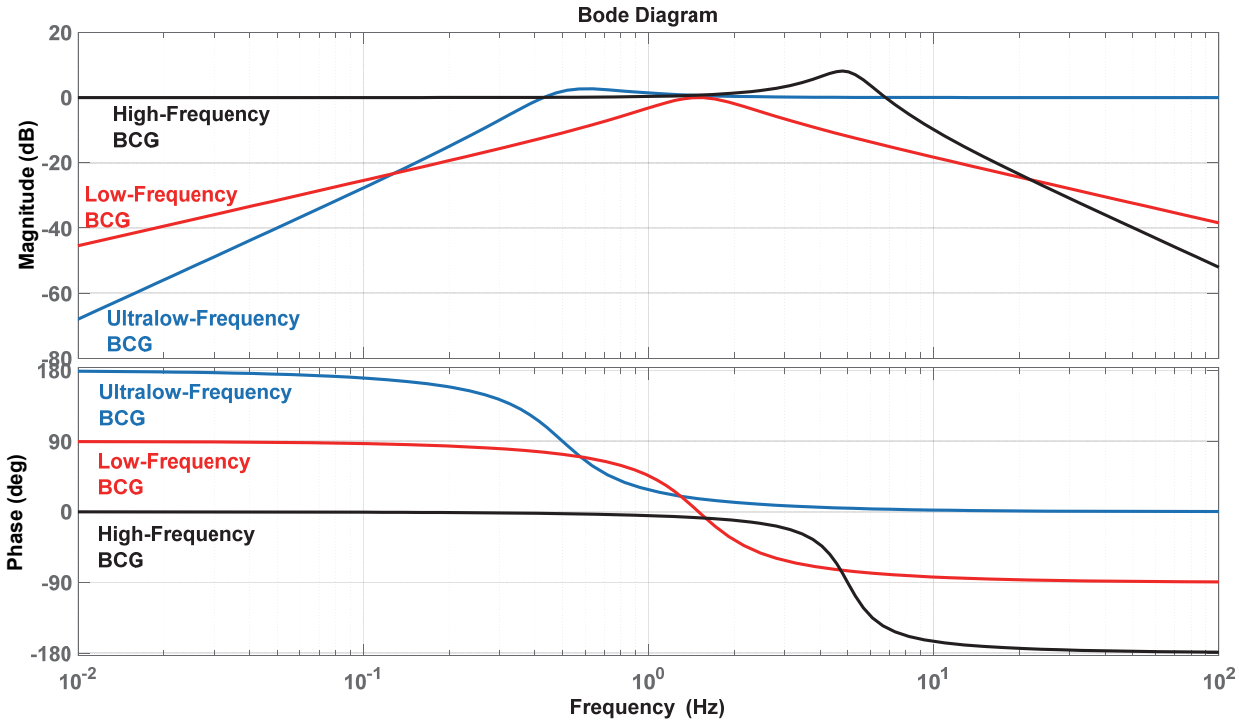

Figure 2-10. Frequency response curves for the three ideal ballistocardiographs using the parameters specified in Table 2-3.

Table 2-3. Functional parameters used to generate the curves in Figure 2-10.

Ideal BCG	Parameter	
	$f_c = {\omega_c}/{2\pi}$ (Hz)	ζ – damping ratio
Type I, ULF-BCG	0.5 Hz	0.4
Type II, LF-BCG	1.5 Hz	0.4
Type III, HF-BCG	5 Hz	0.2

Overview of Modern Measurement Techniques

Modern ballistocardiography came about due to advances in sensor technology (e.g., highly sensitive accelerometers, electromechanical films, polyvinylidenefluoride materials (PVDFs), and load cells), data acquisition hardware and software, and digital signal processing techniques. One of the most attractive aspects of the BCG is that it can be measured unobtrusively and continuously without any effort from the user. In fact, when working with sensitive populations such as the elderly or children with severe disabilities and autism, BCG systems can be integrated into their environments seamlessly without major modifications [70], [87]. With all the sensor advancements that have been made and the flexibility of modern sensors and acquisition systems, it is difficult to describe in detail every kind of ballistocardiograph that has been (or will be) created. Rather, the following sections address the common sensing modalities that have gained popularity and how they relate to the historical models in Figure 2-3 and Figure 2-4.

Standing Ballistocardiograph

To understand the standing ballistocardiograph system (standing-BCG; see Figure 2-11(left)), the frame of reference in Figure 2-4 still applies. The *x* direction corresponds to the head-to-foot BCG component, and the standing-BCG system offers the most straightforward means to collect this component in light of the effect of gravity (measurements made in low gravity environments are discussed in a later section). The force of gravity pushes down on the subject, strengthening the coupling between the person and the measurement device. The skeletal frame provides a rigid travel path for the forces generated by the heart. Note that the following analysis still assumes that the body and heart move together as a single mass. The coupling network between the platform and the ground, β_{PG} and D_{PG}, are determined by the characteristics of the scale/platform. For example, consider the weighing scale used by Inan *et al*. in [42]. The spring constant for the scale is reported to be 1.13 to 1.19 N μm^{-1}. With this large of a spring constant, the system most closely resembles special case III, the HF-BCG system. For example, a spring constant of 0.8 N μm^{-1} was reported for an HF-BCG system [80]. A standing-BCG system is only limited by the bandwidth of the scale or force plate, since the sensing mechanism can cause delays [88].

Chair Ballistocardiograph

Like the standing-BCG systems, chair-based systems (see Figure 2-11(right)) appear to be a good fit for capturing the head-to-foot component of the BCG when the sensor is placed on the seat. However, while the pressure wave does partially travel along the skeletal system, it must also pass through fatty tissue before reaching the sensor. The amount of signal attenuation is dependent on the tissue characteristics. Typically, signal amplitudes tend to be lower for chair-based systems compared to standing-BCG systems [26]. In addition, signal morphology has been found to be dependent on posture [89]. Considering the model in Figure 2-4, the sensor/platform will be strongly coupled to ground. The body is also strongly coupled to the sensor. Thus, to understand this system, modeling the body as a single mass falls short. Instead, the heart and the body must be treated as independent masses coupled by a spring-damper as depicted in Figure 2-3. This model helps to understand the point made above that the tissue characteristics of the body between the heart and the sensor affect or distort the recorded signal morphology. Therefore, one must correct for this distortion before chair- and standing-BCGs can be compared.

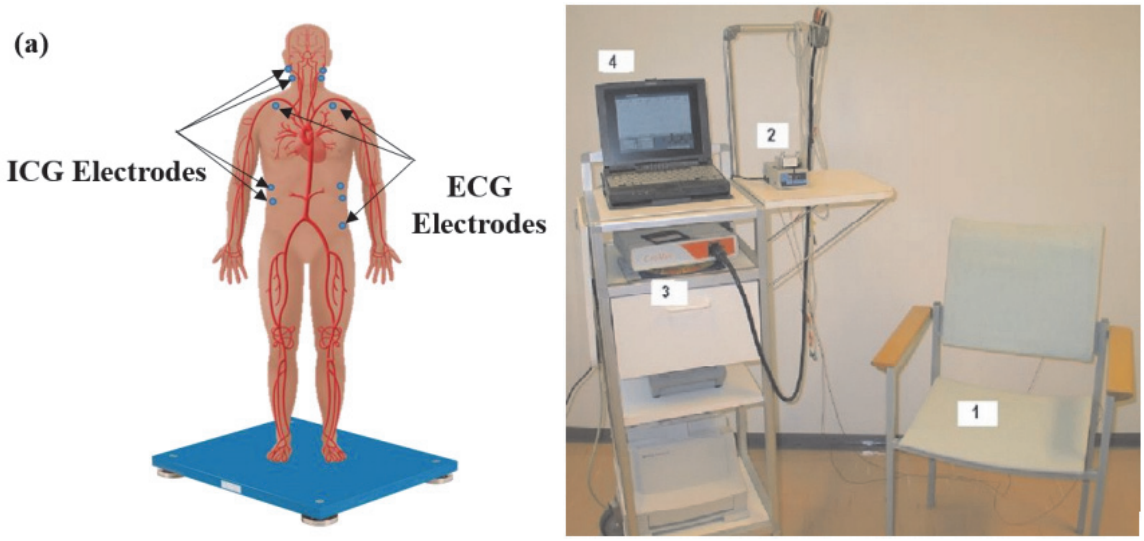

Figure 2-11. Standing-BCG system with force plate (left) ©2016 IEEE [68]. Chair-based BCG system (right) ©2005 IEEE [90].

Bed-Based Ballistocardiograph

A bed-based system (see Figure 2-12) can be difficult to analyze, since it records a combination of the dorsal-ventral and head-to-foot BCG components [26]. There is also the issue

of the body's natural frequency [91], which causes considerable signal distortion because the system acts like a lowpass filter with a large resonance around 3 to 5 Hz [24]. This was apparent in early ballistocardiograph systems, so in response (a) non-slip pads were placed under the person, (b) footplates, head fixtures, and shin-bars were used to raise the resonant frequency of the system, and (c) electrical networks were investigated to "correct" for the distortion [85], [92], [93]. For a modern system designed to be integrated into a standard bed, a springy mattress adds to the distortion seen in the BCG waveforms, sometimes making it impossible to extract any useful information from the acquired signals. A modern bed-based system is most closely related to the original DB-BCG design, since the platform or recording system is held stationary. Further, the head-to-foot component of the BCG is weakly coupled to the sensing mechanism. Looking back at equation 11, both spring and damping factors influence the resultant waveform, making it difficult to interpret the resulting BCG when the sensor is placed beneath the subject's chest.

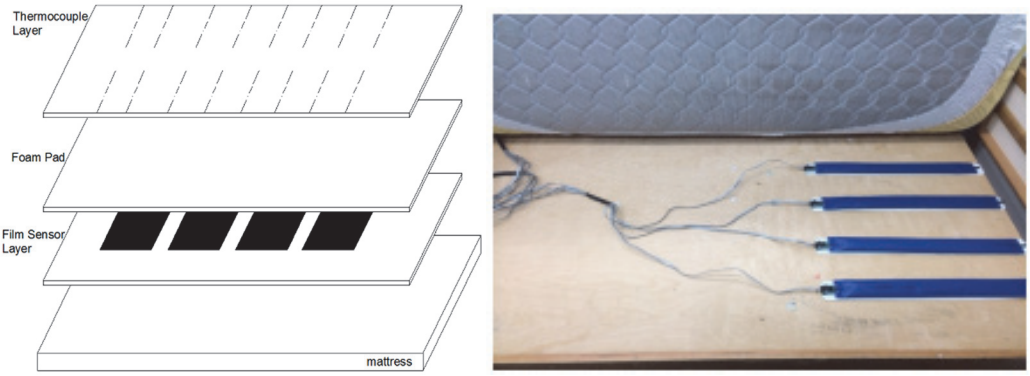

Figure 2-12. Two example bed-based BCG systems: multilayer system using EMFi sensors (left) [46], and four hydraulic sensors placed under the mattress (right) ©2015 IEEE [94].

Wearable Ballistocardiograph

When the subject wears a sensor (e.g., an accelerometer; see Figure 2-13) it is important to consider the sensor's location. If an accelerometer is placed on the sternum, the recorded waveform will be the seismocardiogram (SCG) – the vibration of the thorax due to a heartbeat, *not* the BCG, which has quite a different morphology [26]. However, when the sensor is placed at other body locations, it can record a "BCG"-like waveform. Digital signal processing techniques (i.e., integration) were demonstrated to map recorded acceleration signals to force waveforms that closely resembled BCGs recorded by a force plate for the same subject [43]. This seems reasonable, since the body was strongly coupled to the force plate, so whether the sensing

location was the feet or another spot on the body, the waveform morphology of the head-to-foot-component should be similar to the morphology of a signal acquired with a standing-BCG system. Note that the subject's orientation and coupling to ground is critical to understanding the resulting recorded waveform.

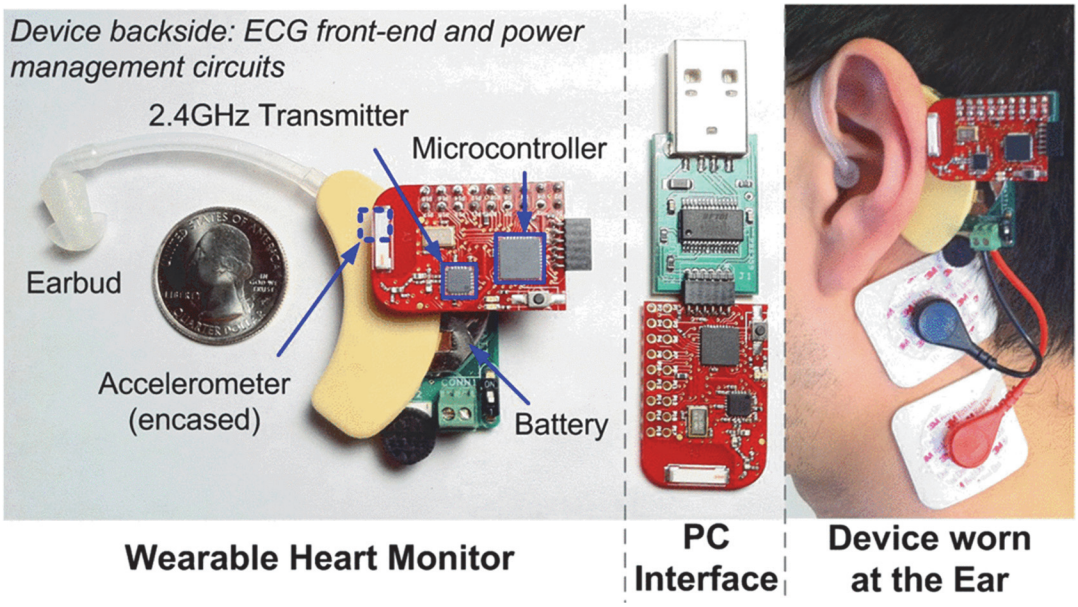

Figure 2-13. Accelerometer-based wearable BCG and ECG system ©2011 IEEE [95].

Non-Contact Ballistocardiograph

Radar and video-based systems have demonstrated the capability to record BCGs. These types of systems have more flexibility in that the person can be standing, sitting, or lying down – as long as the system has a line of sight to the person. The type of BCG recorded will depend on how the subject is situated, as with the wearable systems. Therefore, the analysis in the previous sections (III.A-III.C) can be applied.

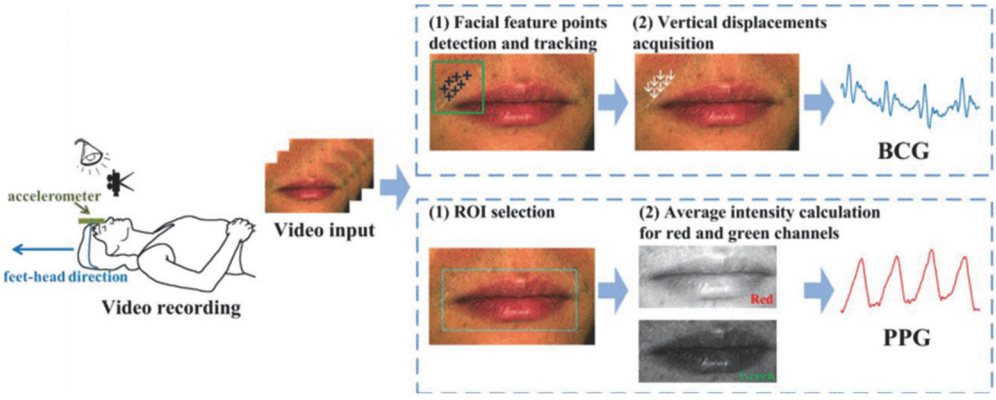

Figure 2-14. Camera-based BCG and PPG system ©2016 IEEE [44].

Reduced-Gravity Measurements

Measurements made in zero- or reduced-gravity environments have been fundamental to understanding the factors that influence the BCG's "true" morphology, i.e., when it is not influenced by gravity. A full history of results gathered from low-gravity measurements would merit its own review. A few anecdotal experiments are noted here. In the late 1960s, the U.S. Naval School of Aviation Medicine performed flight procedures to simulate zero-gravity environments, where tri-axial BCG data were recorded using accelerometers attached to the subject along with simultaneous ECG data [96]. In 1993 during the Spacelab D-2 mission, tri-axial BCG data were gathered noise-free for 146 seconds [97], [98]. Each of these recordings most likely resembles the purest form of a BCG without the influence of gravity. Not surprisingly, the ULF-BCG system offered similar BCGs to those gathered in microgravity [83].

Figure 2-15. Triaxial accelerometer-based BCG measurements made in low gravity in 1964 [96].

Chapter 3 - A Bed-Based Monitoring System

For personalized healthcare to become widely accepted, advances need to occur in medical monitoring technologies. Such systems must operate outside of a clinical setting, e.g., in an individual's home [10], [99]. To that end, medical devices are getting smaller and more powerful, making it possible to monitor physiological signals in a variety of environments. Wireless protocols that are secure and efficient are being proposed to develop frameworks capable of keeping patient information private while achieving efficient network data transfers [100], [101]. However, medical technology designers face a number of challenges if they are to meet the demands of a personalized healthcare system.

One such challenge is the acceptance of these devices for long-term use. Such systems must collect data reliably and accurately for weeks, months, or years, whereas current wearable medical technologies (e.g., blood pressure and heart rate monitors) require consistent, repeated effort from users. For example, in the case of cuff-based blood pressure monitors, periodic measurements need to be performed daily, and each takes several minutes to perform. Previous studies have documented that subjects have extremely low adherence to routine monitoring (e.g., checking their blood sugar level or receiving recommended care for hypertension) [102]. Limiting the effort required from a user is a vital design consideration for a personalized healthcare system.

One approach to address the acceptance of medical technologies is to use unobtrusive or noncontact technologies, which require little to no effort by the user. In [103], infrared motion sensors were placed throughout a subject's home, and machine learning algorithms were devised to detect mild cognitive impairment. Capacitive electrograph systems have been demonstrated to be effective for longer-term monitoring of heart rate and other physiological metrics (e.g., respiration rate) [104]–[106]. A pressure-sensitive sheet placed on top of a mattress has been used for sleep-staging [16]. As stated in the Introduction, ballistocardiography systems can also be used to assess physiological signals unobtrusively.

This chapter describes a new type of multi-sensor, bed-based system capable of robustly and unobtrusively recording ballistocardiogram, respiration, and movement data. The design was motivated by the need to monitor the sleep of children with severe disabilities and low-functioning autism. The system is redundant in its ability to monitor physiological signals: multiple sensors with different sensing modalities are placed throughout the bed system – each

with the ability to capture BCGs. As will be discussed in more detail in Chapter 6, this bed-based system is both redundant and robust in its ability to track the physiological signals of such children – each sensor gathers data that are useful in their own right but can also be compared to slightly different signals gathered from sensors at other locations in the bed system. The bed system was designed to keep all of the sensors hidden. I.e., the bed should not look or feel any different from a normal bed. Further, the system should operate autonomously, not requiring any effort from the user.

Goals and Objectives

The overall goal of this bed-based effort is three-fold: design, validate, and demonstrate the functionality of a new multi-sensor physiological monitoring device that can operate unobtrusively and autonomously. The bed-based system provides a platform for the concepts addressed in this dissertation: custom biomedical sensor design, sensor integration and management, and novel ballistocardiogram processing algorithms for signal quality assessment and heartbeat interval estimation. Five **technical objectives** support the overall goal:

1. Design a multi-sensor, bed-based system that can be integrated into the bedroom of a severely disabled autistic child without disrupting their environment.
2. Design an acquisition architecture to collect data from multiple bed systems, which also includes the collection and management of thermal imagery.
3. Validate the system against gold standard metrics (e.g., respiration rates and heart rate intervals synchronously collected from a patient monitor).
4. Demonstrate the capability of the system to operate and collect data accurately over a long-term period in the environment of children with severe disabilities and low-functioning autism.
5. Propose and validate novel ballistocardiogram signal processing techniques for signal quality and heartbeat interval estimation for this multi-sensor platform.

Technology Overview

The bed system incorporates highly sensitive force sensors (electromechanical films and load cells), custom analog signal conditioning circuitry and signal management, National Instruments (NI) [107] compact data acquisition modules and chassis, and NI virtual instrumentation software. The custom analog circuitry was specially designed to condition low

amplitude physiological signals (e.g., BCGs, including their respiration components). NI hardware and software are utilized to collect and process high-resolution, analog-to-digital channels for real-time or post-collection analyses. The high-level virtual instrument (VI) manages multiple instances of the acquisition hardware, making it possible to collect and store datasets from multiple bed systems with a single VI.

A low-resolution thermal camera controlled by a Raspberry Pi unit [108] is used in conjunction with each bed system. The low-resolution thermal imagery serves as a corroboration source for motion detection. Additionally, a thermal camera is useful to diagnose system failures that result from in-room activity.

The custom analog conditioning module and acquisition hardware were also designed to accommodate signals from a patient monitor – signals gathered synchronously that provide standard "ground-truth" parameters against which bed system parameters can be compared. E.g., R-to-R peak intervals are extracted from electrocardiograms gathered from the patient monitor, and these intervals are used to validate BCG heartbeat intervals estimated from bed sensor data.

The multitude of sensors makes the system a suitable platform to track physiological signals from any individual who may sleep in a variety of positions and bed locations. The system is also highly sensitive, accommodating a wide range of subject heights and weights. Further, the platform is flexible in terms of bed compatibility – the system does not require a special type of mattress.

Currently, the platform does not perform real-time data processing in terms of respiratory rate or heart rate estimation. The VI manages the data collection, and these data are stored directly to a series of LabVIEW measurement files (LVMs) [109], where the file structure is outlined in Appendix C. A subset of the currently collected data is displayed on the VI front panel; this provides a real-time means to verify that the bed system is working correctly.

Bed-Based System Concept Model

An initial diagram illustrating the various upper layers of the custom bed-based system is depicted in Figure 3-1. These layers, consisting of (a) a thermocouple layer, (b) a foam pad, (c) a film sensor layer, and (d) a mattress, only represent the top portion of the bed system. The approximate locations of the load cells and the system acquisition hardware are depicted in Figure 3-2, where the dotted white lines represent analog channels. Custom breakaway cables are used to route the output from each EMFi sensor to the conditioning board housed in the bed's

cavity. An accompanying block diagram for the acquisition system is contained in Figure 3-3. An example of a typical Heartspring bed fitted with the sensor system is illustrated in Figure 3-4.

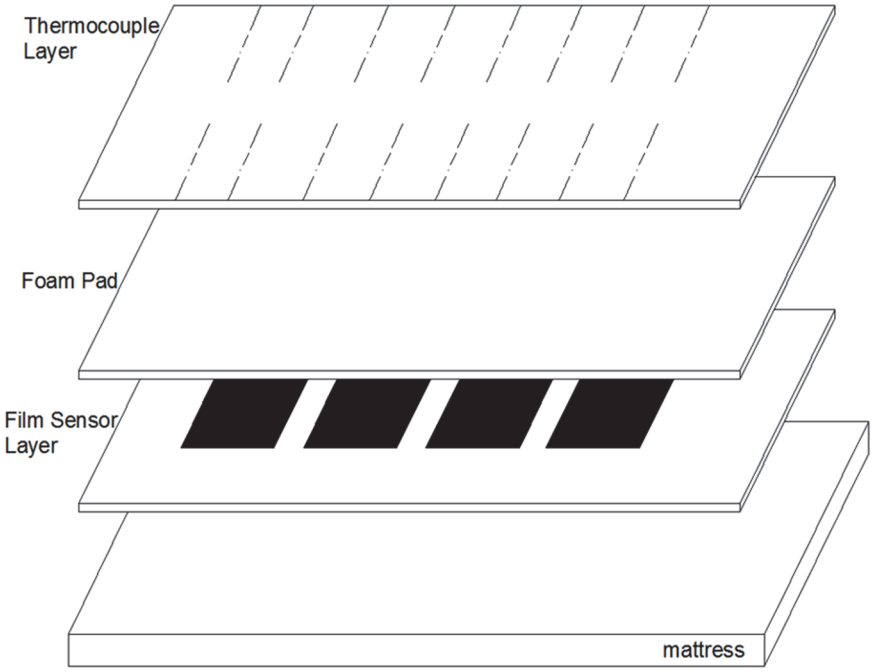

Figure 3-1. Upper layers of the bed.

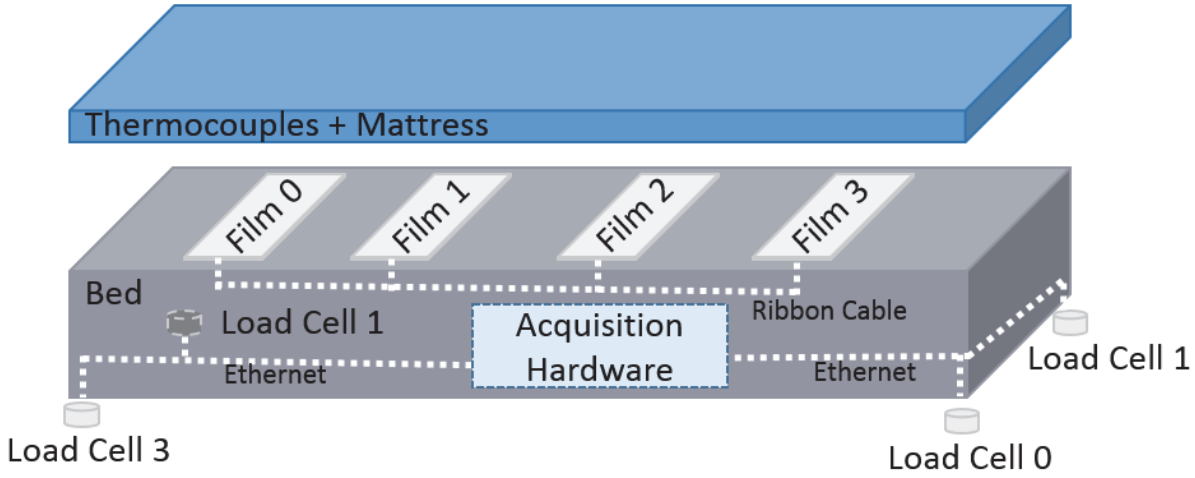

Figure 3-2. Approximate sensor and hardware acquisition locations within the bed system.

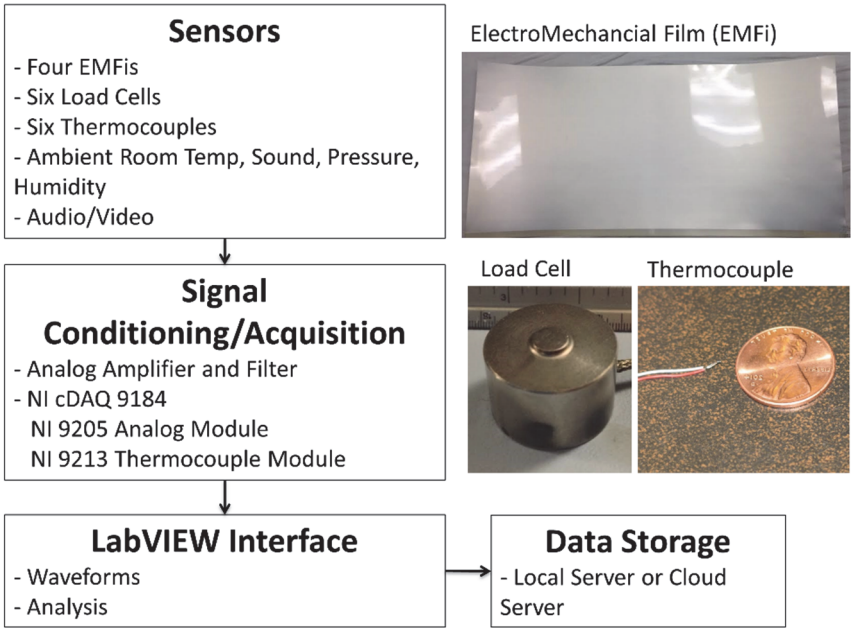

Figure 3-3. Overall system diagram and primary sensor set.

Figure 3-4. Typical Heartspring captain's bed fitted with the monitoring system.

This platform fits well within the personalized health-monitoring model. The eight primary film and load cell sensors, each capable of recording BCGs, make the system robust in its ability to track physiological signals regardless of sleeping position. I.e., no restrictions are

placed on how a person must sleep – a limitation of commercial BCG-based sleep monitoring technologies. Load cells make it easy to track bed entrance and exit events, and these load cell data can be processed to offer center of position (see the next chapter). The bed system can be programmed to operate autonomously – a user does not need to start or stop the system when they get into bed at night or when they wake up the next morning, respectively. The VI management aspect also makes the system capable of real-time analysis. For example, for individuals in need of constant monitoring, parameters estimated from the bed system (e.g., respiration rate, heart rate, heart rate variability, ambient temperature, motion, etc.) can be monitored continuously and unobtrusively. Another aspect to note is that these physiological parameters can be monitored over time, making it possible to track trends over weeks, months, or even longer. Parameters such as weight, resting heart rate, and sleep efficiency offer insight into general wellbeing when tracked over a longer time period.

Chapter 4 - Bed System Architecture

This chapter details the sensors, custom hardware, and NI hardware and software that work together to comprise the bed-based platform. Given that BCG forces are in the approximate range of a few newtons, highly sensitive force sensors capture these micro-movements [26]. Custom hardware conditions these small signals, amplifies the signal components in the frequency ranges of interest, and filters out unwanted noise. The National Instruments hardware provides means for remote configuration, data management, signal synchronization, and timing control. The NI hardware and software allow the platform to simultaneously record data streams from two bed systems located in separate rooms via a single VI. An added benefit of the NI toolset is that selected waveforms can be viewed in real time, making it possible to debug elements of the system without the need for additional test equipment (e.g., an oscilloscope).

Sensor Selection

As discussed in earlier chapters, several sensing modalities exist to monitor BCGs. When acquiring these signals from children with severe disabilities and low-functioning autism, the bed system needs to hide the sensors, making it appear no different from a standard bed. To this end, different types of sensitive force sensors were considered. Given that little prior nighttime research has been conducted on this population, it was unclear which types of sensors or sensor placements would work well. The team ultimately decided to place large, sensitive electromechanical film (EMFi) sensors beneath the mattress, and load cells were also placed under the four corner bedposts. The initial design was planned to be redundant, with the thought that it could be simplified in future implementations. However, the team soon discovered that the multi-sensor system is robust as opposed to just redundant – an aspect detailed in Chapter 6.

Electromechanical Films

EMFis are thin (37 or 70 μm thick) polypropylene sheets that are sensitive to forces applied normal to their surfaces. I.e., a voltage measured at a film's contacts will be proportional to the applied force due to the film's structure [110]. This high sensitivity makes it possible to capture micro-movements of the body caused by cardiac activity (the BCG). For the bed-based system, four EMFi sensors (EMFit; L series; 300 mm x 580 mm) are placed in a row under the mattress and therefore coincide with a large amount of the mattress surface area (see Figure 4-1).

Figure 4-1. Example film sensor and pockets sewn into a fitted sheet that hold sensors in place. The mattress is turned upside down to illustrate EMFi sensor and pocket locations.

Typically, a bed-based BCG monitoring system only uses one EMFi sensor placed under the torso to capture both BCG and respiration data [69]. However, children sleep in a variety of positions throughout the night, making a single sensor system impractical. This multi-film design choice was justified during the pilot study to be discussed in Chapter 6 [70].

Two analog conditioning circuit designs were considered to amplify and filter the acquired EMFi signals – either a charge or a voltage amplifier configuration can work well with an EMFi sensor. A review of these two approaches, describing the pros and cons of each, is contained in [110]. The film sensors are located a short distance from the acquisition hardware (one or two feet), but this distance is great enough that cable capacitance needs to be considered. Further, these EMFi sensors have a large surface area, resulting in a high structural capacitance. By using the selected charge amplifier configuration, the sensor and cable capacitances are shorted out, leading to the output voltage being dependent only on the circuit's feedback capacitor.

BCG frequency components cover a range from approximately DC up to around 30 Hz, so other investigators have suggested a lowpass conditioning filter with a cutoff frequency not lower than 25 Hz [111]. However, with regard to retaining the low-frequency signal components, it would be impractical to design the charge amplifier without a feedback resistor parallel to the feedback capacitor (see Figure 4-2), which creates a simple RC highpass filter that blocks a percentage of the DC and lower-frequency components. (The feedback resistor bleeds off the charge buildup on the capacitor, preventing the amplifier from going into saturation. Further, the

resistor provides a DC bias current path for the operational amplifier's negative input.) Therefore, the primary task is to choose a sensible cutoff frequency for this highpass filter that allows the meaningful acquisition of both the respiration baseline and the BCG pulsatile components while avoiding saturation at the output of the signal conditioning circuitry. Note that the forces due to breathing are much greater than the forces that correspond to the BCG pulsatile components, and typical respiration rates range from 6 to 30 breaths per minute, or 0.1 to 0.5 Hz [112].

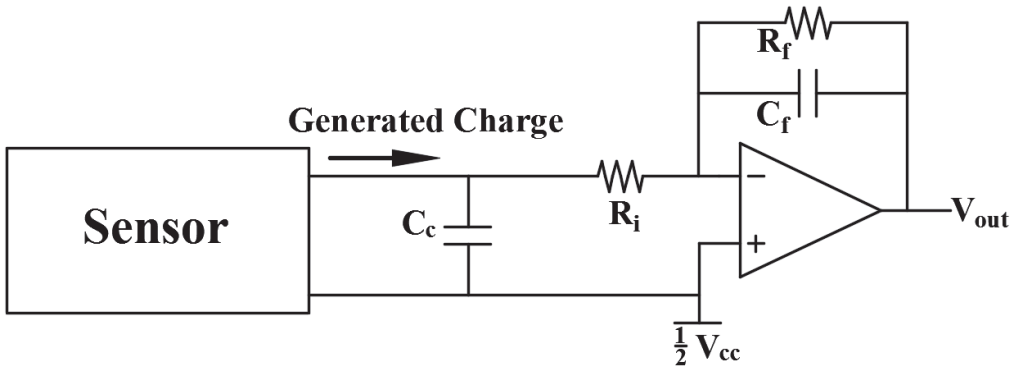

Figure 4-2. Charge amplifier analog conditioning circuit topology. C_c represents cable capacitance, R_i provides ESD protection, and R_f and C_f are the feedback resistor and capacitor, respectively.

A short analysis was performed to determine which of two candidate highpass cutoff frequencies, 0.3 and 1 Hz, would be more suitable in this context. While these cutoff frequencies appear high, recall that the recorded respiration signals are strong and require attenuation so that they do not overwhelm the pulsatile BCG signal components. A data collection exercise was conducted as part of this short analysis, where one subject laid in a supine position with their chest above EMFi sensor 1 (F1 – see Figure 3-2). Twenty seconds of clean data were analyzed in the frequency domain for each film-and-cutoff-frequency combination, yielding the single-sided amplitude spectra in Figure 4-3, where each blue trace (S1) and red trace (S2) correspond to 1 Hz and 0.3 Hz cutoff frequencies, respectively.

The respiration component is visible in the spectrum for each configuration in Figure 4-3, but the BCG harmonics are sharper for the 0.3 Hz cutoff frequency (the BCG sampling frequency is 250 Hz). A comparison of the time domain signals for the two highpass cutoff frequencies is depicted in Figure 4-4. Note that both configurations captured the respiration and

BCG components without allowing the system to saturate. Thus, to preserve as much signal information as possible, the high-pass cutoff frequency was set to 0.3 Hz: $1/(2\pi RC) = 0.32$ Hz, where the feedback resistance, R, is 4.99 MΩ and the feedback capacitance, C, is 0.1 μF (refer to Figure 4-5). Figure 4-5 also depicts the 2nd-order, lowpass Sallen-Key Butterworth filter (cutoff frequency = 25 Hz) used to limit the higher frequency content, including 60 Hz power line interference. To avoid aliasing the first harmonic of the 60 Hz interference into the BCG frequency range of interest, the sampling frequency was chosen to be 250 Hz: more than twice the Nyquist sampling requirement. This allows the 60 Hz signal's 2nd harmonic (120 Hz) to also be properly sampled.

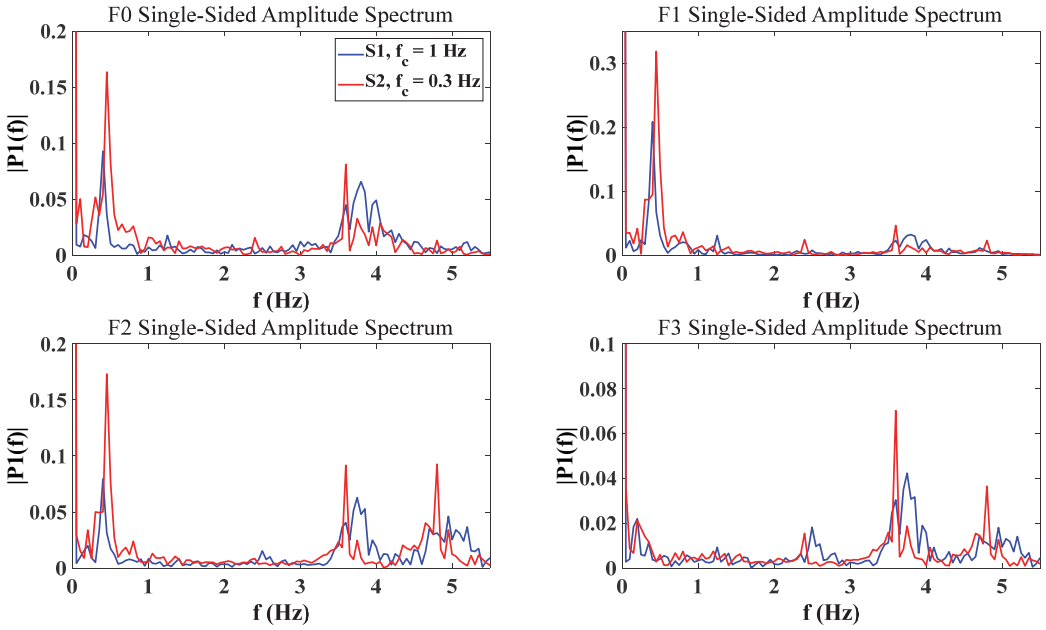

Figure 4-3. Single-sided amplitude spectra for the BCG data acquired using each film sensor, where two highpass cutoff frequencies are considered: f_c = 1 Hz (blue) and f_c = 0.3 Hz (red).

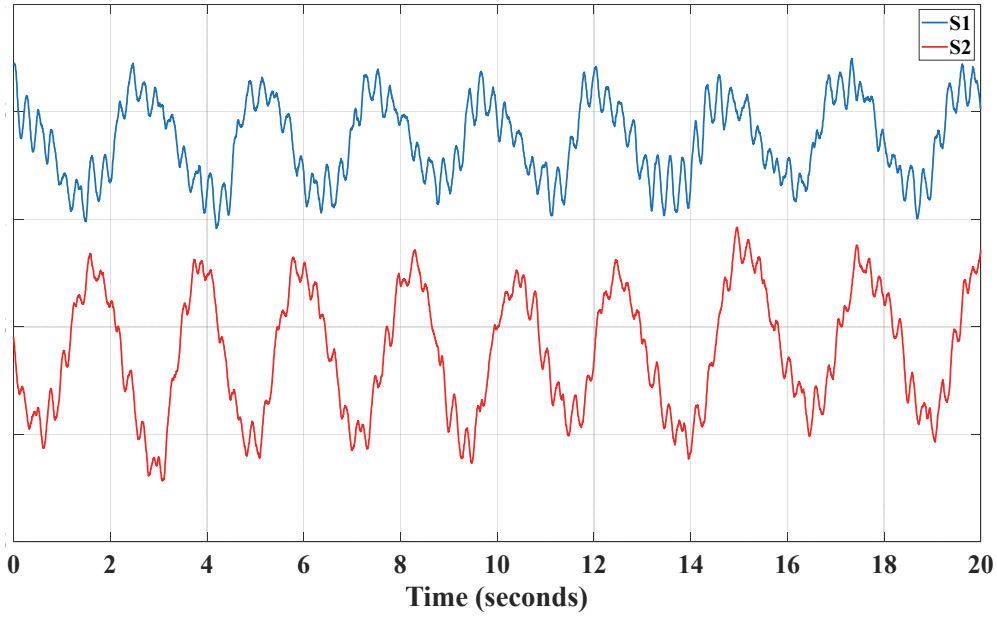

Figure 4-4. Time domain counterparts for the spectra illustrated in Figure 4-3 given a cutoff frequency of 1 Hz (blue) and a cutoff frequency of 0.3 Hz (red). Note each small-amplitude BCG riding on a larger-amplitude respiration baseline.

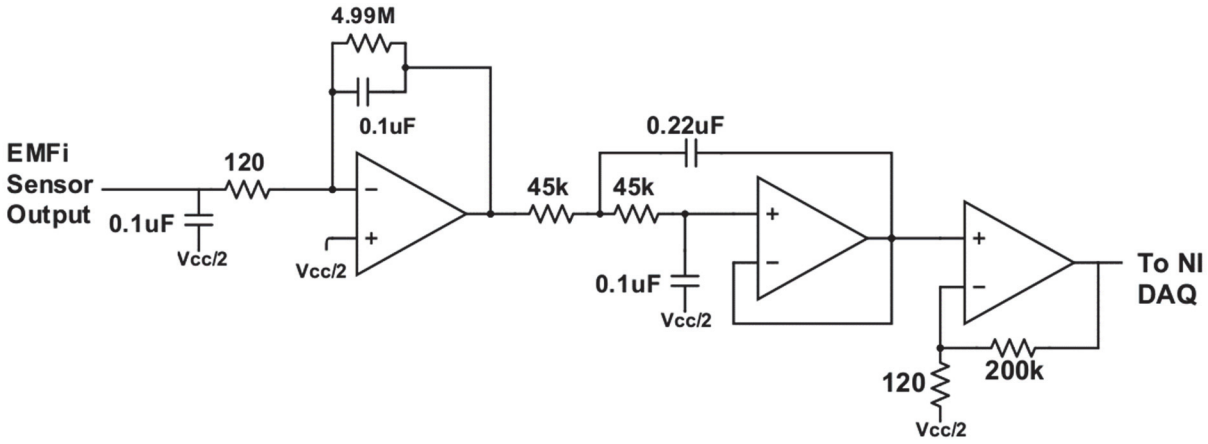

Figure 4-5. Electromechanical film analog conditioning circuitry.

Load Cells

The load cells, which operate on a Wheatstone bridge principle, are also highly sensitive to forces applied normal to their surfaces. Although a wide variety of load cells are available on the market, choosing the right type of load cell for BCG acquisition proved to be a challenge given that load cells are not specifically designed to record such signals. The team experimented with several different types of load cells and found the TE Connectivity Measurement Specialties FX1901-0001-0200-L to work well in the bed system in terms of the resulting BCG signal-to-

noise ratio. A load cell is placed underneath each bedpost (see Figure 3-2). These load cells can individually acquire BCGs and can collectively provide center of position (COP) data, since the output voltage of each cell is directly proportional to the applied static and dynamic forces. In comparison, a film sensor only measures changes in applied force.

Since the load cell sensors are mechanically coupled to the BCG through the bed frame, their signals also need conditioning. The analog circuitry for the load cells consists of an instrumentation amplifier and active filters with an aggregate passband of 0.05 to 35 Hz (see Figure 4-6). The load cell PCB illustrated in Figure 4-7 contains an implementation of the circuit depicted in Figure 4-6 (for Load Cell 1 (B)) and routes the signal from a second load cell board (Load Cell 0 (A)) – two load cell boards were daisy chained together to reduce the number of wires.

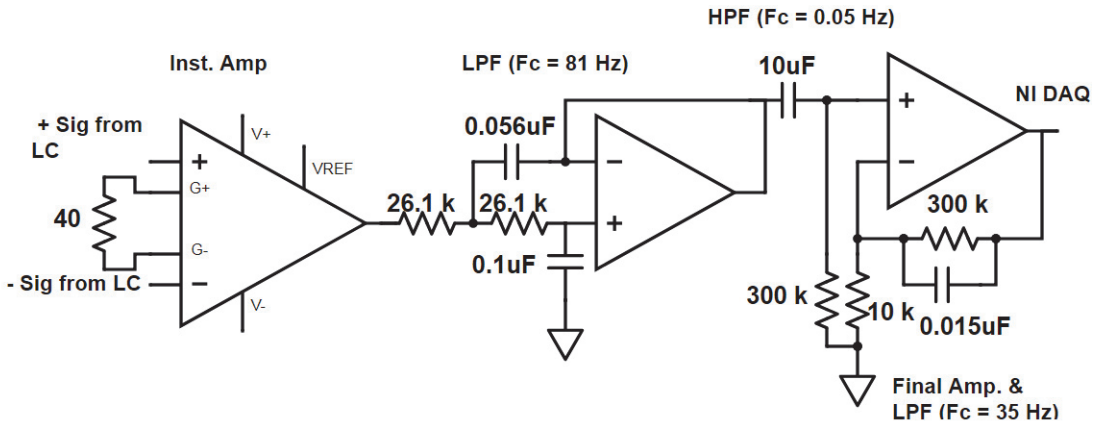

Figure 4-6. Load cell analog conditioning circuitry.

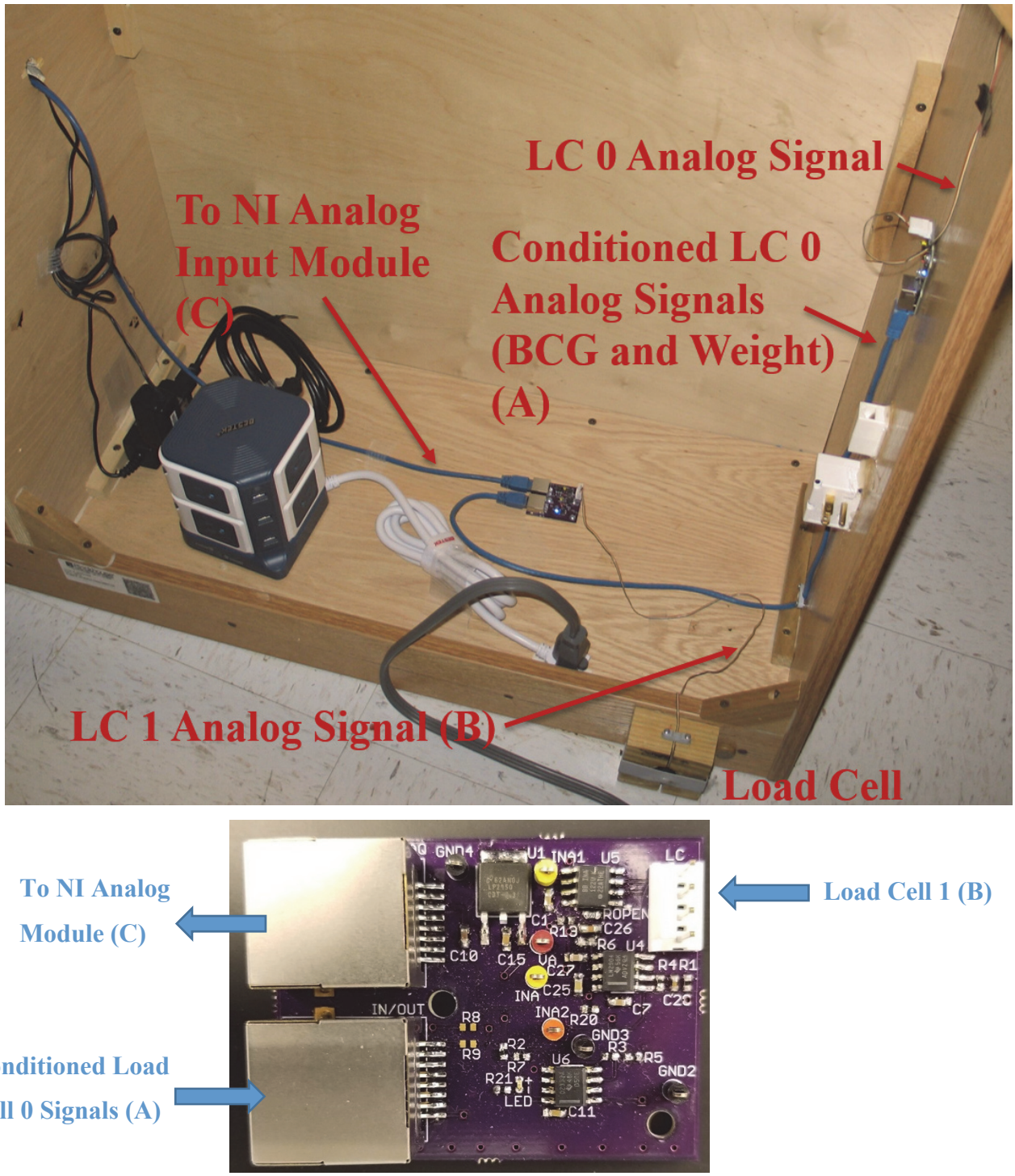

Figure 4-7. Load cell analog conditioning PCB (bottom) and example implementation in a captain's bed (top), courtesy Ahmad Suliman.

Custom Conditioning Hardware

Several design iterations were made to the custom analog conditioning hardware. The first version of the EMFi acquisition design included a separate PCB for each EMFi sensor – see Figure 4-8. Further, the first version did not include routing of the load cell channels alongside the EMFi channels – each load cell had to be separately wired to the NI 9205 module. Additionally, the first version was purposefully made more modular and flexible (e.g., the final gain stage was set using a 10 kΩ potentiometer), since at the time the optimal settings to acquire EMFi signals were unclear. This hardware worked well for the three-night pilot study detailed in a later chapter. However, it was cumbersome, and it was not aesthetically pleasing due to the multiple wires running to/from each component (see Figure 4-9). Further, the design included a switched-capacitor voltage converter to provide the negative power supply. Therefore, to reduce the amount of voltage ripple seen on the output, a separate power supply module was used as the negative power supply, leading to a bulkier design. To be clear, the setup worked well, since a great deal of data were collected during the three-night study. However, updates were clearly needed in order for the design to become practical for larger-scale scenarios.

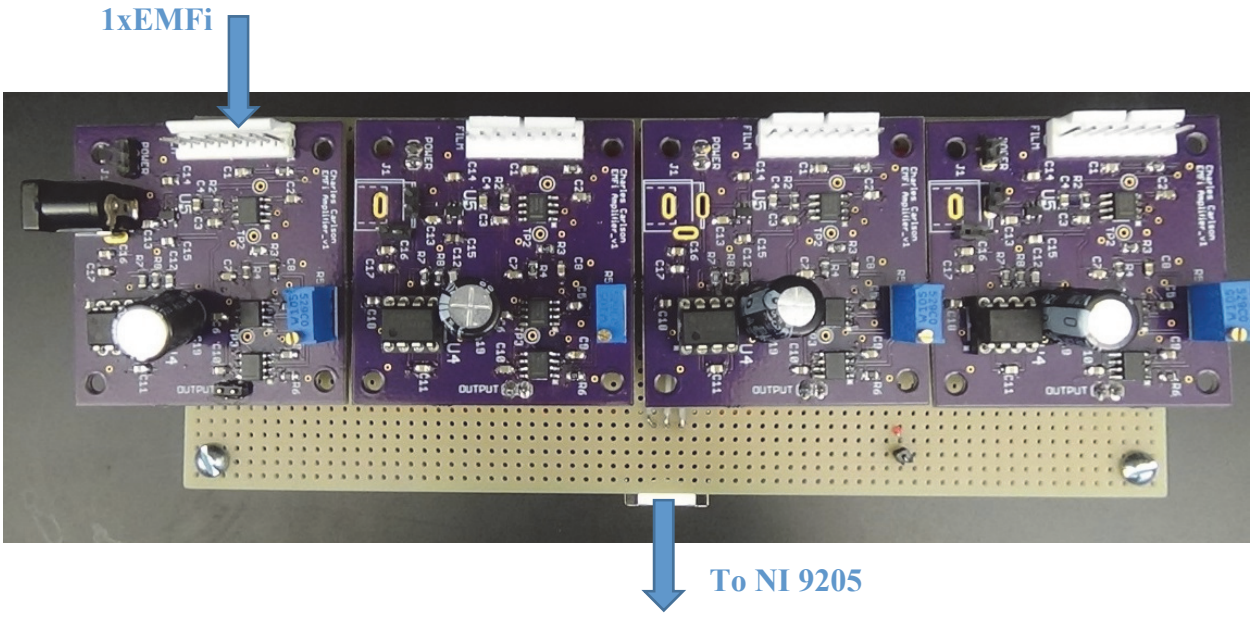

Figure 4-8. Custom EMFi analog conditioning hardware – version 1.

Figure 4-9. Bed system setup for the three-night pilot study at Heartspring, illustrating the version 1 hardware/wiring system hidden under the bed's cavity.

A second hardware iteration included the use of a single power supply plus the aggregation of the four EMFi channels onto a single PCB. An image of the PCB for the second version can be seen in Figure 4-10, and Figure 4-11 depicts the PCB interfaced to the NI 9205. Even though this version had a considerably smaller footprint and fewer wires, it still took several minutes to set up – each conditioned EMFi signal output from the custom PCB (a wire within the yellow Ethernet cable in Figure 4-11) had to connect to an NI 9205 spring terminal.

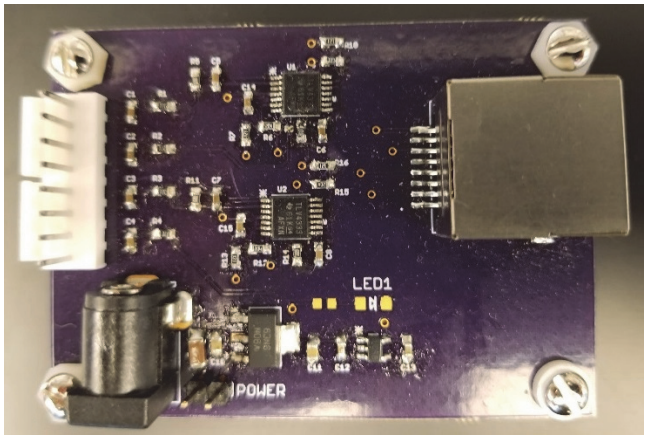

Figure 4-10. Custom EMFi analog conditioning hardware – version 2.

Figure 4-11. Connections between the version 2 analog conditioning circuitry, the NI 9205, and the NI 9184.

The final iteration of the hardware (custom PCB revision 3) includes these updates:

- interfaces to the load cells via two RJ-45 connectors and to the EMFi sensors with an 8-pin Molex connector,
- combined signal conditioning for the four EMFi channels and shared routing of the EMFi and load cell channels,
- a 37-pin D-SUB connector to directly connect to the NI analog module (the NI 9220), and
- a 44-pin D-SUB connector to interface to a GE Datex-Ohmeda Cardiocap^{TM}/5 vital sign monitor, allowing synchronous collection of electrocardiogram (ECG), respiration, photoplethysmogram (PPG), pulse rate, and respiration rate data to be used as comparison standards for corresponding health metrics determined with bed-based sensor data.

An example image of the EMFi signals, load cells, and patient monitor channels interfaced with the version 3 design is contained in Figure 4-15 later in this section. The D-SUB connectors

make it easy to connect the conditioning PCB to the NI analog module and the patient monitor. The overall design was vastly improved compared to the first version – a visual comparison is shown in Figure 4-12. Board schematics and layout files are included in the appendices.

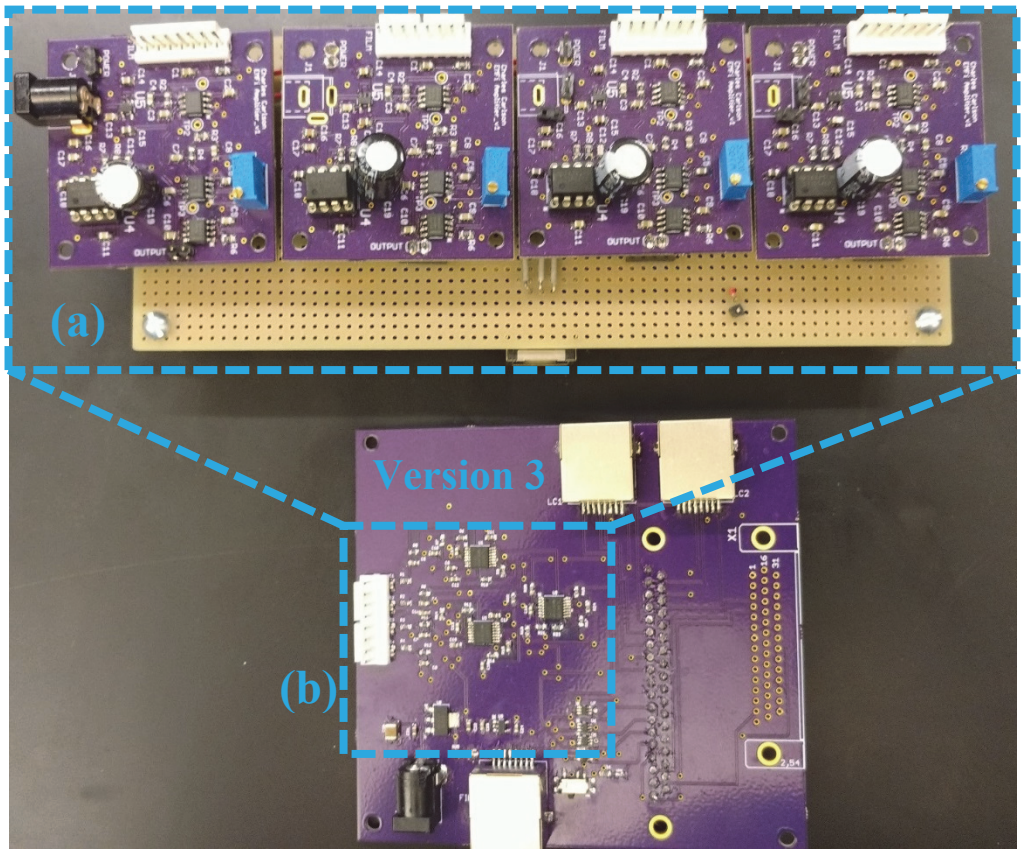

Figure 4-12. The final iteration of the analog conditioning hardware – version 3 (b) vs version 1 (a). The physical board size needed to perform the data acquisition and signal conditioning functionality has been substantially reduced.

System Configurations

Two versions of NI hardware used for data collection and analysis are presented in this dissertation. The first system is based on a more configurable NI 9205 analog input module and an NI 9184 Ethernet-based compact DAQ chassis. This system worked well during the testing phase and the three-day pilot study described in the next two chapters. However, due to reliability issues encountered with the NI 9205 module, the team decided to upgrade to the NI 9220 analog input module. At the beginning of the six-month study described in Chapter 9, the children's rooms did not have easily accessible Ethernet connection points. Consequently, the NI 9184 compact DAQ chassis were replaced with Wi-Fi capable NI 9191 compact DAQ chassis. Thus, system two replaces the NI 9205 module and NI 9184 Ethernet chassis with the NI 9220

module and NI 9191 Wi-Fi chassis, respectively. In each system, four channels are used for EMFi signals, four are used for load cell BCG signals, four are used for load cell DC values (used for COP), and four are interfaced to the GE Datex-Ohmeda Cardiocap^{TM}/5 patient monitor.

System 1 Data Acquisition

The C series NI 9205 module was selected due to its flexibility in terms of signal configuration (single-ended or differential) and its high-resolution, selectable voltage input ranges. The main features of the NI 9205 module are

- 32 single-ended or 16 differential channels,
- selectable signal ranges to manage resolution (±200 mV, ±1 V, ±5 V, or ±10 V),
- a maximum sample rate of 250 kS/sec, and
- 16-bit resolution on each channel.

Figure 4-13 contains the high-level block diagram for System 1, and images that depict the custom circuit board, NI analog module, and chassis connection interface are contained in Figure 4-14. A complete setup, including all cabling for the sensors and the patient monitor, is contained in

Figure 4-15.

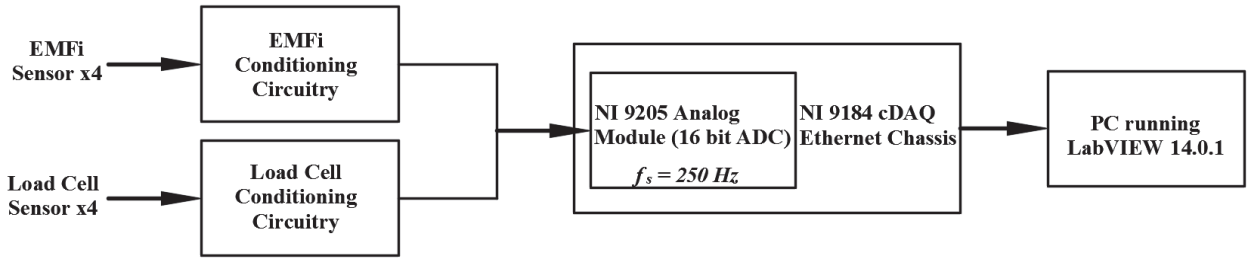

Figure 4-13. System 1 data acquisition block diagram.

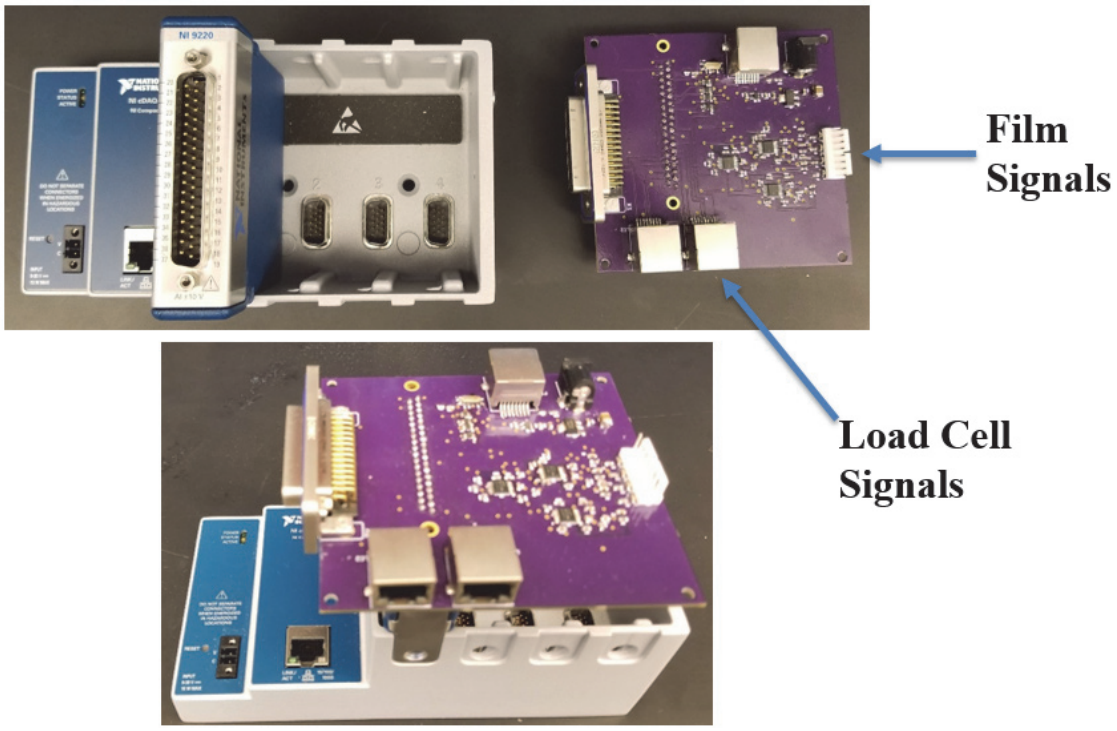

Figure 4-14. National Instruments hardware and custom analog signal conditioning hardware.

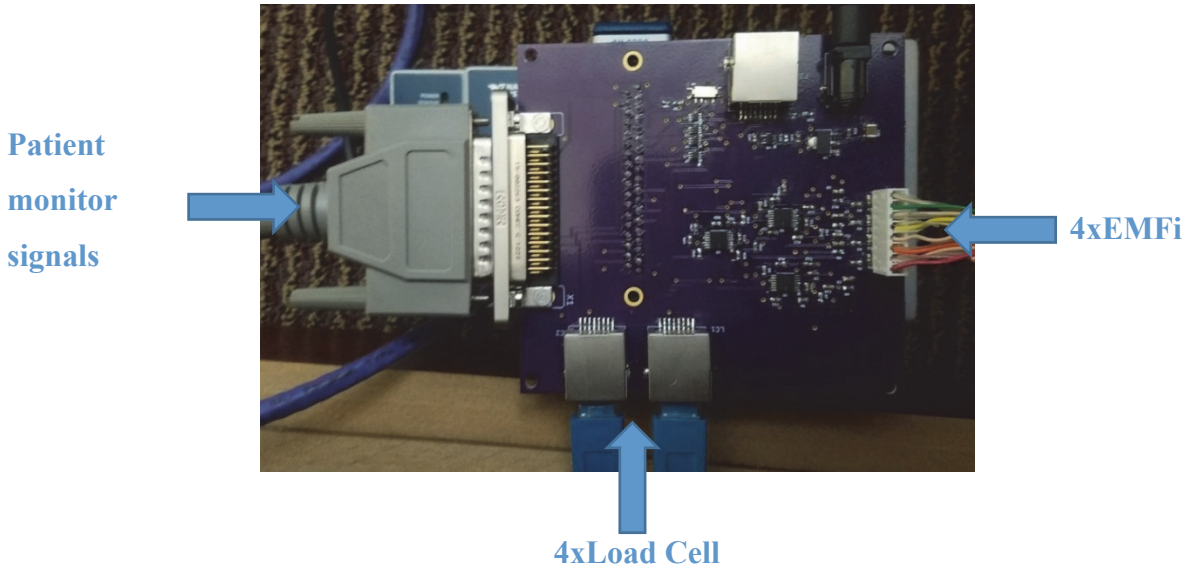

Figure 4-15. Analog signal conditioning and signal management hardware, including a 37-pin DIN connector to a patient monitor (left), two RJ-45 connections that provide load cell signals (bottom), and a Molex connector to acquire EMFi signals (right).

System 2 Data Acquisition

The C series NI 9220 analog module also has 16 16-bit differential channels, but it offers a much higher sampling rate – 1.6 MS/s compared to 100 kS/s offered by the NI 9205 unit. The module is connected to an NI 9181 wireless cDAQ chassis that is controlled remotely from a PC running LabVIEW 14.0.1. The high-level block diagram and an example setup illustrating how the custom hardware connect to the NI hardware are contained in Figure 4-16 and Figure 4-17, respectively.

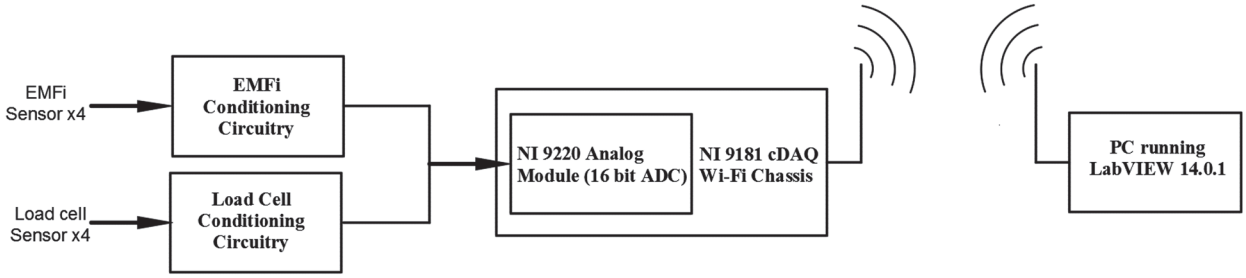

Figure 4-16. System 2 data acquisition block diagram.

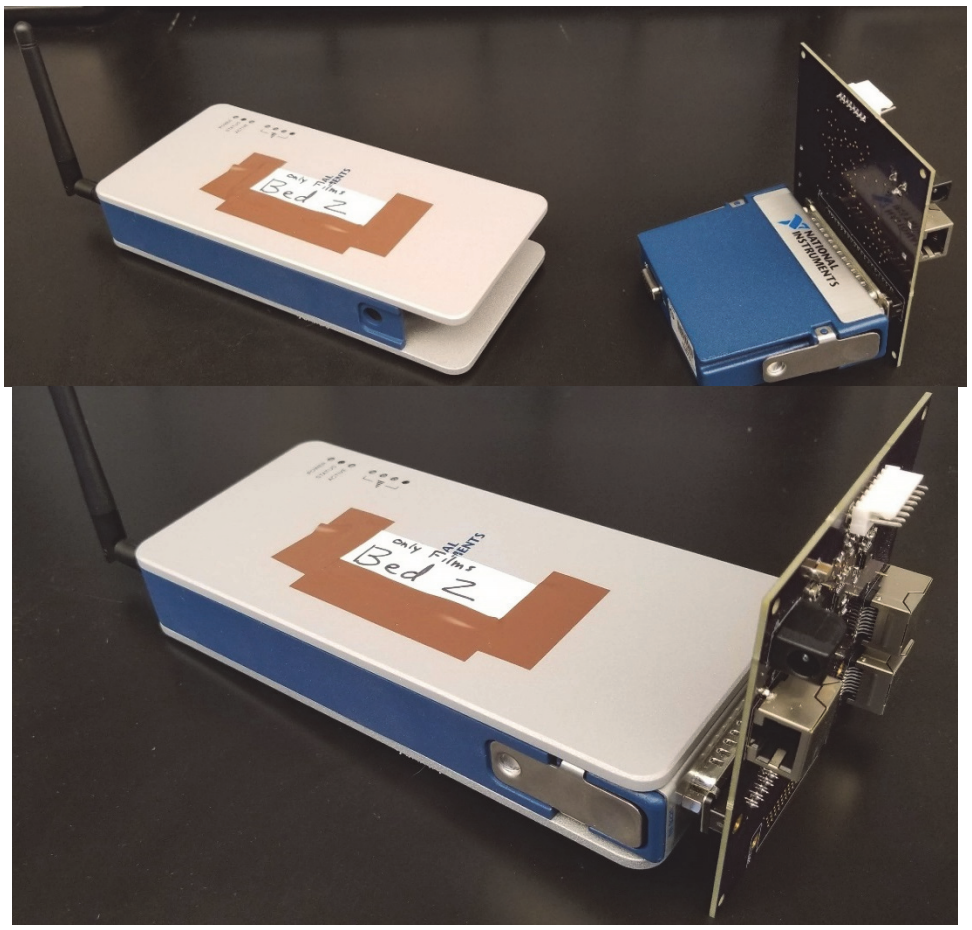

Figure 4-17. System 2 data acquisition modules (analog input and Wi-Fi chassis).

Virtual Instrumentation and Data Management

A Virtual Instrument (VI) running on a remote PC manages the data acquisition system and controls the sampling rates of all twelve signals. A producer-consumer architecture, see Figure 4-18, was implemented within the VI to collect and consolidate data. The example depicted in Figure 4-19 and Figure 4-20 manages data collected from the two bed systems. The front panel design (a) makes it possible to configure start and stop times for data collection and (b) utilizes chart graphs to display a subset of the acquired signals in real time – see Figure 4-18. A BCG waveform from film sensor 0 is clearly visible in the real-time waveform chart contained in Figure 4-20.

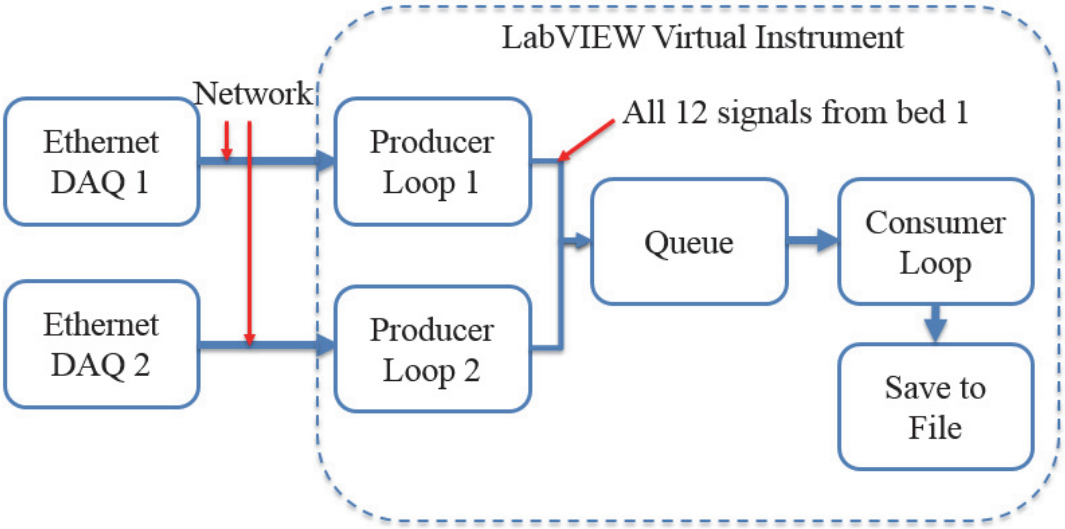

Figure 4-18. Producer-consumer architecture for the two bed systems.

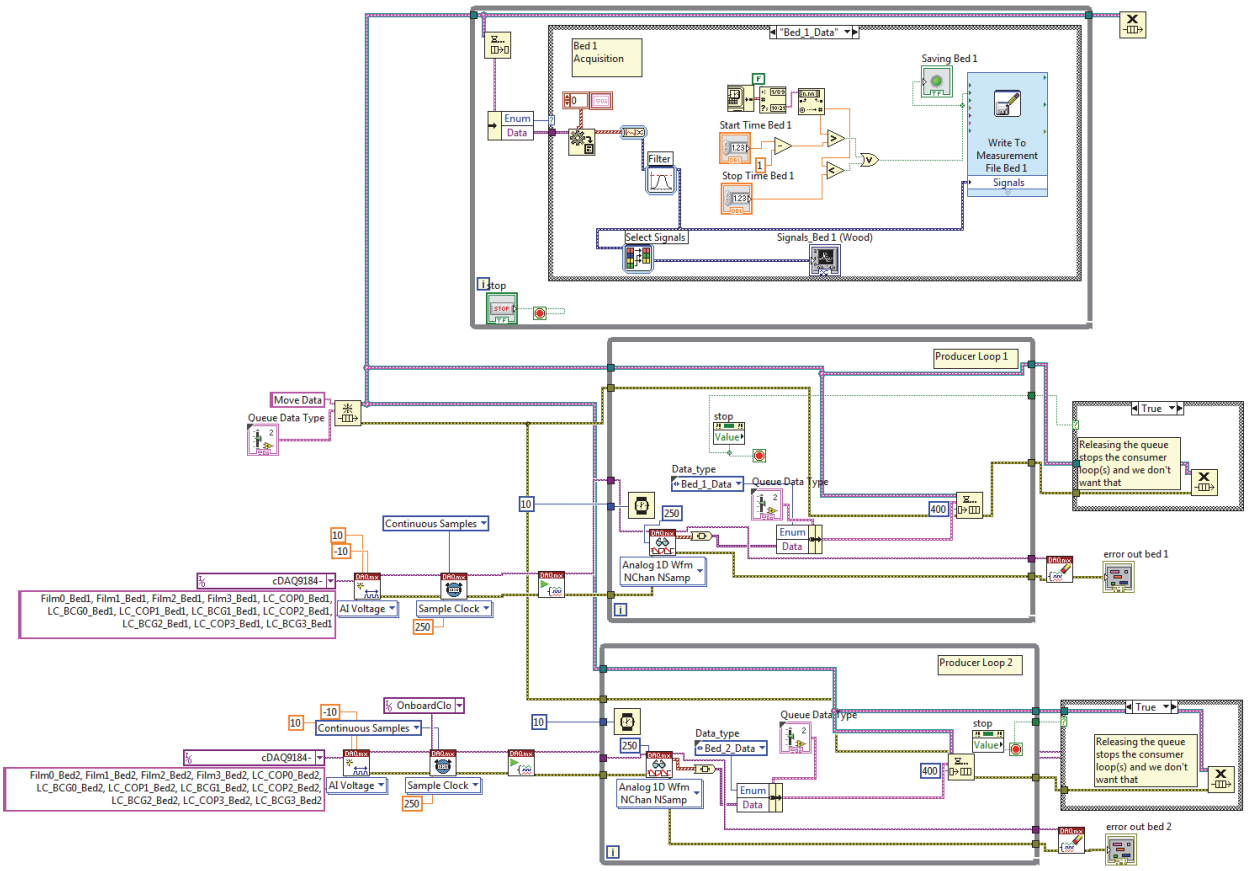

Figure 4-19. Example LabVIEW virtual instrument block diagram implementation of the producer-consumer architecture.

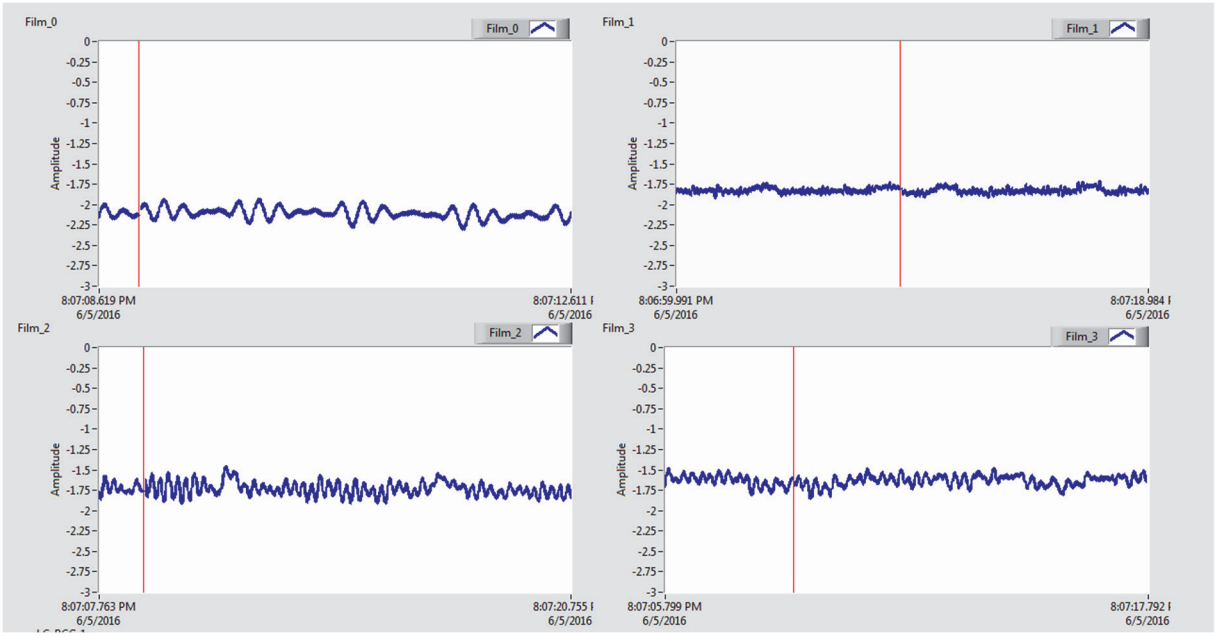

Figure 4-20. Example LabVIEW virtual instrument front panel display depicting real-time waveforms from four EMFi sensors.

Center of Position with Load Cells

Load cells placed under each bedpost make it possible to calculate the subject's center of position (COP). The BCG signal from each load cell rides on top of a static offset due to the weight of the bed. The COP is calculated from these four DC offsets using equations 18 and 19, with load cell 1 acting as the (0, 0) point for the coordinate system (see Figure 4-21):

$$X_{position} = \frac{X_{max}(LC_2+LC_3-(LC_{20}+LC_{30}))}{LC_0+LC_1+LC_2+LC_3-(LC_{00}+LC_{10}+LC_{20}+LC_{30})} \quad (18)$$

$$Y_{position} = \frac{Y_{max}(LC_0+LC_3-(LC_{00}+LC_{30}))}{LC_0+LC_1+LC_2+LC_3-(LC_{00}+LC_{10}+LC_{20}+LC_{30})} \quad (19)$$

where LC_z is the DC voltage measured at load cell z with z = 0, 1, 2, or 3. Here, LC_{z0} is the initial voltage measured at load cell z with the bed unoccupied.

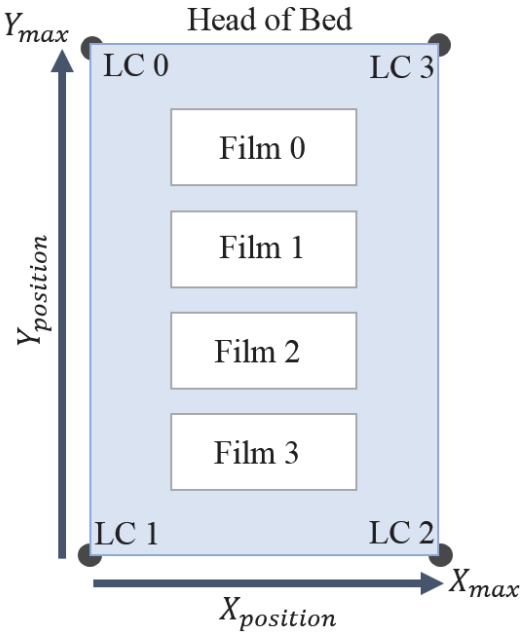

Figure 4-21. Sensor locations and center-of-position reference coordinate system.

Thermal Camera to Track Movement and Position

After the first pilot study (detailed in Chapter 6), it was evident that an automated imaging system was needed to validate movement and position. Standard video recording would compromise the privacy and dignity of the children, so an alternative solution was needed. As a compromise, a FLiR Lepton® thermal imaging module was selected to monitor each child's

movements and possibly track their positions. The FLiR Lepton® module is a small, low-resolution longwave infrared imager. An accompanying breakout board, purchased as a kit from Sparkfun, makes it simple to interface the module to a Raspberry Pi unit. The thermal imaging module is connected to a breakout board and interfaced to a Raspberry Pi 3 B+ using a serial peripheral interface. The Pi unit saves and transmits the low-resolution thermal images (80 by 60 pixels; captured every 1 to 2 seconds) to a remote PC over Wi-Fi using WinSCP.

The low-resolution thermal camera makes it possible to analyze each child's movement without comprising their integrity. In addition to providing a visual reference for movement and position, bed entrance and bed exit events can be tracked. An example thermal camera setup and the associated camera module and breakout board are depicted in Figure 4-22 and Figure 4-23 (left), respectively. An example thermal image illustrating two students working at a lab bench is contained in Figure 4-23 (right).

Figure 4-22. 3D printed housing (left), swivel (center), and wall mount setup (right).

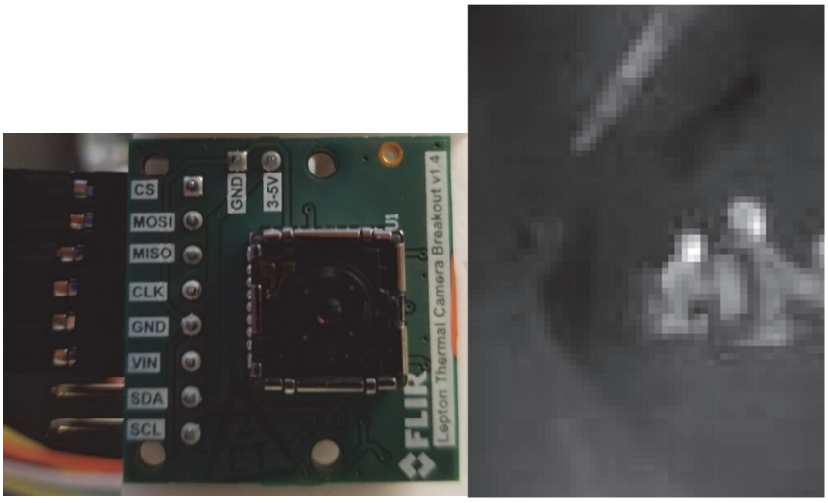

Figure 4-23. FLiR Lepton ® module and breakout board (left) and example grey scale thermal image (right).

Chapter 5 - Preliminary System Results

The bed system was carefully tested in a laboratory setting to verify its ability to track parameters such as pulse rate, respiration rate, and movement. A captain's bed just like the ones used by many of the children at Heartspring was modified and fitted with sensors and a data acquisition system. An example setup showing the locations of the load cells is depicted in Figure 5-1. The original load cell configuration included six load cells, but the team reduced the load cells to four (one at each corner) to minimize the number of redundant channels while retaining the ability to calculate center of position. This also freed up some NI analog input channels (only sixteen are available) to collect signals from the patient monitor. The four film sensors are not visible in Figure 5-1 since they were placed under the mattress (for film sensor placement, see Figure 4-1 or Figure 4-21).

This chapter presents representative signals and preliminary estimated heartbeat interval data collected from one subject to verify the system's capabilities. Three activities (rolling left and right on the shoulders, moving around, and sitting on the long side of the bed) were performed to test the load cells' ability to track movement and center of position – see Figure 5-2, where the upper plot and lower plot illustrate data acquired relative to the *x* (short) axis and *y* (long) axis of the bed, respectively. Lastly, a subject laid on the bed for a few minutes in a prone position to test the system's ability to estimate heartbeat intervals from acquired BCGs.

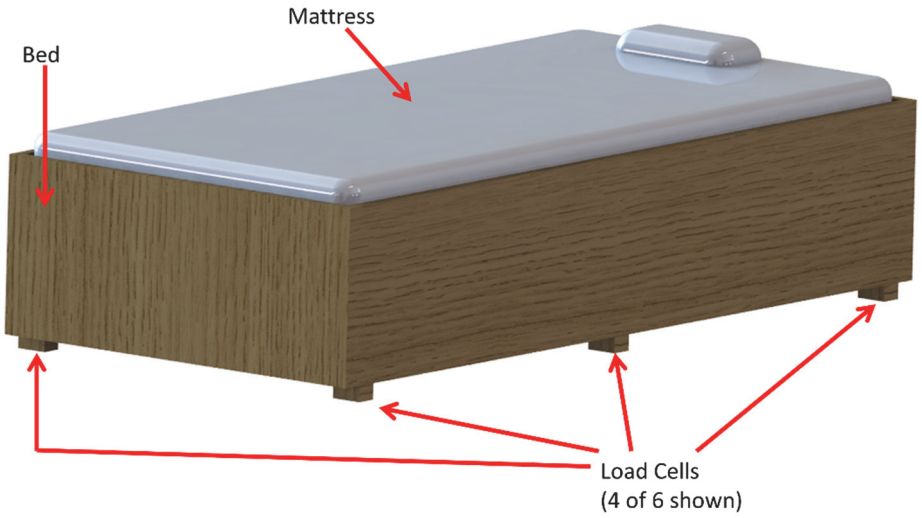

Figure 5-1. Load cell placement.

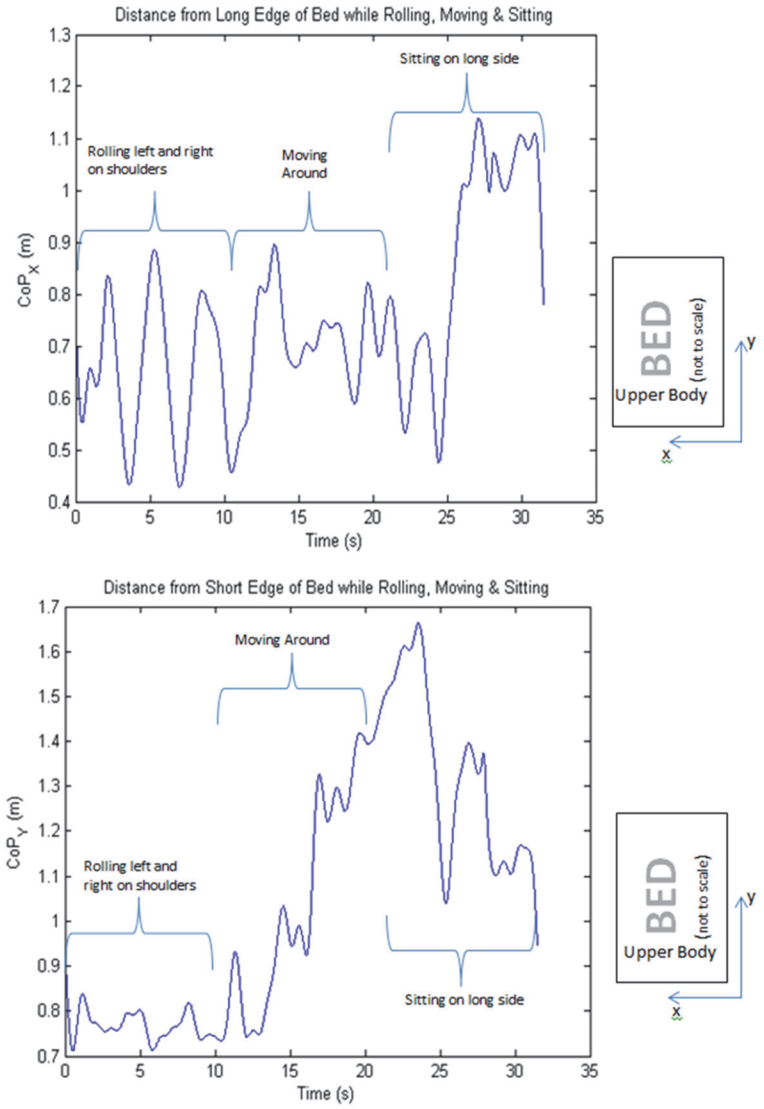

Figure 5-2. Center of position along the *x* axis (upper plot) and *y* axis (lower plot) measured with four load cells.

Preliminary Heartbeat Interval Estimation

Heartbeat Interval Estimation

A peak detection algorithm described in [54], coupled with a template matching approach described in [113], were implemented in MATLAB and used to estimate the heart beat intervals (HBIs) from the acquired BCG. An example output from the HBI extraction script is depicted in Figure 5-3, where the blue trace is the correlation coefficient computed with a local sliding

window function and the green squares depict the local maxima that represent individual heart cycles.

Ballistocardiogram and Electrocardiogram Data Collection

Several minutes of data were recorded with a subject lying in a supine position on the bed. ECG data were collected (iWorx ECG module with an iWorx ETH-255 bioamplifier) in concert with data from four EMFi sensors. The Pan Tompkins algorithm [114] was used to find the ECG R peaks, and the method described in the previous section (with and without template matching) was used to locate BCG heart beats and estimate the HBIs. Figure 5-4 and Figure 5-5 display the comparative results, where the HBI values more closely track the ECG RR intervals when template matching is used (r^2 = 0.9890/0.0204 with/without template matching).

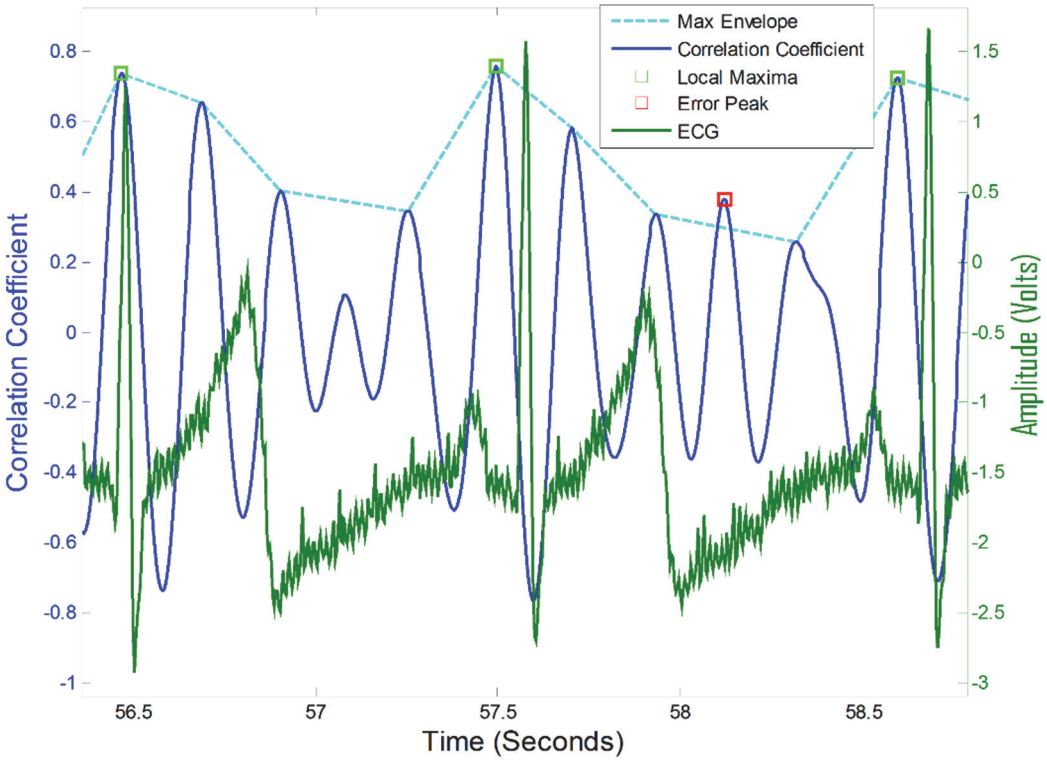

Figure 5-3. Heartbeat interval estimation – BCG compared to ECG.

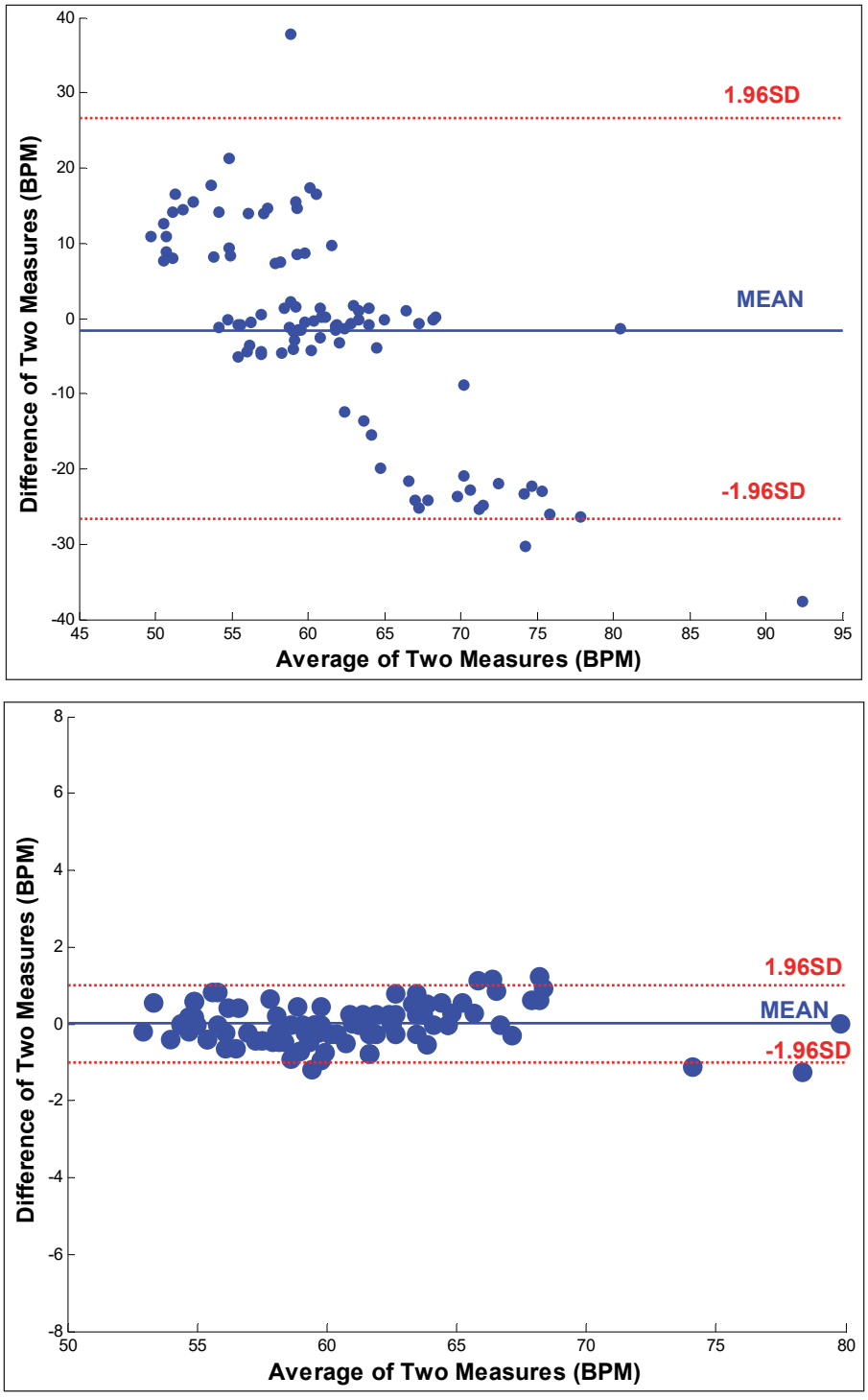

Figure 5-4. Bland-Altman plots comparing BCG HBI to ECG RRI without (top) and with (bottom) the use of template matching.

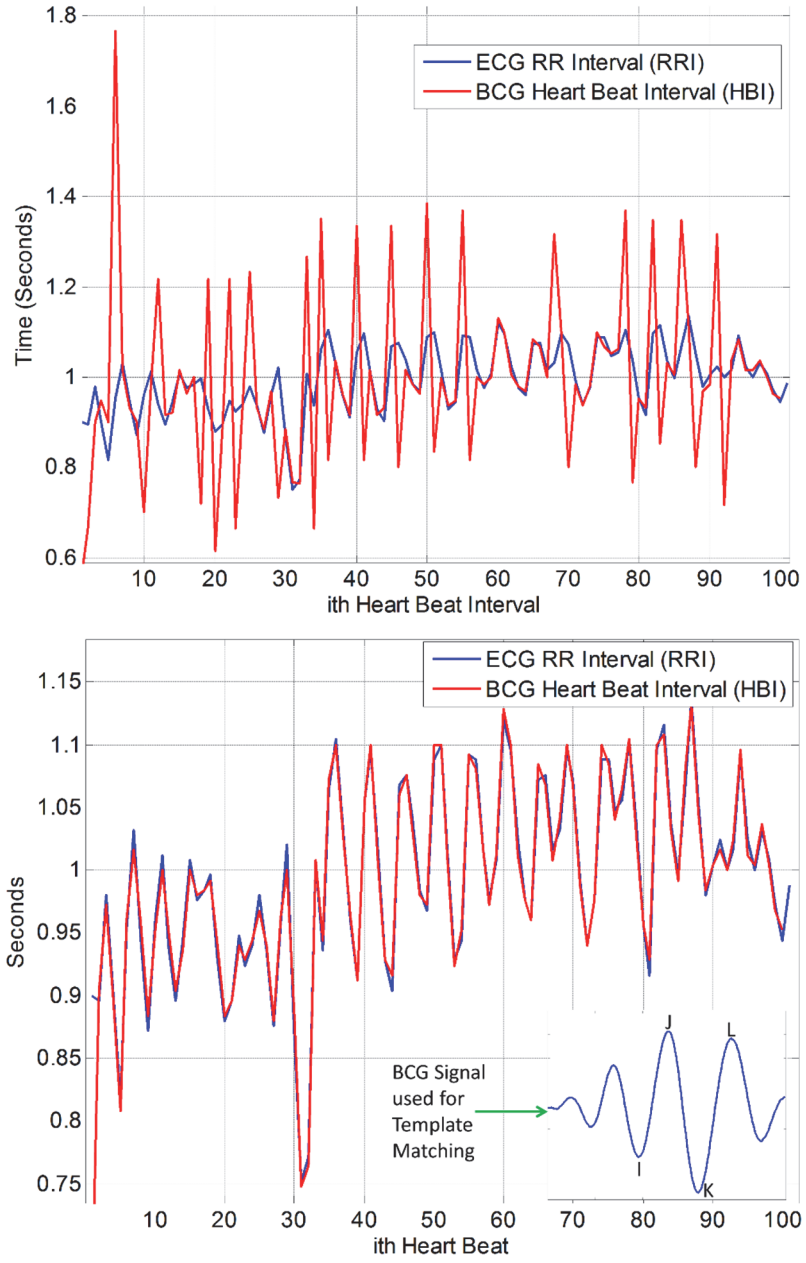

Figure 5-5. Estimated BCG heartbeat intervals compared to ECG R-to-R intervals with (bottom) and without (top) template matching.

Chapter 6 - Heartspring Three-Night Pilot Study and Follow-On Data Analyses

This chapter presents data collected from a three-night pilot study performed at Heartspring. This was the first test of the system in the room of a child with severe disabilities and autism. The main goal of this short study was to determine if the system could operate and provide valid data in such an environment. A secondary goal was to see if all of the film and load cell sensors were necessary for the bed system to prove useful. I.e., are eight sensors redundant for monitoring the sleep of each child? The team learned almost immediately that these children sleep in a wide variety of positions and bed locations. Nonetheless, the system worked well and collected high quality data from the child. Early analyses indicated that the presence of the entire sensor set is useful, since the BCG with the highest signal-to-noise ratio can be collected from a different sensor for each of the three different sleeping positions that were analyzed.

Overnight Data Collected at Heartspring

The sensor-laden bed system was placed in one severely disabled autistic child's residential apartment bedroom, and a team of Kansas State University (KSU) students collected data from the bed system overnight for three consecutive nights after receiving consent from the child's parents.[1] Over 30 hours of data were collected with each of the eight sensors (four EMFis and four load cells). Students on the KSU team also tracked the movement and position of the child in real time during each of the three nights via a wall-mounted baby monitor with a black and white camera (no video recordings were conducted during this pilot study in order to protect the privacy and dignity of the child). During each subsequent day, para-educators tallied a set of daytime behaviors for the child, which is standard practice for all children at the facility.

As discussed in the previous chapter, the existence of four EMFi sensors hidden under the mattress and four load cells placed under the corners of the bed means the system is redundant in its ability to monitor BCGs. This redundancy is helpful and arguably necessary. E.g., when a subject lies in a supine position, their BCG is measurable with all sensors. However,

[1] This research protocol and the accompanying informed consent documents were approved by the Kansas State University Institutional Review Board under protocol #7783. This protocol became active on June 26, 2015 and has since been renewed annually. It is currently active through June 26, 2019.

the team learned that a child may rarely sleep in such a position, choosing instead to lay sideways, perhaps even at the end of the bed, so the sensors must exhibit broad coverage.

Ballistocardiogram and Respiration Signal Separation

Early BCGs acquired with EMFi sensors and load cells were digitally bandpass filtered in MATLAB over the frequency range of 1 to 25 Hz to reduce noise and to remove the respiration baseline. While a 1 Hz highpass cutoff frequency seems high compared to expected pulse rates, most of the BCG information is contained in the secondary signal harmonics at frequencies up to 15 Hz [115]. The higher cutoff frequency helps to reduce the effects of respiration. Representative time-domain signals and frequency-domain spectra from a short data segment are depicted in Figure 6-1 and Figure 6-2.

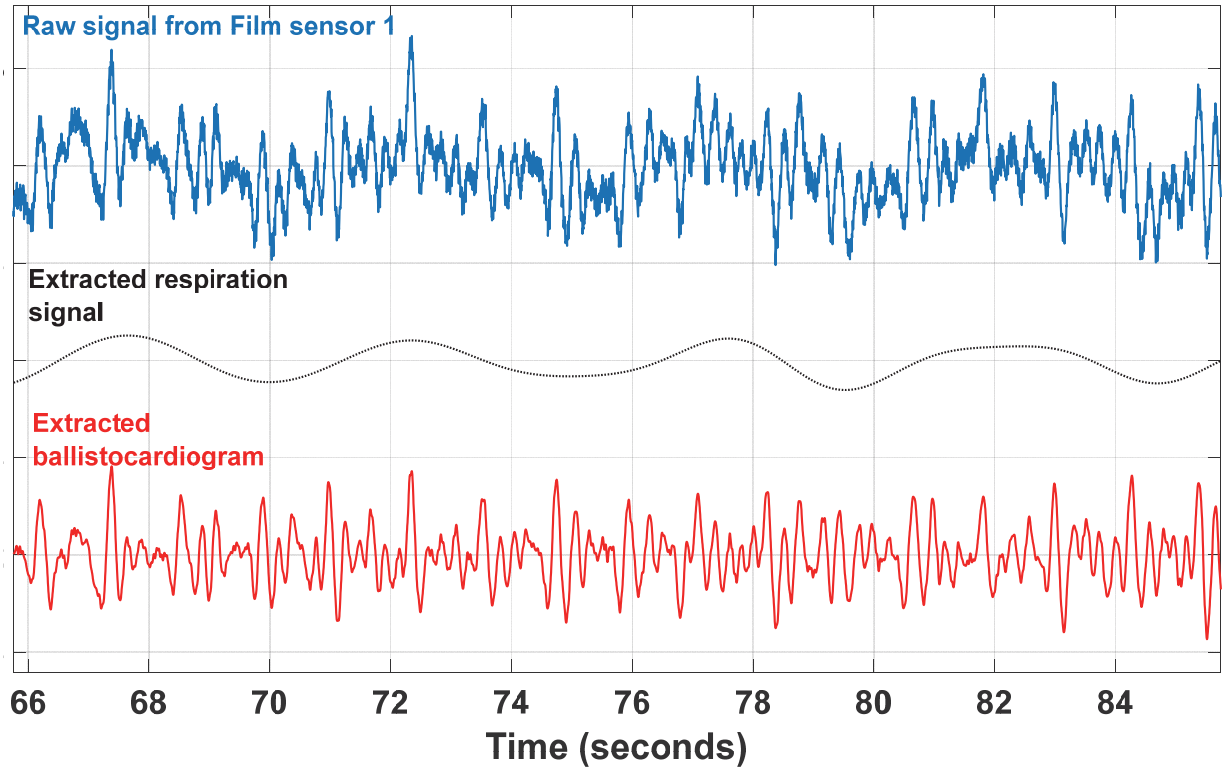

Figure 6-1. Twenty-second section of data acquired from film sensor 1 during night three: raw waveform (blue), extracted respiration signal (black), and extracted BCG (red).

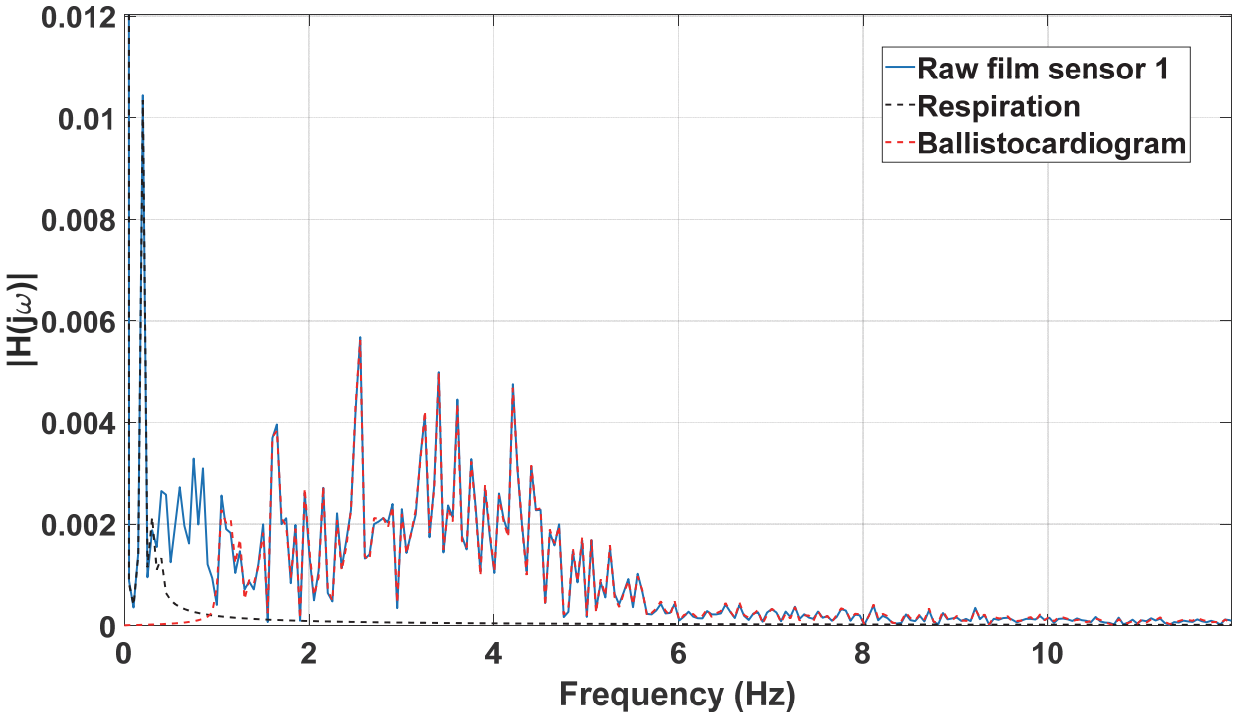

Figure 6-2. Single-sided frequency spectra for the raw film signal (blue), the extracted respiration signal (black), and the extracted BCG (red).

Sensor Comparison

Simultaneous data collection with load cells and films allows for straightforward comparison of the respective signals. Approximately two minutes of BCG data were used for each comparison presented here, where three different subject positions (prone, supine, and left side) were identified when choosing data intervals. To clarify, the goal is to see how BCG morphology changes, depending on both the sensing method and the position of a film or a load cell relative to the body.

BCG Cycle Separation and Ensemble Averaging

Since ECG data time-aligned with these BCGs were unavailable (as in [116]), the BCG J peaks were first located using an adapted form of the algorithm presented by Brüser *et al*. in [69]. The implementation of the algorithm is outlined in Appendix A. Each individual BCG cycle was identified as starting 0.25 seconds to the left of the estimated J peak and ending 0.50 seconds to the right of the same peak. These surrogate R peak locations will not cause consecutive BCG cycles to overlap given that a heartbeat interval was never shorter than 0.75 seconds (heart rate of 80 beats per minute), which the team felt was reasonable for this subject

while they were asleep. These single-cycle waveforms were then aligned based on J-peak locations, and an ensemble average was computed. The ensemble average was calculated and plotted to visualize how the BCG morphology changed for each sensor and position. Figure 6-4 depicts an example ensemble average computed from the BCGs extracted from film sensor 0 using 156 individual cycles.

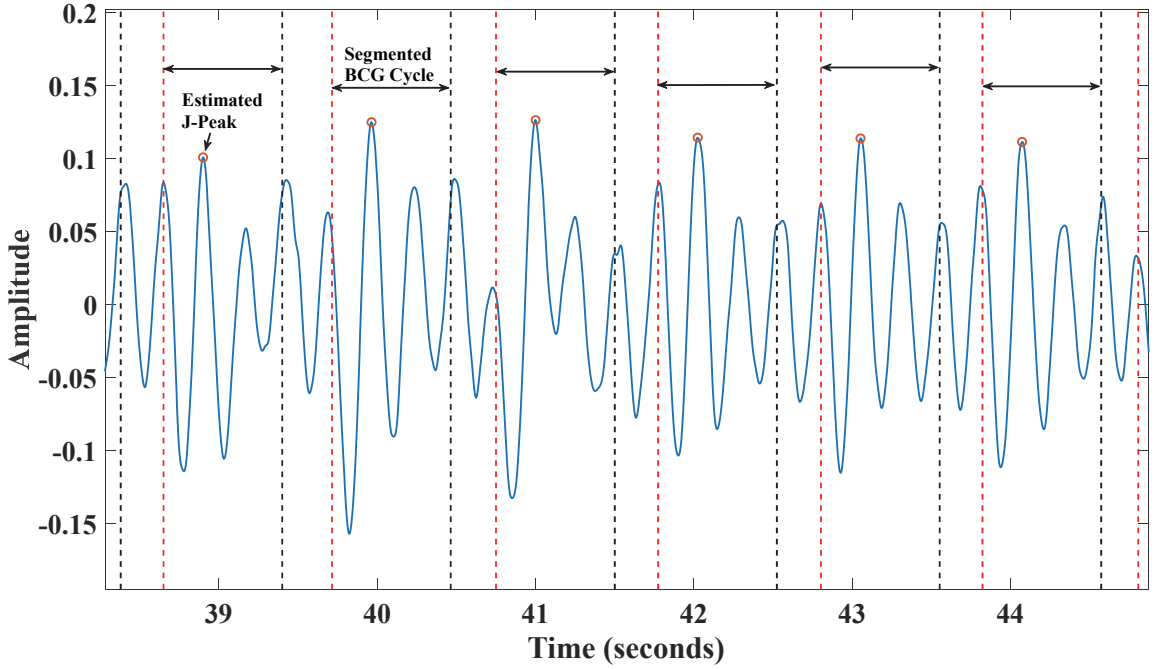

Figure 6-3. Example BCG waveform illustrating how the individual BCG cycles were segmented.

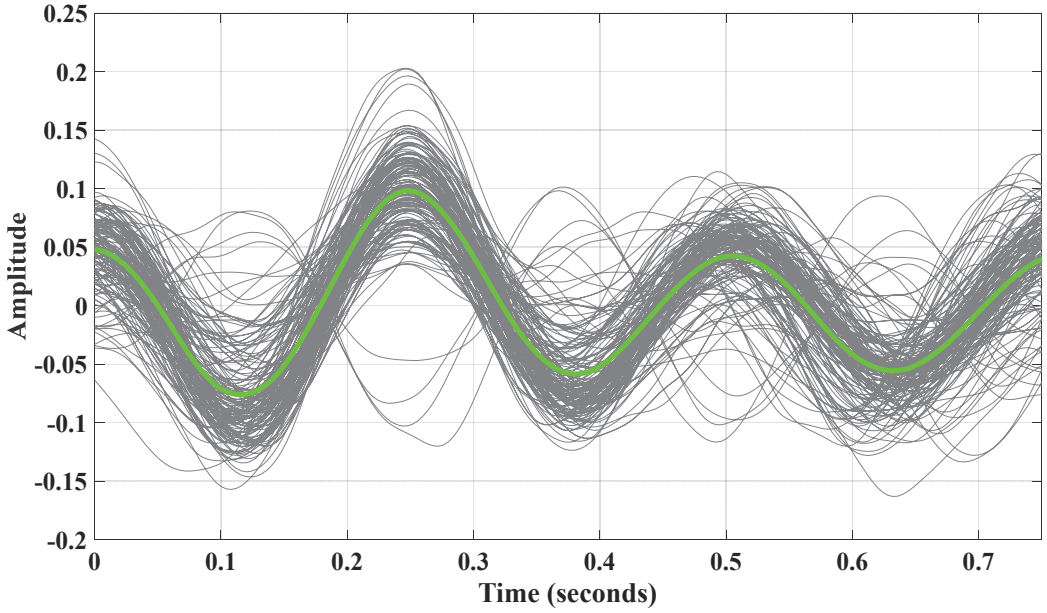

Figure 6-4. 156 Individual cycles (grey) and ensemble average (green) for film sensor 2.

Sample Correlation Coefficient Signal-To-Noise Ratio

After determining the individual BCG cycles, the signal-to-noise ratio (SNR) was estimated using the sample correlation coefficient [117]. The sample correlation coefficient, *r*, was computed for each adjacent pair of BCG cycles, $\{(x_1, x_2), (x_3, x_4), \ldots (x_{M-1}, x_M)\}$, where M is the total number of individual cycles (number of heartbeats), from a given sensor as

$$r_m = \frac{\frac{1}{N}\sum_{i=1}^{N}(x_j[i]-\overline{x_j})(x_k[i]-\overline{x_k})}{\sqrt{\frac{1}{N}\sum_{i=1}^{N}(x_j[i]-\overline{x_j})^2 \frac{1}{N}\sum_{i=1}^{N}(x_k[i]-\overline{x_k})^2}}, \quad m = 1, \ldots, \frac{M}{2} \tag{20}$$

where $N = 188$ is the length of a given cycle for this study (0.75 seconds at a sampling rate of 250 Hz). Note that each pair of BCG cycles is used to compute one sample correlation coefficient. The estimated SNR is then calculated as

$$SNR_r = A * \frac{r}{1-r} + B \tag{20}$$

The constants *A* and *B* are defined in [117] and computed as

$$A = \exp\left(\frac{-2}{N-3}\right) \tag{21}$$

and

$$B = -0.5 * (1 - A) \tag{22}$$

The mean sample correlation coefficient SNR was computed using two minutes of data for each sensor and position (see Table 6-1). Comments regarding these data are included at the end of this section.

Table 6-1. Mean sample correlation coefficient signal-to-noise ratio comparison between BCG segments acquired with different sensors given different subject sleeping positions.

Sensor	Prone (position 1)	Supine (position 2)	Left Side (position 3)
Film 0	14.4	1.8	7.7
Film 1	7.4	1.9	4.5
Film 2	1.8	1.4	2.4
Film 3	4.2	4.3	5.0
Load Cell 0	1.3	3.1	2.1
Load Cell 1	3.2	6.5	19.9
Load Cell 2	7.3	3.6	5.5
Load Cell 3	NA	6.1	28.3

During the first night of this three-night test, the baby monitor feed indicated that the subject laid close to the head of the bed in a nearly prone position – the first position analyzed. During the third night, the subject stayed on the lower quarter near the foot of the bed for the entire night, transitioning back and forth multiple times between a supine-like position (second analyzed position) and their left side (third analyzed position). The ensemble averages for the film BCGs acquired at the various sensor locations are depicted in Figure 6-5, where the four films are numbered relative to the top (head) of the bed. Load cells LC0 through LC3 are numbered counter-clockwise around the bed corners. Each illustrated ensemble average was computed using the same BCG cycles that were used to compute the mean sample correlation coefficients. Comments regarding these data are included at the end of this section.

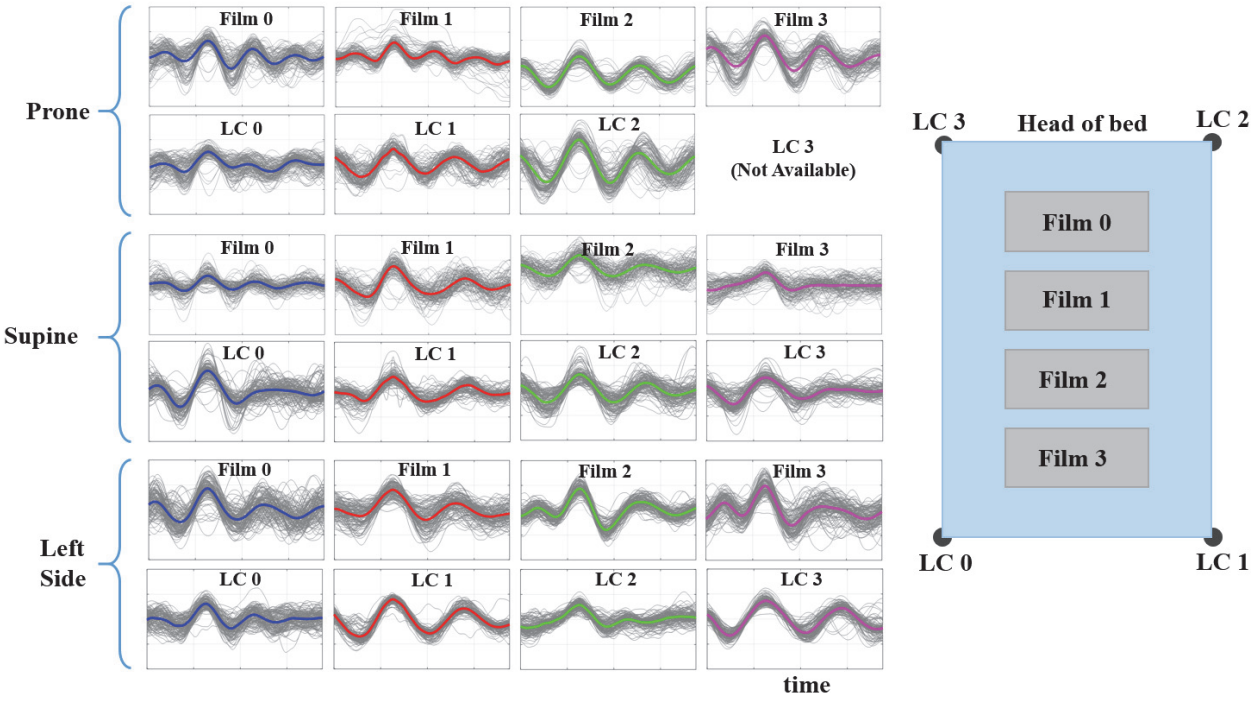

Figure 6-5. BCG ensemble averages and approximate sensor locations (not to scale). Each ensemble average has a duration of 0.75 seconds.

Daytime Behaviors

Heartspring day school classrooms are tailored to the needs of the children, who lack communication and social interaction skills. The Heartspring staff systematically track specific behaviors for each child to better understand and quantify the effects of intervention strategies (e.g., therapies and medications), where the most common behaviors are aggression, self-injurious behavior, and property destruction [118]. Daytime behaviors tracked for the child who participated in this short three-day study are noted in Table 6-2, where each day followed a nighttime data collection period.

Preliminary Sleep Quality Estimates

In [52], two motion-detection algorithms geared toward classifying restlessness as a surrogate sleep quality indicator are presented. The first technique involves a frame-by-frame Neyman-Pearson detection test based on the time-domain signal variance. For the second approach, a sequential detection test uses a fitted Gaussian distribution on the BCG data, where the parameters (mean and variance) are used in the decision process. In each approach, assessments of "clean" and "motion-corrupted" one-second BCG data frames are formulated

based on training data, where a binary hypothesis test determines if a given data frame is clean or motion-corrupted. Any continued movements longer than one minute are then classified as "restlessness," and all other periods are classified as "sleep." This makes it possible to estimate sleep quality based on a subject's sleep-restlessness states for each night. Sleep quality estimates derived using the sequential detection algorithm are listed in Table 6-2.

Table 6-2. Number of recorded daytime behaviors and estimated sleep quality from each prior night.

Day	AGG	PDE	SIB	Total	Estimated Sleep Quality
1	1	0	4	**5**	**73%**
2	0	0	4	**4**	**69%**
3	0	2	7	**9**	**82%**

AGG = Aggression; PDE = Property destruction; SIB = Self injurious behavior

Discussion and Lessons Learned

During the first night of data collection, the team noticed that the floor in the subject's room was not level. Also, the subject slept on the upper portion of their bed for most of the night, shifting from their left side to a supine-like position several times throughout the night. Coupled with the non-level-floor issue, the movement of the upper left corner of the bed caused load cell 3 to yield an intermittent signal, so the team was unable to calculate its SNR estimate or ensemble average for the first sleeping position. Thus, load cell 3 results for the first position are not included in Table 6-1. The bed was adjusted to improve contact between load cell 3 and the floor for the second and third nights.

When considering the SNR estimate values in Table 6-1, neither sensing modality proved consistently superior. The "best" signal was heavily dependent on the subject's position. When the subject lay in a more prone position, film sensor 0 had the highest SNR. When the subject was positioned on their left side, load cell 3 had the highest SNR. It is also interesting to note that the ensemble averages varied for each sensor and position, which is reasonable considering the coupling between the body and each sensor is different. Table 6-2 provides only preliminary sleep quality estimates based on sleep-wake state classifications, like wrist-worn actigraphy systems. Given only three nights worth of data, it is difficult to draw conclusions or parallels between the recorded daytime behaviors and the sleep quality estimates. Nonetheless, the pilot

study demonstrates that the system is capable of unobtrusively monitoring physiological and activity parameters indicative of sleep quality for a disabled autistic child.

Chapter 7 - A Ballistocardiogram Signal Quality Index

The BCG can be a difficult signal to process and extract information from depending on the instrumentation device and the characteristics of the measurement setup, i.e., how the forces of the heart are coupled to the sensor. Accurately pinpointing heartbeat occurrences in a BCG can be a problematic task if the waveform becomes altered due to motion, other artifact-inducing phenomena, or due to the measurement system. Thus, an ECG is often gathered synchronously with a BCG. ECG R-to-R intervals (RRIs) typically serve as the gold standard for heartbeat intervals (HBIs) estimated with BCG analysis algorithms [119]. ECGs offer additional benefits, including R-peaks that can act as separation points to determine individual BCG cycles [55]. Further, timing parameters can be extracted when both waveforms are collected together (e.g. R-J, R-I, R-K, etc.) – parameters which have been linked to hemodynamic features [120], [121].

In some circumstances, however, it is infeasible to collect ECG and BCG data simultaneously, such as when monitoring the sleep of children with severe disabilities and low-functioning autism, as noted in earlier chapters [70], or in situations that involve long-term physiological monitoring [122]. Wearing the required ECG electrodes often and for extended periods is not sensible. In these types of situations, an approach is desired to quantify BCG quality independent of ECG availability. For example, investigators have found that posture and BCG instrumentation affect signal morphology [88], [89], but in such cases the need still remains to estimate cardiopulmonary parameters based on BCG morphology and to understand the quality of those estimates (e.g., heartbeat intervals).

Thus, is it possible to gage the quality of BCG-based heartbeat interval estimates in terms of error, false alarm rate, or false negative rate without access to corresponding ECG data? This chapter seeks to address this question by investigating the relationship between a proposed BCG signal quality index and the aforementioned performance metrics.

Modified Signal Quality Index Definition

In [55], a signal quality index (SQI) is presented to determine the quality of a BCG acquired with a weighing scale. In that study, ECG R waves are used to partition individual BCG cycles. For the modified approach proposed here, each individual BCG cycle is centered on an estimated J-peak location, where J-peak locations are determined by the detection and interval estimation algorithm proposed by Brüser [69]. Figure 7-1 contains an illustration depicting the proposed method. Once the BCG J-peaks are estimated, each individual cycle is defined as a

one-second segment of data centered on a J-peak. All individual cycles during a one-minute analysis window are used to create an ensemble average or parent template. Then, a correlation coefficient is calculated between each individual cycle and the parent template. The mSQI is computed as the average of the correlation coefficients for the one-minute window. This parameter is similar to the SNR metric in Chapter 6, but the mSQI bounds are [0, 1], making it (a) simpler to compare mSQI values computed for different BCGs gathered from different sensors with different circuit gains at different time periods and (b) sensible to map a linear relationship to this performance metric.

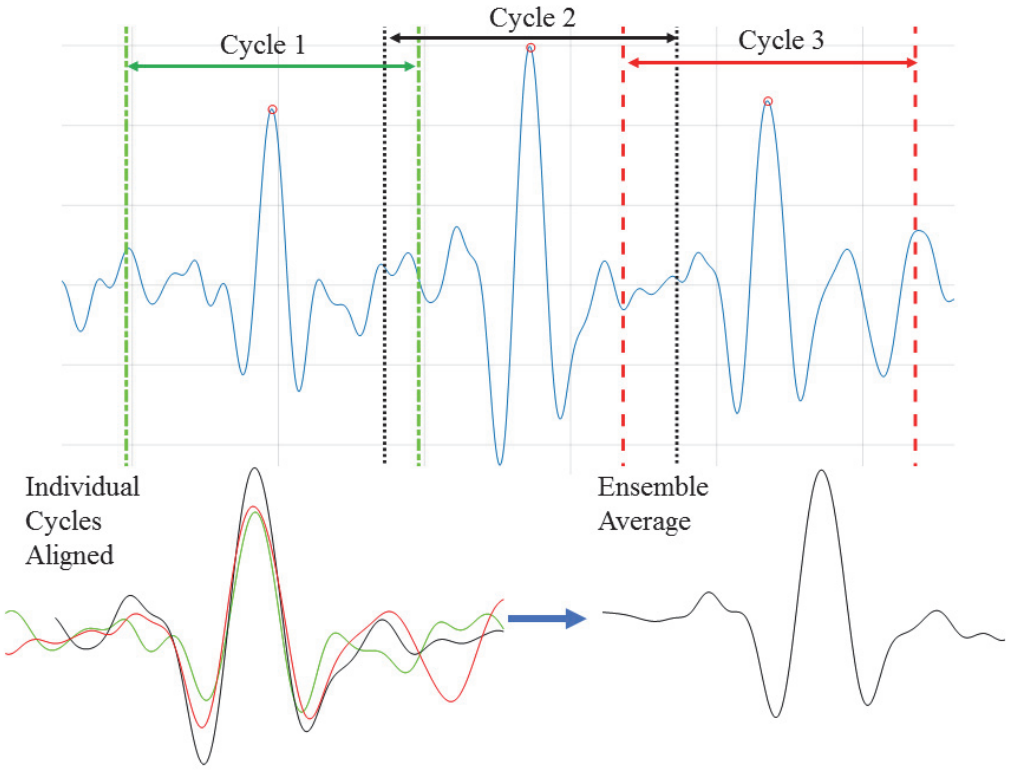

Figure 7-1. Generating an ensemble average from individual ballistocardiogram cycles.

Performance Metrics

To gage the sensibility of the BCG intervals used to determine the mSQI, a sum-squared error (SSE) metric is computed between the *N* J-peak times and their corresponding ECG R times as identified using the Pan-Tompkins algorithm [114]:

$$SSE = \left(\frac{1}{N}\right)\sum_{i=1}^{N}\left(\hat{T}_i - T_i\right)^2 \tag{23}$$

where $\hat{T}_i$ and T_i represent the times associated with the i^{th} J peak and the i^{th} R peak, respectively. For determining which estimated BCG J peak to use with $\hat{T}_i$ in equation 23, consider the time window between the i^{th} and $(i+1)^{th}$ ECG R peaks (T_i to T_{i+1}). Within this window, the BCG J peak associated with $\hat{T}_i$ is the closest estimated peak to Ti where $\hat{T}_i > T_i$ (the initial electrical activity of the ventricular contraction must precede the corresponding BCG J peak). Any additional peaks within the window are considered "false alarms", and if no estimate exists, a false negative (miss) is tallied. The false alarm rate (FAR) and false negative rate (FNR) are computed as the total number of false alarms or total number of misses, respectively, divided by the total collection time.

Linear Models

Two linear models were considered to map the mSQI to the performance metrics. The linear model fits were computed using MATLAB. For the first linear model (equation 24), all performance metrics (SSE, FAR, and FNR), were considered. For the second linear model (equation 25), only the FAR was considered. The adjusted R-squared and the root mean square error were computed for both models considered – equations 24 and 25 below:

$$\widehat{mSQI} = x_0 + x_1 SSE + x_2 FAR + x_3 FNR + \epsilon \tag{24}$$

$$\widehat{mSQI} = x_4 + x_5 FAR + \epsilon \tag{25}$$

Data Collection

Film- and load-cell-based BCG data were collected from 27 subjects – twelve male (weight = 79.9 ± 18.6 kg, height = 175.7 ± 3.6 cm, and age = 32.8 ± 8.8 yrs. (mean ± standard deviation)) and fifteen female (weight = 67.5 ± 11.2 kg, height = 168.7 ± 10.3 cm, and age = 47.2 ± 18.2 yrs.) under Kansas State University Institution Review Board (IRB) protocol No. 9386. After providing consent, each subject was asked to lie on their back in a supine position on the bed system for approximately five to ten minutes.

Results

The coefficients for the above equations were determined using 1,208 estimates (151 one-minute segments of data from eight sensors) from 27 subjects whose demographics are explained in the next section. See Table 7-1 and Table 7-2 for the coefficients and the associated fitting parameters.

Table 7-1. Parameter estimates for equation 24.

Parameter	Value
x_0	0.88
x_1	-0.34
x_2	-0.43
x_3	-0.21
RMSE	0.08
Adjusted R^2	0.64
Model p-value	$p < 0.001$

Table 7-2. Parameter estimates for equation 25.

Parameter	Value
x_4	0.88
x_5	-0.45
RMSE	0.09
Adjusted R^2	0.61
Model p-value	$p < 0.001$

The relationship between the mSQI and the FAR parameters becomes more apparent when examining a scatter plot of the two parameters (see Figure 7-2). For the 1,208 estimates, the correlation coefficient between the two was -0.78. The negative result and the negative coefficient, x_5, verify that the mSQI is inversely proportional to the FAR.

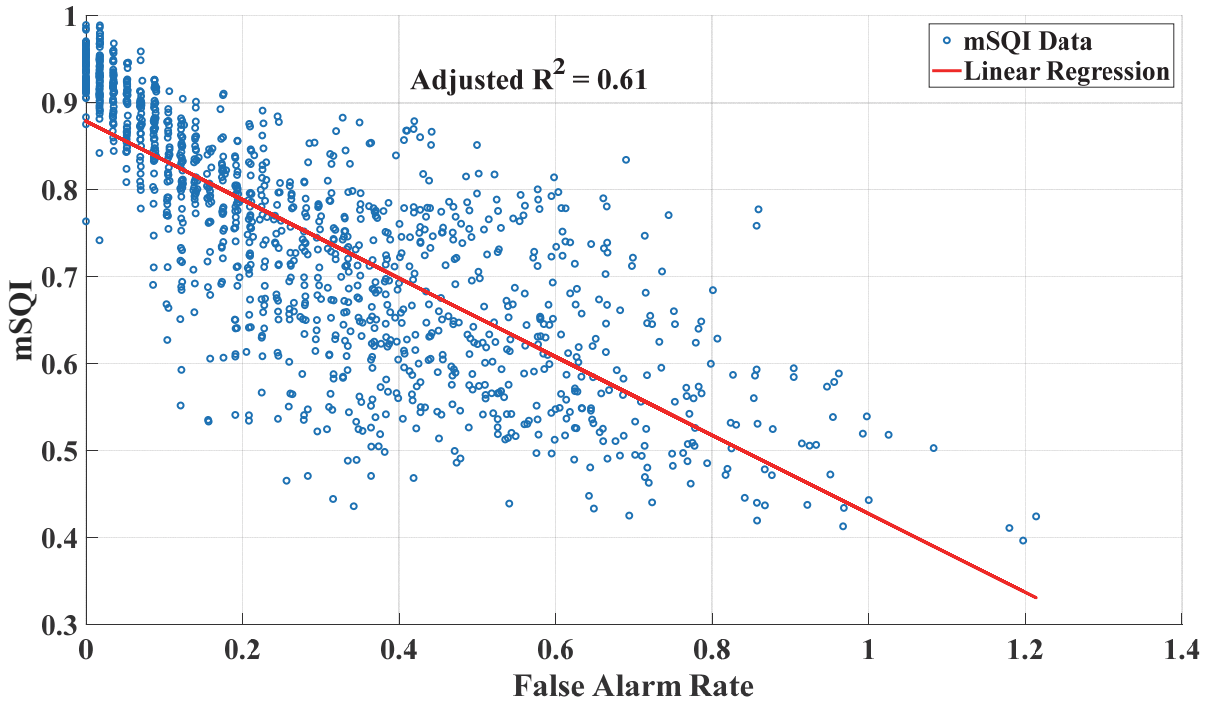

Figure 7-2. Scatter plot indicating the inverse relationship between the mSQI and the false alarm rate (FAR).

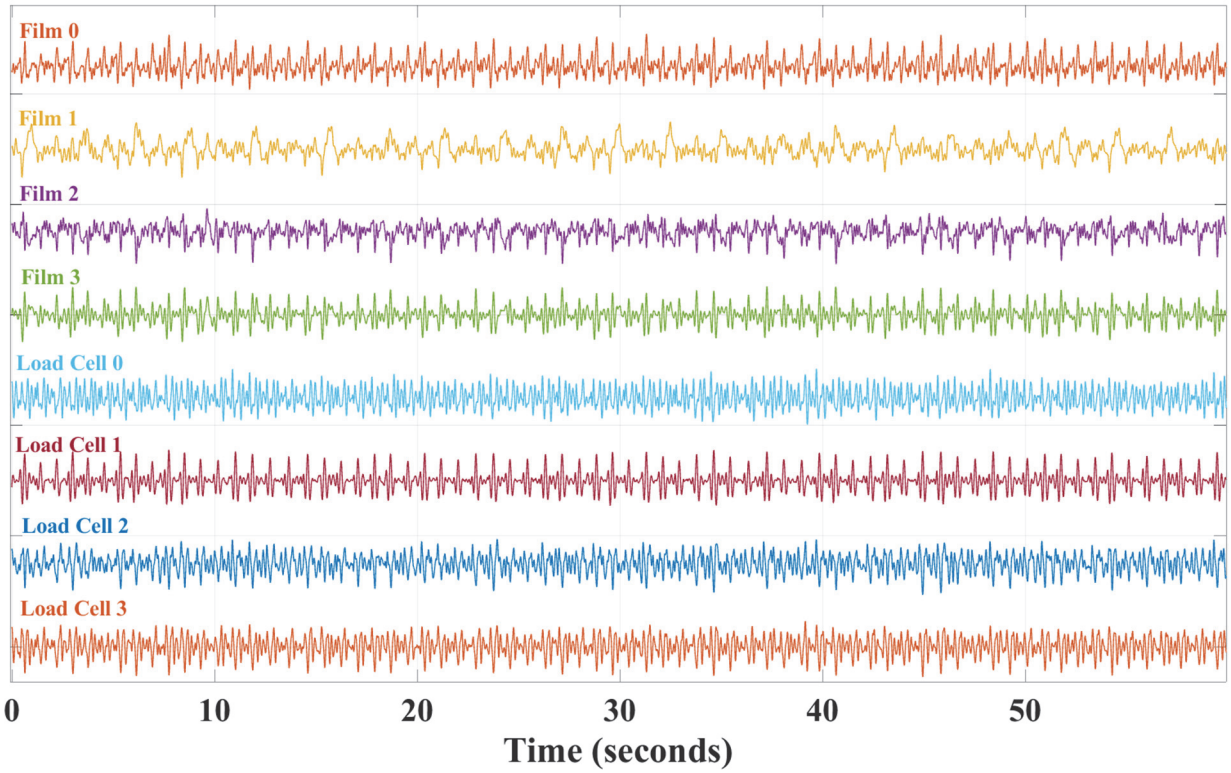

Figure 7-3. Representative ballistocardiograms acquired from all eight sensors. The accompanying mSQI values are in Table 7-3.

Table 7-3. mSQI for each BCG plotted in Figure 7-3.

Signal	Modified SQI
Film 0	0.87
Film 1	0.67
Film 2	0.41
Film 3	0.90
LC 0	0.68
LC 1	0.97
LC 2	0.58
LC 3	0.64

Discussion

The work presented in this chapter quantifies the quality of clean BCG data for the purpose of estimating HBIs. In earlier work published by our group, a model was presented to classify BCG data as noisy or clean [123]. The work presented here seeks to further quantify the suitability of BCG data for the purpose of extracting HBI estimates.

This study was limited in that only one BCG HBI estimation algorithm was used. If alternative HBI estimates are available, the corresponding BCG mSQIs can be computed. Further, data were only collected from subjects that laid in one position on the mattress (supine). However, the bed system used to collect these BCGs consists of two sensing technologies, and the sensors are spread out throughout the bed, meaning that this approach did analyze BCGs of varying morphology due to the presence of different sensing technologies that reside at a variety of sensor locations relative to the subject.

Chapter 8 - Robust Heartbeat Interval Estimation

As discussed in the last chapter, a challenge with ballistocardiography is the extraction of heartbeat intervals (HBIs). Estimating HBIs from bed-based BCGs has been the focus of several research groups [54], [113], [124]–[126], some of whom have demonstrated that their methods for extracting HBIs are accurate when those HBIs are compared to gold-standard ECG R-R intervals.

The redundancy built into the multi-sensor KSU system appears to give it a natural advantage over single-sensor systems in terms of the potential accuracy of the resulting HBI estimates. However, determining which sensor signal to use for HBI estimates is not a straightforward process. Chapter 6 confirmed that subject position and sensor location are factors that affect which sensor will ultimately provide the "best" signal in terms of a signal-to-noise metric. Fusion methods that combine multi-sensor, bed-based data have demonstrated better accuracy when estimating HBIs compared to methods that employ data from only one sensor in such a system [53], [67].

The KSU system differs from previous systems that utilized fusion approaches in that it collects BCG signals from more than one type of sensor: electromechanical films (EMFis) and load cells. Furthermore, the distance between a given sensor and the chest of the subject can be far greater because the sensors cover a large percentage of the mattress surface area and also reside under the corners of the bed posts: the team wanted to ensure that BCGs could be detected regardless of where a child slept on the bed. Given the availability of both EMFis and load cells, one of the questions of interest was, "Does the fusion technique always provide better accuracy compared to a single sensor?" If not, then the mSQI method discussed in the previous chapter could be used in selecting the "best" sensor signal for estimating HBIs.

Another characteristic that is often overlooked in bed-based systems is the "bed filtering effect." When examining BCG time-domain characteristics, it is quite clear that the bed system itself filters BCG data and causes resonance to occur in the range of 3 to 5 Hz – see Figure 8-1. These effects make it difficult for algorithms to estimate HBIs due to the multiple prominent peaks for most of the BCG cycles (see Figure 8-2). When dealing with bed-based systems, one could model the body and mattress as a spring-mass system, which is driven by the forcing function of each heartbeat, similar to the models outlined in Chapter 2. Therefore, a

deconvolution or “bed effect removal” preprocessing step is a sensible goal toward improving the accuracy of the HBI estimation technique.

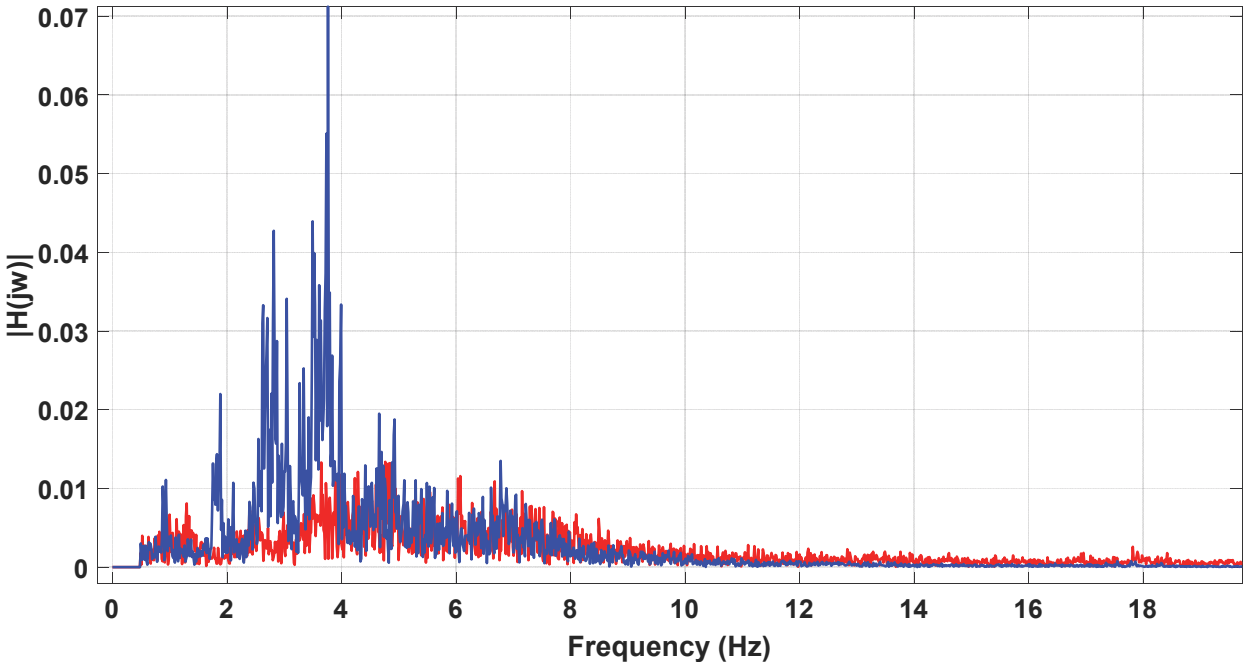

Figure 8-1. Comparison of single-sided frequency spectra: 30 seconds of standing BCG data (red) and bed-based BCG data (blue).

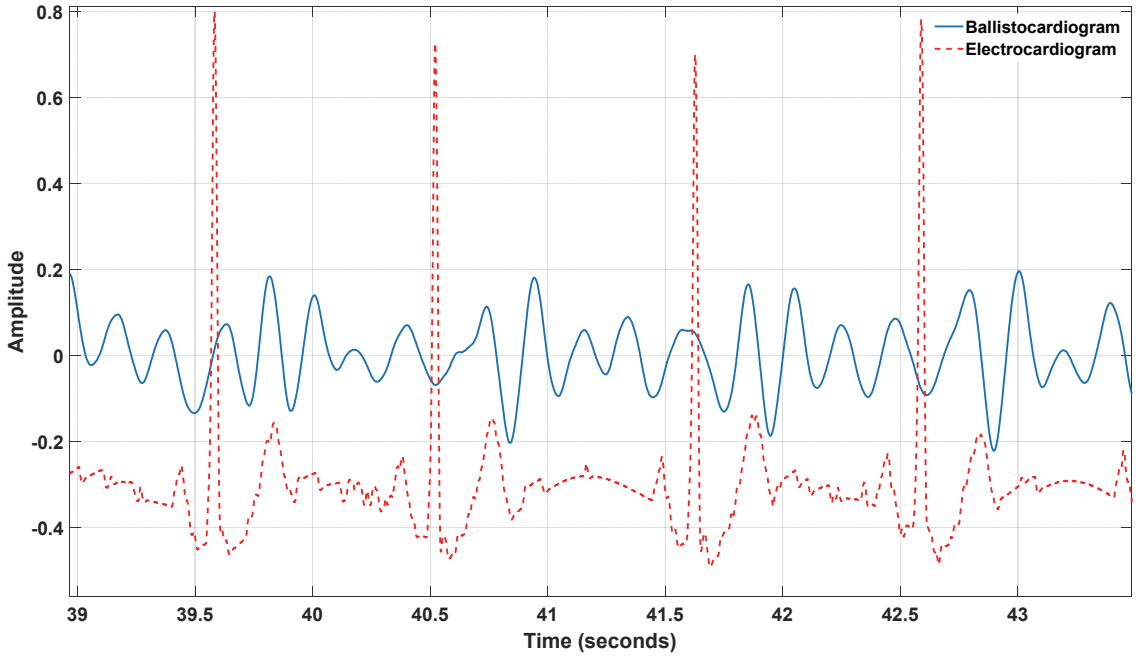

Figure 8-2. Multiple BCG and ECG cycles. The BCG J-peaks are not easy to visually distinguish from the secondary waves.

Study Approach

BCG data were collected from five subjects (three male and two female; ages 31 ± 4 years; weights 70.8 ± 3.8 kg; heights 166.4 ± 6.0 cm). Two types of mattresses were employed: one plush mattress that induces obvious resonant, BCG-filtering effects, and one firm mattress that induces minimal filtering. All five subjects are part of the KSU research team and have no known cardiovascular health issues. The short study was conducted at the Kansas State University Lafene Health Center, Manhattan, Kansas. Data were collected from each subject, who laid in five different positions on each mattress:

1. supine, with their head close to the top of the mattress,
2. on their right side,
3. on their left side,
4. prone, and
5. supine, with their head toward the bottom of the mattress.

For each position, a subject laid still to minimize motion artifacts. The signal quality metric outlined in the previous chapter was used to select the best sensor signal to estimate HBIs. To compare the four different HBI estimation approaches illustrated in Figure 8-3, the sum-squared error (SSE), false alarm rate (FAR), and false negative rate (FNR) were calculated for the estimated HBIs given the gold-standard ECG R-R intervals.

In addition to comparing all four methods using data from the entire sensor set, a secondary comparison was made using only the HBIs determined from EMFi sensor 1 BCGs, with and without a deconvolution filter (refer to the next section for deconvolution algorithm details). Figure 8-3 presents another diagram of the bed system that illustrates the sensor locations. Often, systems only utilize one film sensor placed under the torso (e.g., EMFit QS [18] and Beddit Sleep Monitor [19]), so one goal was to determine if an inverse filter (a deconvolution filter) provides improved performance at this location.

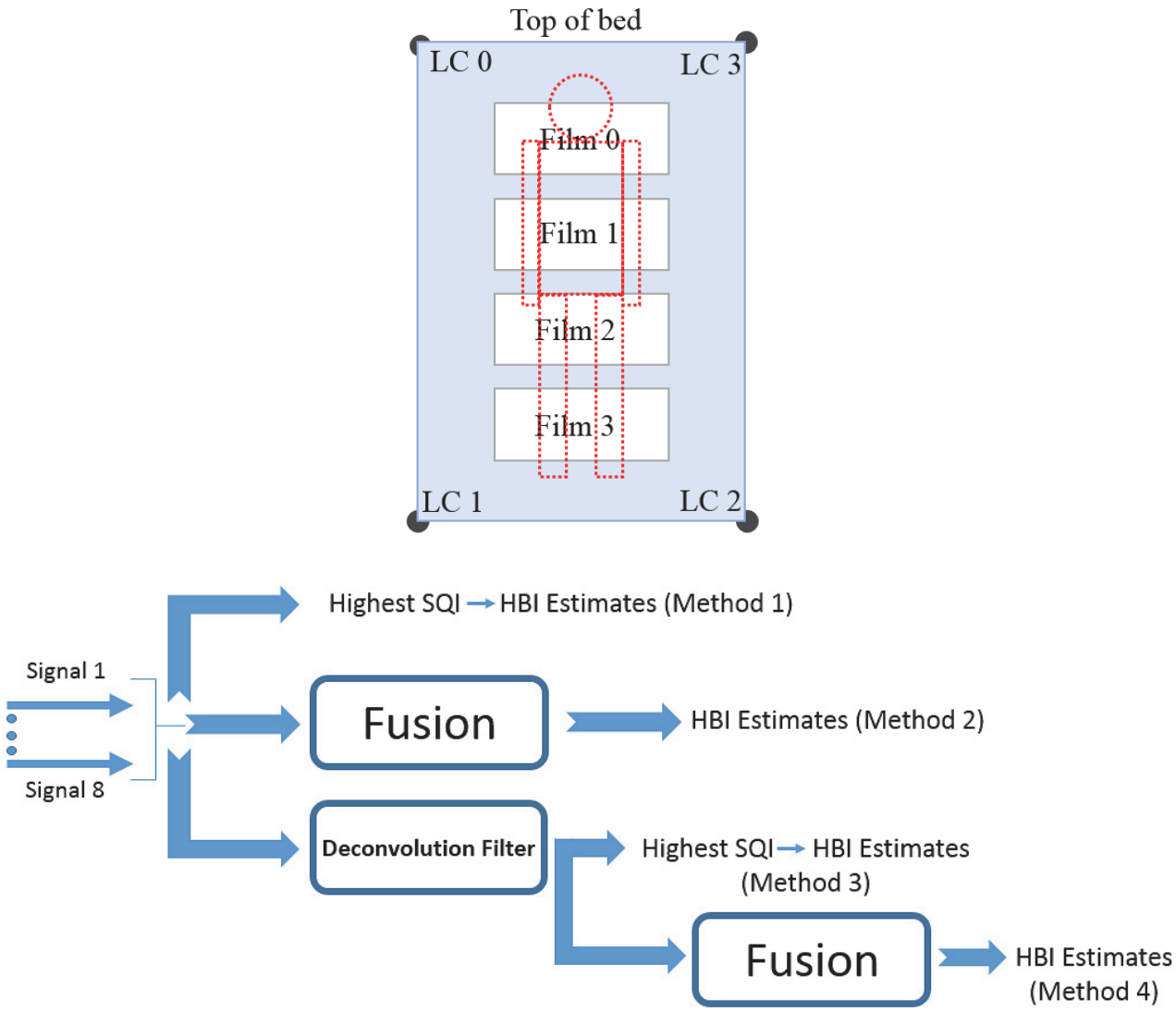

Figure 8-3 Sensor locations (top) and four different approaches for estimating heartbeat intervals (bottom).

Deconvolution Process Using an Inverse Filter

Overall Signal Preprocessing Process

No additional software filtering was applied to these BCG data before they were saved to files. During the post-processing phase, the signals were bandpass filtered in MATLAB using a sixth-order Butterworth filter with a passband of 1.0 to 10 Hz. The deconvolution ('inverse') filtering method described in the following section was then applied to the EMFi and load cell data – see HBI estimation methods 3 and 4 in Figure 8-3.

Deconvolution Approach

The following algorithm was used to apply an inverse filter:

1. Find the coefficients for an inverse filter that will apply linear predictive coding (LPC) on a window of BCG data (100 seconds for this study) that have already been bandpass filtered.
2. Apply the inverse filter, followed by a lowpass filter with a cutoff frequency of 10 Hz.

The MATLAB function, `LPC()`, was used to find the inverse filter coefficients. Three weights appeared sufficient for the inverse filter to remove the bed's filtering effect – this determination is discussed further in the Results section. A brief description of LPC is provided in the following section.

Linear Predictive Coding

The following provides a brief summary of linear predictive coding and how the method was utilized for this study. For further details, see [127]. If the force signal, $u(t)$, generated by the heart is assumed to be stationary, and the oscillation distortion is modeled as a shaping filter, $h(t)$, then the bed output signal can be formulated as

$$S(z) = U(z)H(z) \tag{26}$$

where $S(z)$ is the z-transformed version of the observed signal, $s(t)$. LPC can be used to estimate the coefficients of the filter, $\widehat{H}(z)$ where the ^ symbol indicates estimation:

$$\widehat{H}(z) = \frac{\hat{S}(z)}{\hat{U}(z)} = G\,\frac{1+\sum_{l=1}^{q} b_l z^{-l}}{1-\sum_{k=1}^{p} a_k z^{-k}} \tag{27}$$

An all-pole model is assumed for this problem (see Figure 8-4). Thus, the inverse filter, with p being the number of poles, can be written as

$$A(z) = 1 - \sum_{k=1}^{p} a_k z^{-k} \tag{28}$$

The output error signal can then be written as

$$e(n) = s(n) - \sum_{k=1}^{p} a_k s(n-k) \tag{29}$$

where n is an integer and represents a periodically sampled time domain signal, i.e., $s(t)$ sampled every T seconds results in $s(n) = s(nT)$. The above equation is solved to determine the weights, a_k, using a least-squares method to minimize the mean error signal [127]. An example BCG waveform with and without the inverse filter applied is illustrated in Figure 8-5.

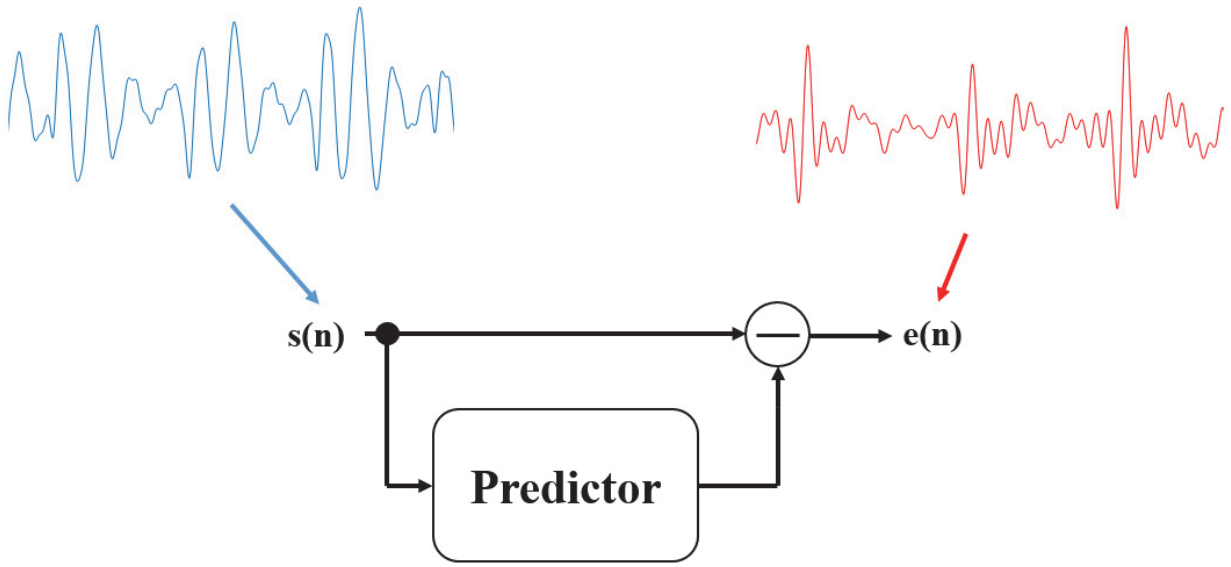

Figure 8-4. All-pole model (adapted from [127]) with representative BCG signals before (blue) and after the applying the inverse filter (red).

Heartbeat Interval Estimation and Fusion Technique

The heartbeat interval estimation technique proposed by Brüser in [69] was used for this study. In a previous study [119], the KSU team implemented and compared multiple BCG HBI and peak-detection algorithms, finding the robust single sensor HBI algorithm outlined by Brüser to work best for the bed system. For the fusion approach, the multichannel continuous interval estimation algorithm, referred to as xCLIE, proposed by Brüser in [53] was used. A description of the heartbeat interval estimation techniques is provided in Appendix A.

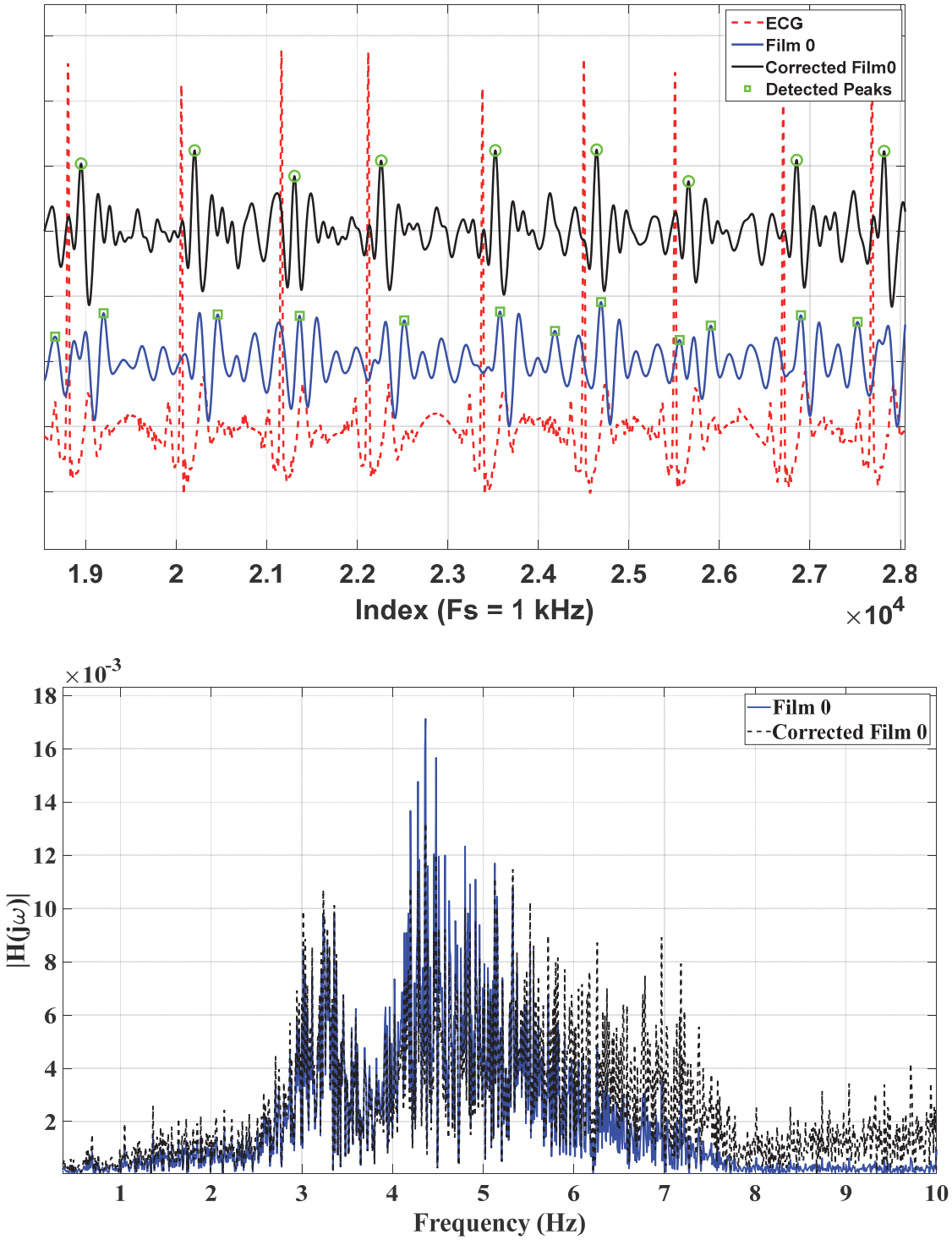

Figure 8-5. Top: BCG acquired from Film sensor 0 for subject A (blue) and corrected film 0 BCG (black), along with the estimated heartbeat locations identified via the algorithm described in the *Heartbeat Interval Estimation and Fusion Technique* section. Bottom: corresponding frequency spectra computed on two-minutes of data.

Quantifying the Performance

To compare the accuracy of each approach's estimated HBIs, the sum-squared error (SSE) was computed between the corresponding estimated heartbeat interval times, $\hat{T}_i$, and the ECG R-R interval times, T_i, in the same way as outlined in Chapter 7. Also computed were the false alarm rate (FAR) as the total number of false alarms divided by the total collection interval time and the false negative rate (FNR) as the total number of misses divided by the same total interval time. The HBI estimates were determined by finding estimated J-peak locations that occurred after the corresponding ECG R peaks. If no estimated J peak exists between two R-peak locations, that heart beat cycle is considered a "miss." If multiple estimated peaks exist between two R-peak locations, the J peak closest to the corresponding R peak is considered a "hit" and any additional peaks are considered "false alarms".

Paired *t*-tests [128] were performed on log-transformed SSE, FAR, and FNR metrics to reduce the abnormality of the distributions. A one-sample Kolmogorov-Smirnov (KS) test [129] was conducted to test the normality of the log-transformed metrics. All testing was performed at the five percent significance level. Both tests were performed using MATLAB.

Results

Inverse Filter Weights

Three different inverse filter lengths, i.e., number of weights = p from equation 28, were considered: 2, 3, and 5. The bias and limits of agreement are tallied in Table 8-1. Boxplots for each performance metric are depicted in Figure 8-6. The paired *t*-test results are included in Table 8-2. Considering the boxplots in Figure 8-6, all of the distributions are quite similar. However, the inverse filter with three weights has the tightest limits of agreement. Thus, three weights are used for the rest of the analyses presented in this chapter.

Table 8-1. Bias and limits of agreement for three different inverse filter lengths.

Number of Weights	Bias	1st Percentile	99th Percentile	(P_{99}-P_1)
2	-9.6 ms	-651 ms	448 ms	1099 ms
3	15.8 ms	-98 ms	484 ms	582 ms
5	52.6 ms	-412 ms	526 ms	938 ms

Table 8-2. Mean (stdev) and paired *t*-test *p* values for three different filter lengths. SSE and FAR data were log-transformed for each metric.

Number of Weights	SSE	FAR	FNR
2	0.029 (0.024)	0.238 (0.225)	0.051 (0.080)
3	0.028 (0.023)	0.249 (0.223)	0.046 (0.069)
5	0.027 (0.021)	0.246 (0.213)	0.041 (0.068)
***t*-test *p* values**			
2 vs 3	0.89	0.19	NA
5 vs 3	0.37	0.82	NA

Note that the KS test did reject the hypothesis that the log of FNR for method 3 with 3 weights came from a normal distribution – the *p* value was 0.006.

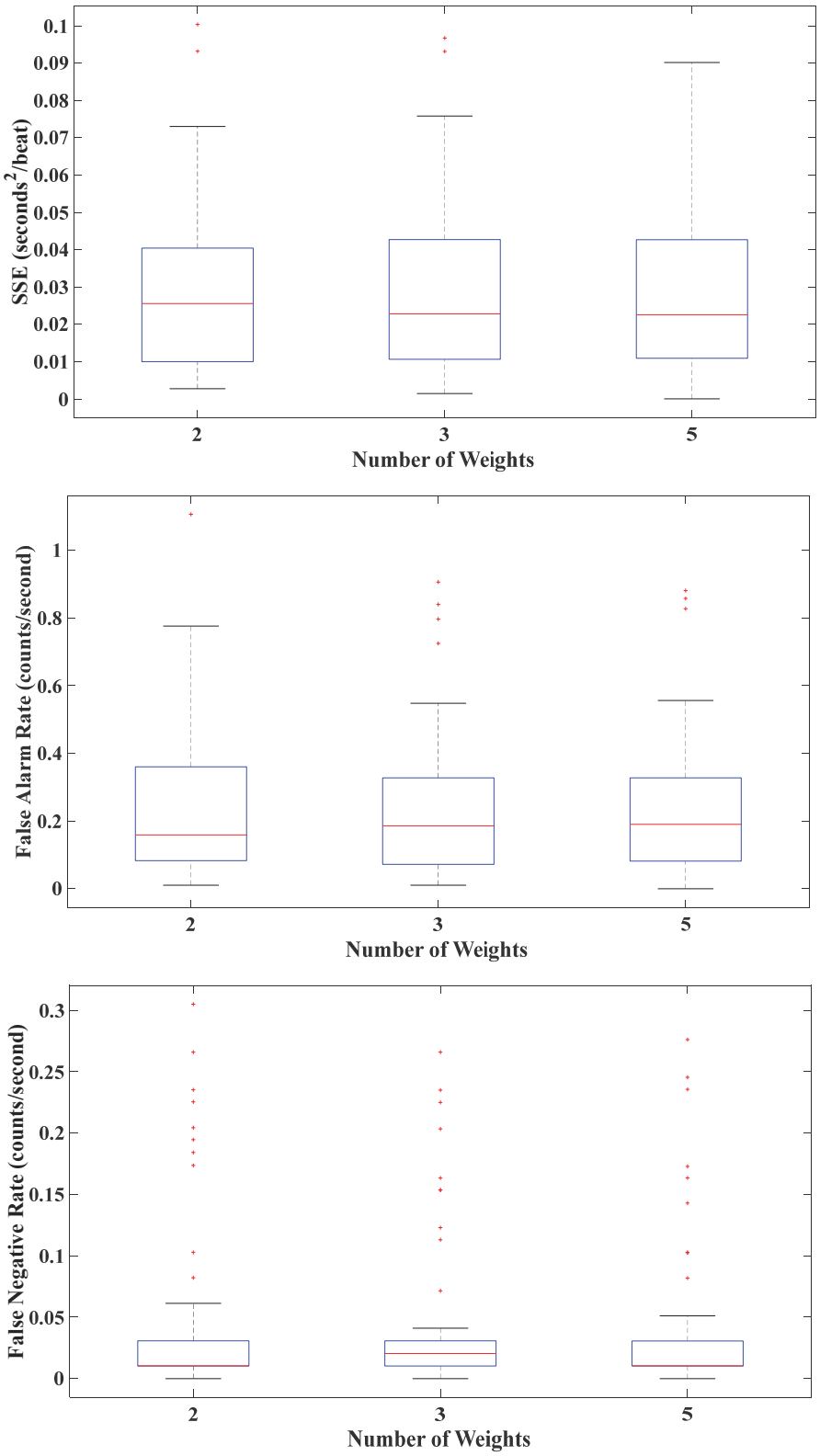

Figure 8-6. Boxplots of SSE, FAR, and FNR for inverse filters with the number of weights being 2, 3, and 5.

Results for Each Method

The average heartbeat interval and BCG signal quality index (see Chapter 7) for each subject/mattress combination is listed in Table 8-3. Note that the highest mean HBI was 1.12 seconds, or 53.6 beats per minute, and the lowest mean HBI was 0.74 seconds, or 81.1 beats per minute, so each method was tested over a reasonably broad range of heart rates. The average BCG signal quality index for each position is provided in Table 8-4.The performance metrics, bias, limits of agreement, and *p* values were computed for each of the four methods (see Table 8-5 and Table 8-6), where three weights were used for the deconvolution filter. The paired *t*-test results are included in Table 8-6. Bland-Altman plots can be seen in Figure 8-7 (Methods 1 and 2) and Figure 8-8 (Methods 3 and 4). The corresponding box plot are illustrated in Figure 8-9.

Table 8-3. Mean (stdev) heartbeat-interval durations (seconds) and mean (stdev) signal quality index for each subject and mattress. The average was calculated for all five laying positions.

Subject - Mattress	Mean (stdev) heartbeat interval	Mean (stdev) signal quality index
A – 1	1.05 (0.09)	0.876 (0.051)
A – 2	1.12 (0.10)	0.895 (0.048)
B – 1	0.94 (0.046)	0.856 (0.109)
B – 2	0.98 (0.66)	0.779 (0.081)
C – 1	1.01 (0.063)	0.872 (0.066)
C – 2	1.00 (0.063)	0.838 (0.054)
D – 1	0.74 (0.063)	0.808 (0.062)
D – 2	0.76 (0.073)	0.742 (0.100)
E – 1	0.90 (0.043)	0.805 (0.082)
E – 2	0.96 (0.043)	0.818 (0.143)

Mattress 1 – plush; Mattress 2 – firm

Table 8-4. Mean (stdev) BCG signal quality indexes for each position.

Position	Mean (stdev) Signal Quality Index
1	0.858 (0.070)
2	0.714 (0.101)
3	0.865 (0.043)
4	0.862 (0.074)
5	0.881 (0.087)

Table 8-5. Bias and limits of agreement.

Method	Bias	1st Percentile	99th Percentile	(P_{99}-P_1)
1	6.4 ms	-209 ms	427 ms	636 ms
2	-5.6 ms	-783 ms	398 ms	1181 ms
3	15.8 ms	-98 ms	484 ms	582 ms
4	0.3 ms	-155 ms	261 ms	416 ms

Table 8-6. Paired *t*-test *p* values for each method. SSE, FAR and FNR data were log-transformed for each metric.

Method	SSE	FAR	FNR
1	0.034 (0.029)	0.212 (0.177)	0.052 (0.073)
2	0.038 (0.047)	0.508 (0.216)	0.081 (0.085)
3	0.028 (0.023)	0.249 (0.223)	0.046 (0.069)
4	0.028 (0.035)	0.430 (0.199)	0.067 (0.082)
***t*-test *p* values**			
1 vs 2	0.35	< 0.001	< 0.001
3 vs 2	0.75	< 0.001	NA
4 vs 2	< 0.001	< 0.05	< 0.05
3 vs 1	0.22	0.40	NA
3 vs 4	< 0.05	< 0.001	NA

Note that the KS test did reject the hypothesis that the log of FNR for method 3 came from a normal distribution – the *p* value was 0.006.

In terms of the limits of agreement, method 4 (deconvolution filter plus fusion) had the tightest bounds. However, both fusion methods had a much higher false alarm rate compared to the single-sensor HBI estimation methods. Given that (a) methods 3 and 4 had similar SSEs, (b) method 3 had only a slightly higher FAR compared to method 1 (not a significant difference), and (c) method 3 had the lowest average FNR, method 3 can be considered the best option. However, there is the tradeoff of a larger bias and wider limits of agreement compared to method 4.

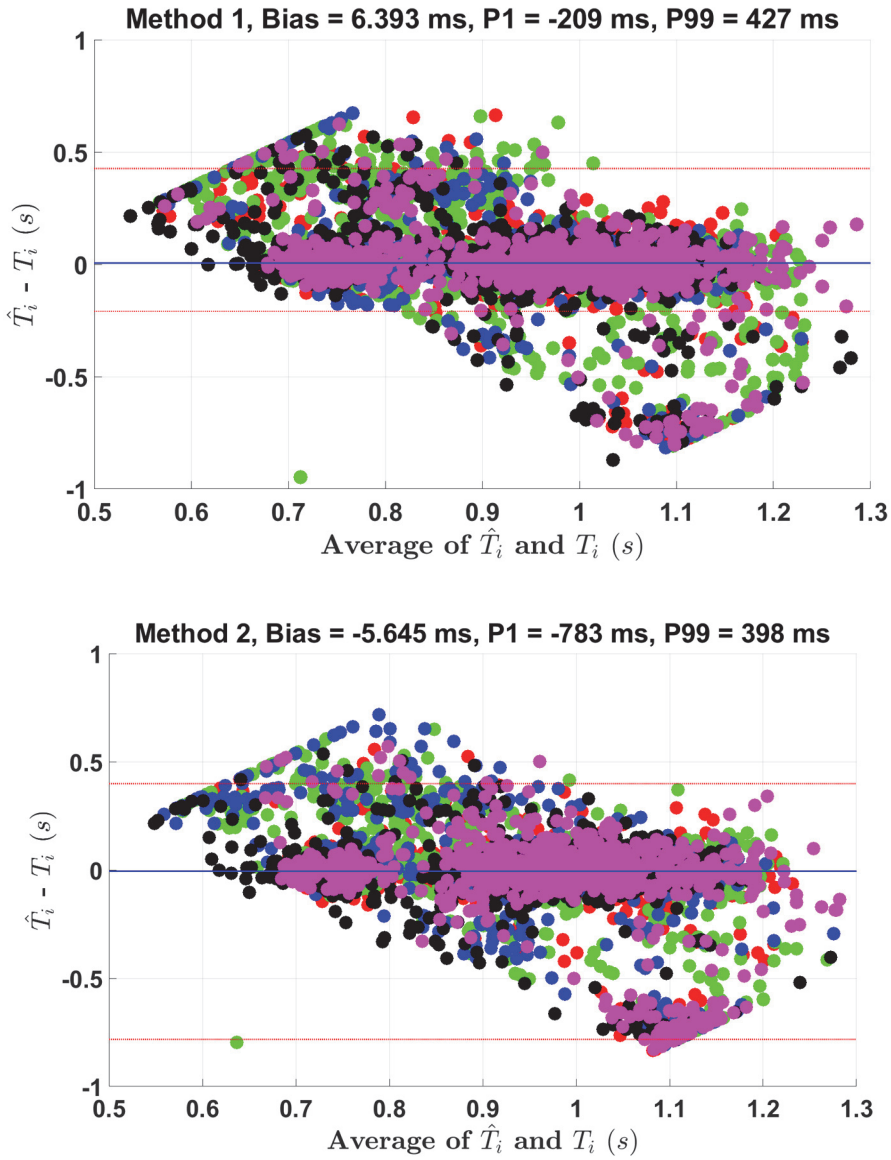

Figure 8-7. Bias and limits of agreement for HBI estimation methods 1 and 2 considering both mattresses. Different colors represent the five positions analyzed. Red = position 1, green = position 2, blue = position 3, black = position 4, and magenta = position 5.

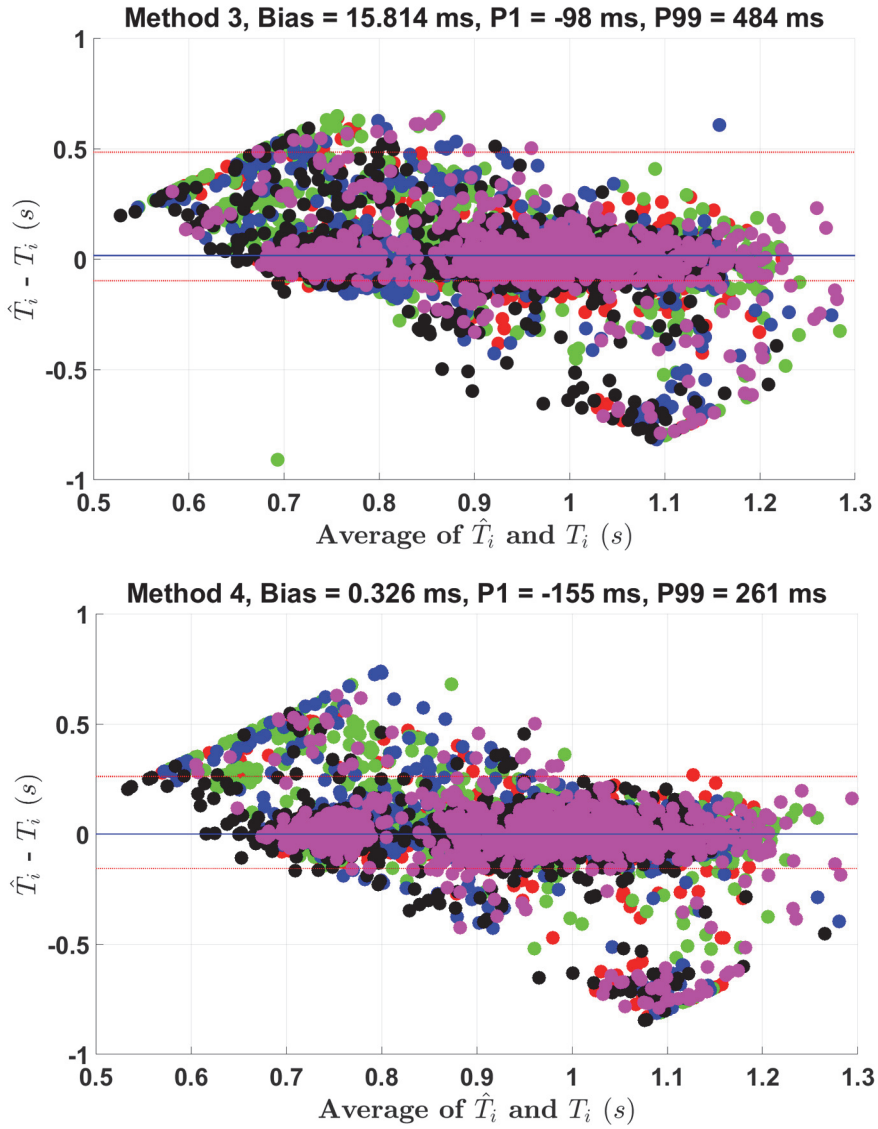

Figure 8-8. Bias and limits of agreement for HBI estimation methods 3 and 4 considering both mattresses. Different colors represent the five positions analyzed. Red = position 1, green = position 2, blue = position 3, black = position 4, and magenta = position 5.

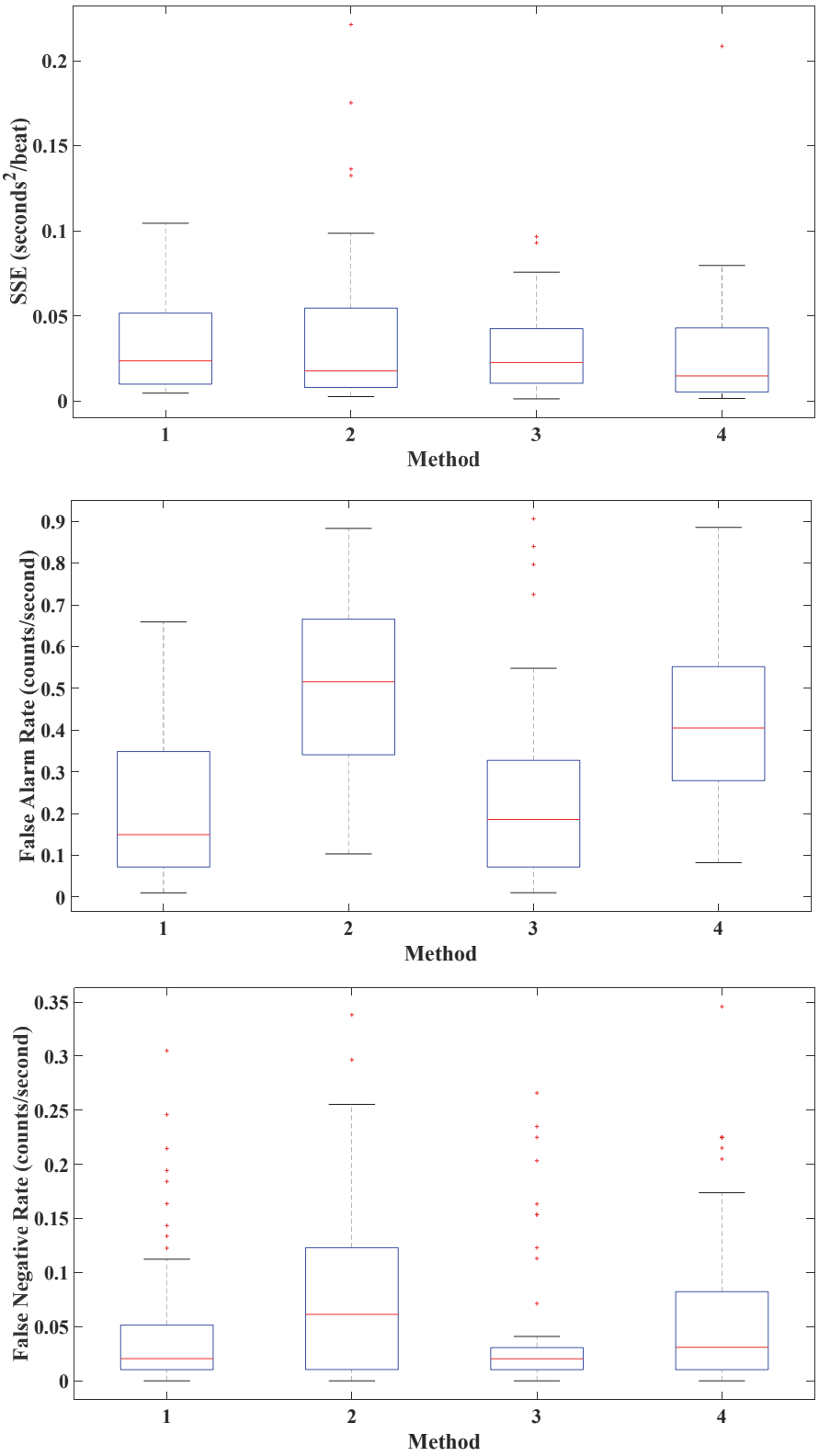

Figure 8-9. Boxplots of SSE, FAR, and FNR for each method.

Results for Each Mattress – Mattress 1 (Plush)

This section provides analysis results for the plush mattress. The bias, limits of agreement, mean (stdev), and *t*-test results for the performance metrics are provided in Table 8-7 and Table 8-8. Corresponding box plots are illustrated in Figure 8-10.

Table 8-7. Bias and limits of agreement for the plush mattress.

Method	Bias	1st Percentile	99th Percentile	(P_{99}-P_1)
1	-5.2 ms	-619 ms	455 ms	1074 ms
2	-24.1 ms	-611 ms	406 ms	1017 ms
3	-0.92 ms	-580 ms	380 ms	960 ms
4	3.3 ms	-555 ms	438 ms	993 ms

Table 8-8. Mean (stdev) and paired *t*-test *p* values for the plush mattress analysis. SSE, FAR, and FNR data were log-transformed.

Method	SSE	FAR	FNR
1	0.039 (0.034)	0.241 (0.184)	0.060 (0.085)
2	0.040 (0.045)	0.614 (0.184)	0.108 (0.094)
3	0.027 (0.022)	0.242 (0.198)	0.052 (0.079)
4	0.031 (0.044)	0.470 (0.164)	0.084 (0.091)
***t*-test *p* values**			
1 vs 2	0.43	< 0.001	< 0.001
3 vs 2	0.55	< 0.001	< 0.001
4 vs 2	< 0.001	< 0.001	< 0.05
3 vs 1	0.10	0.90	0.24
3 vs 4	0.13	< 0.001	< 0.001

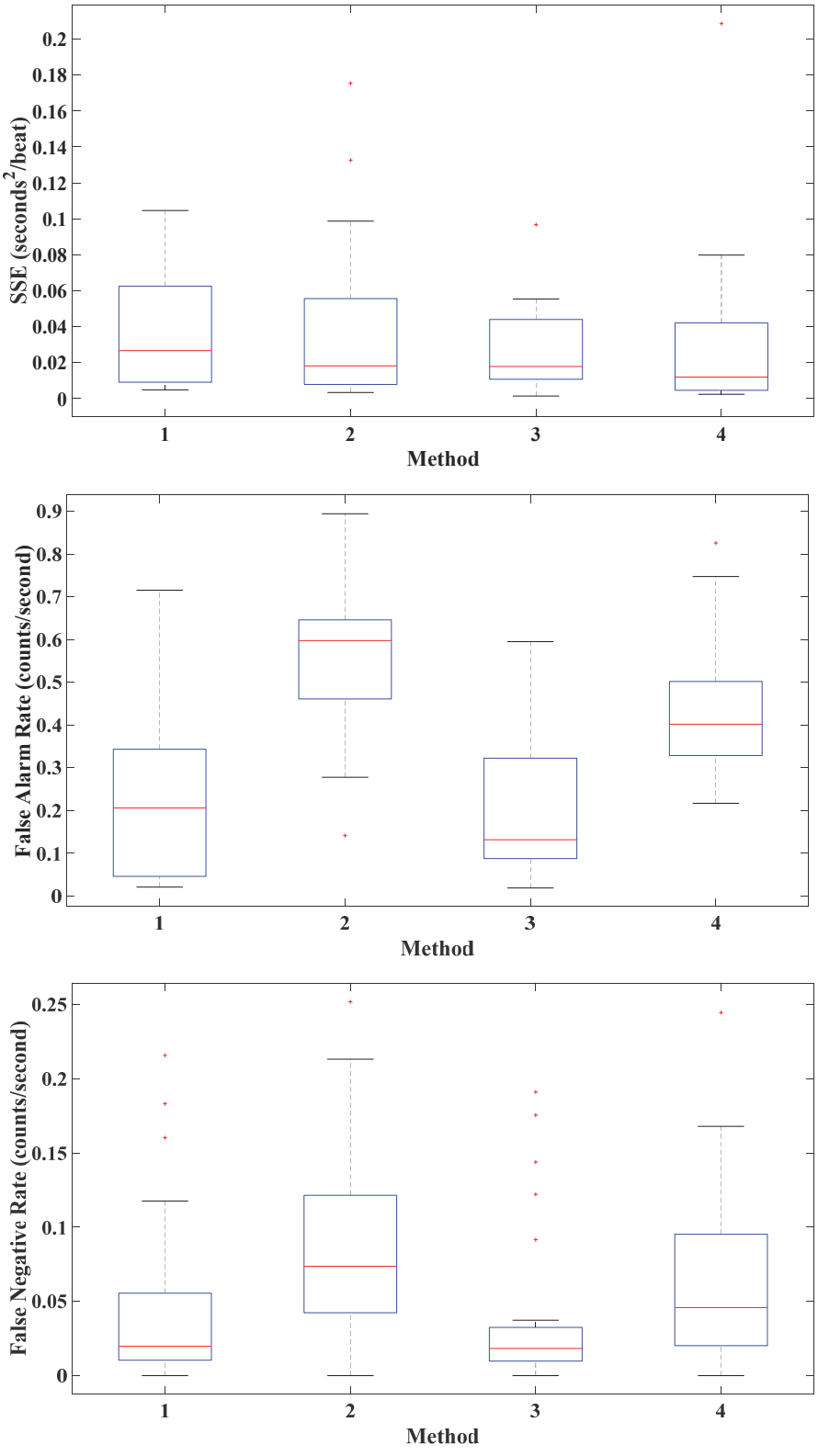

Figure 8-10. Boxplots of SSE, FAR, and FNR considering only mattress 1 (plush).

Results for Each Mattress – Mattress 2 (Firm)

This section provides analysis results for the firm mattress. The bias, limits of agreement, mean (stdev), and *t*-test results for the performance metrics are provided in Table 8-9 and Table 8-10. Corresponding box plots are illustrated in Figure 8-11.

Table 8-9. Bias and limits of agreement for the firm mattress.

Method	Bias	1st Percentile	99th Percentile	(P_{99}-P_1)
1	1.0 ms	-502 ms	427 ms	929 ms
2	-12.4 ms	-783 ms	399 ms	1182 ms
3	9.5 ms	-296 ms	484 ms	780 ms
4	5.4 ms	-155 ms	381 ms	536 ms

Table 8-10. Mean (stdev) and paired *t*-test *p* values for the firm mattress analysis. SSE, FAR, and FNR data were log-transformed.

Method	SSE	FAR	FNR
1	0.029 (0.024)	0.183 (0.169)	0.044 (0.059)
2	0.037 (0.050)	0.403 (0.196)	0.055 (0.066)
3	0.029 (0.024)	0.256 (0.250)	0.039 (0.059)
4	0.025 (0.022)	0.389 (0.225)	0.050 (0.069)
***t*-test *p* values**			
1 vs 2	0.63	< 0.001	0.10
3 vs 2	0.87	< 0.001	< 0.05
4 vs 2	0.11	0.45	0.42
3 vs 1	0.88	0.31	0.07
3 vs 4	0.12	< 0.05	< 0.05

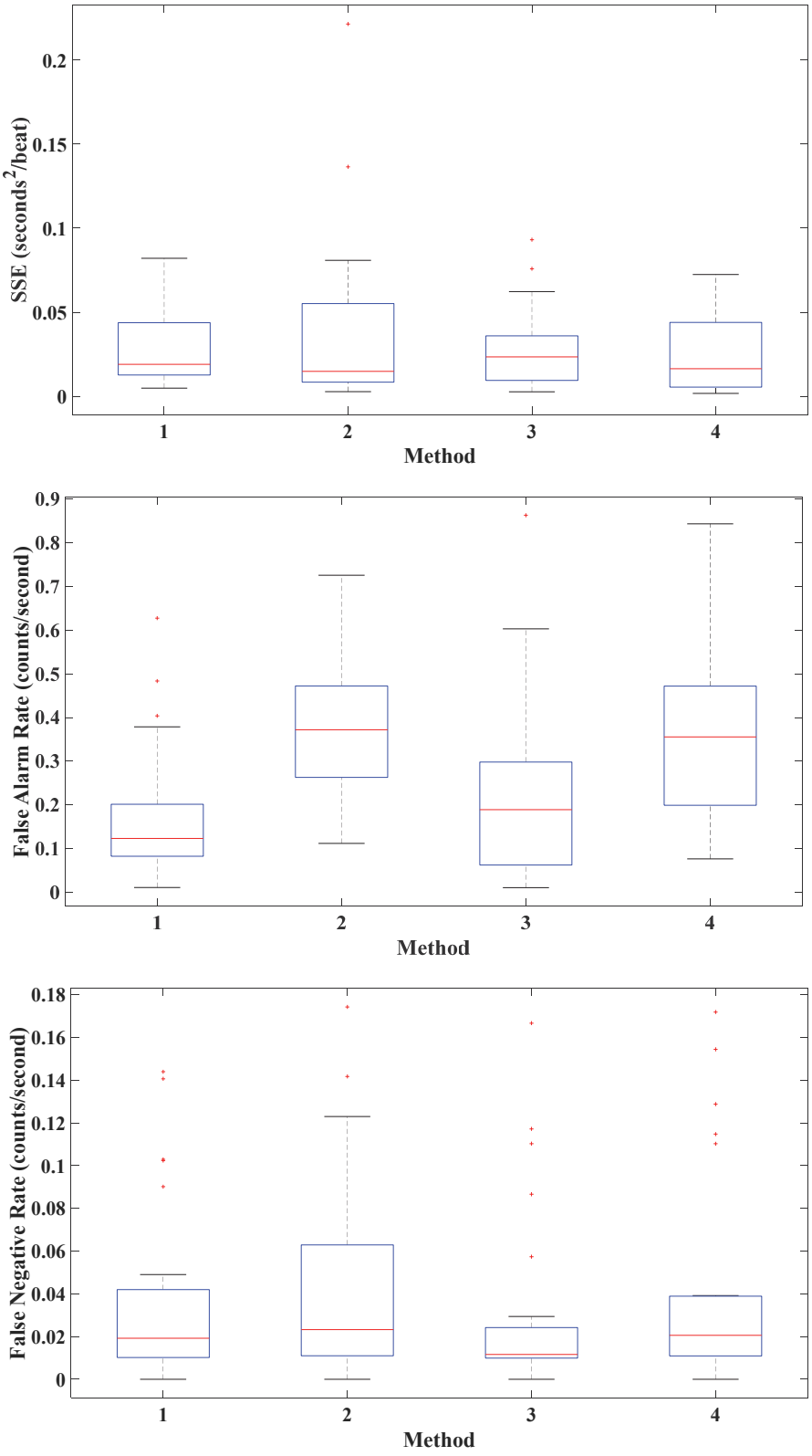

Figure 8-11. Boxplots of SSE, FAR, and FNR considering only mattress 2 (firm).

Results Only Considering EMFi 1

For this comparison, only HBIs from EMFi sensor 1 and the first four positions were considered for analysis since EMFi sensor 1 was located approximately under each subject's mid-section for these trials (for position 5, their head was closer to the foot of the bed). The bias, limits of agreement and performance metrics are listed in Table 8-11 and Table 8-12.

Table 8-11. Bias and limits of agreement.

Method	Bias	1st Percentile	99th Percentile	(P_{99}-P_1)
1	12.7 ms	-658 ms	554 ms	1212 ms
3	63 ms	-636 ms	484 ms	1120 ms

Table 8-12. Mean (stdev) and paired *t*-test *p* values for both methods. SSE, FAR, and FNR data were log-transformed.

Method	SSE	FAR	FNR
1	0.071 (0.047)	0.519 (0.266)	0.082 (0.092)
3	0.060 (0.045)	0.510(0.291)	0.063(0.087)
***t*-test *p* values**			
3 vs 1	< 0.05	0.34	< 0.05

The addition of the inverse filter slightly improved the limits of agreement but did increase the bias. In terms of the performance metrics, the inverse filter substantially improved the SSE without significantly influencing the FAR or FNR. Boxplots for each metric are provided in Figure 8-12.

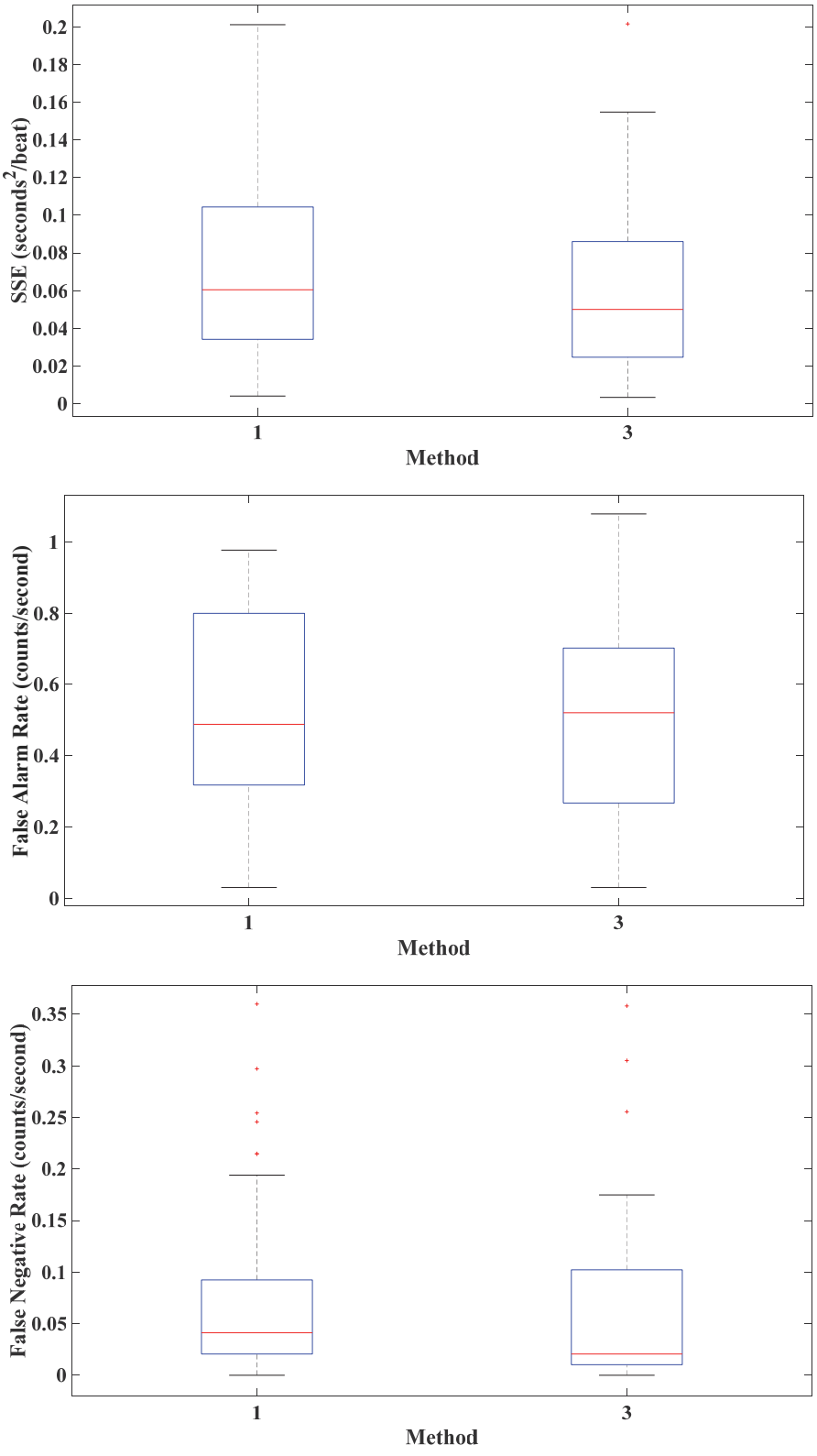

Figure 8-12. Boxplots of SSE, FAR, and FNR for method 1 and 3 considering only the first four positions and EMFi sensor 1.

The findings presented in this chapter confirm that the multi-sensor bed-based system can accurately estimate HBIs regardless of sleeping position and mattress type. Further, an inverse-filter preprocessing step improves the performance of already proven, robust HBI estimation techniques. Therefore, this inverse-filtering step could be used as a preprocessing step for other BCG HBI or peak-detection algorithms to improve performance, especially for a single sensor system that utilizes a sensor placed under the torso.

Some study limitations existed. First, the number of subjects was low – only five. However, by asking each subject to lie in different positions and by using two different mattresses, the team was able to gather 50 data points for each performance metric (5 subjects *x* 5 positions *x* 2 mattresses). Another limitation was the consideration of only healthy individuals. Future studies will investigate how different heart conditions (e.g., arrhythmias) affect the performance of the various algorithms.

Chapter 9 - Heartspring Six-Month Study

After verifying that the system can successfully operate in the room of a child with low-functioning autism, and thus help to quantify their sleep, a longer study was needed. First, these data were required to better understand the relationship linking sleep quality to daytime performance/behaviors. Second, a longer study would test the feasibility of the system to operate for weeks to months without the presence of KSU staff on-site at Heartspring, allowing the team to vet the methods employed for remote access and storage. Two bed systems were developed: the original system that utilized a "captain's bed" design (the traditional wood panel bed design used with Heartspring children), and another system that utilized an Endurance Bed 2.0, since an Endurance bed was used by a second child participating in the study. The Endurance bed design, a much heavier-duty plastic form factor, is the design to which Heartspring residential staff are migrating because it is more robust, harder for a child to move, and less susceptible to bed-wetting damage. The team sought to minimize the number of changes and disturbances made to each child's environment to minimize any influence on the quality of their sleep.

In summary, these two male children with severe disabilities and low-functioning autism had their standard beds at the Heartspring campus replaced with KSU custom bed-based systems: one captain's bed and one Endurance bed. Nighttime physiological data and daytime behavioral data were collected under KSU IRB protocol #7783. Both systems were put in place March 20, 2018 and remained in these boys' rooms until the beginning of September 2018, at which point the Endurance bed system was removed. The remaining captain's bed system continued to operate until the middle of October 2018. In total, over 200 nights of data were collected for bed system 1 and over 150 nights of data were collected for bed system 2.

Each bed system was configured to collect data between 7:00 p.m. and 9:00 a.m. to increase the likelihood that the system would capture bed entrance and bed exit events. Each child generally went to bed around 8:00 p.m. and awoke the next morning anywhere between 7:00 and 8:00 a.m. This fourteen-hour timeframe typically generated 168 8 MB LabVIEW measurement files (LVMs) per night. The LVM file structure is illustrated in Appendix C. Low-resolution thermal camera images were acquired every 1-2 seconds during the same fourteen-hour period, where each image is 5 kB (60 by 80 pixels). Considering all of the bed system and

thermal camera data, approximately 1.5 GB of data were collected per bed per night, for a total of 576 GB of data over the full six-month study.

Signal Preprocessing

All signal processing and analysis is performed in MATLAB. A sixth-order Butterworth bandpass filter with a 1 to 10 Hz passband is applied to these BCG data to accentuate the BCG signal components and attenuate the respiration and noise components. Prior to the bandpass filter, a simple lowpass filter with a 0.3 Hz cutoff is used to extract the respiratory component. A visual example of this BCG signal preprocessing is illustrated in Figure 9-1.

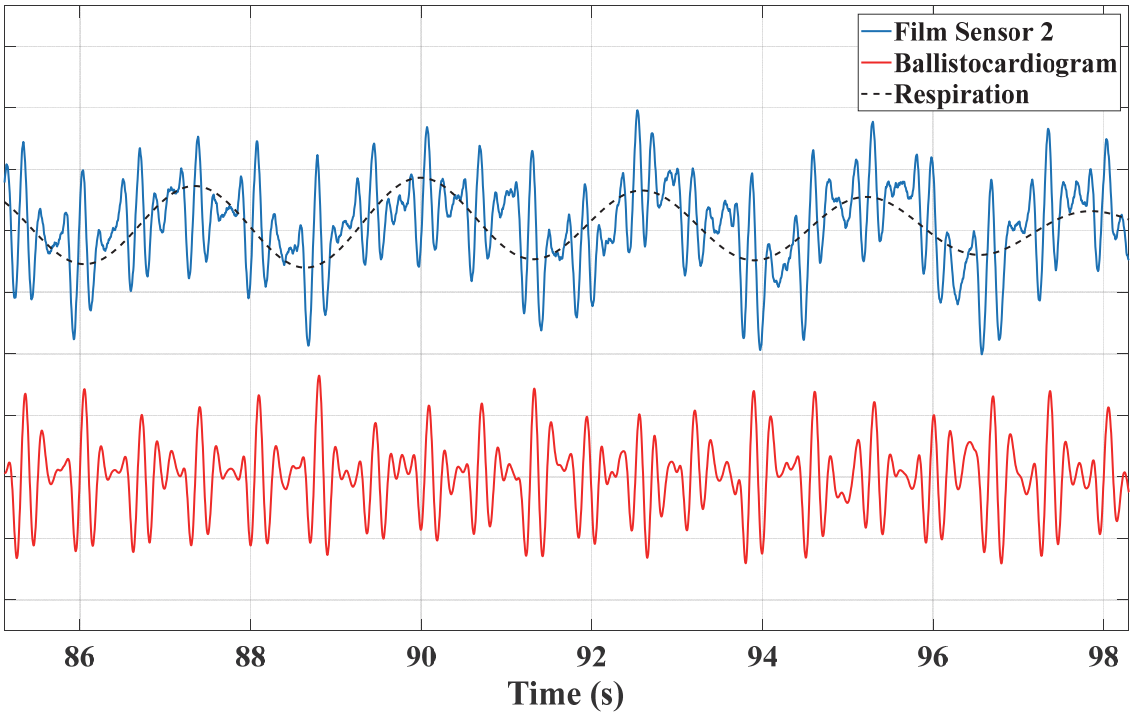

Figure 9-1. Signal preprocessing example – separation of the respiration and BCG components given the composite recorded waveform.

Overnight Analysis

Seven consecutive nights of data for each bed system are selected for overnight analyses as a means to illustrate the processing performed on these data sets. The nights of June 7th-8th through June 13th-14th are chosen for bed system 1, while Aug. 9th-10th through Aug. 15th-16th are chosen for bed system 2. For these time periods, each night within the respective time window offers a full set of data from both the bed system and the thermal camera. BCG signal quality indexes, heartbeat intervals, and respiration rates are estimated from BCG signals acquired

between 8:00 p.m. and 7:00 a.m. the next morning. Other than limiting the time window from 8:00 p.m. to 7:00 a.m. the next day, no additional data were removed from these analyses (e.g., data corrupted by motion). First, two representative short, raw waveforms (one film BCG and one load cell BCG) acquired with bed system 1 and corresponding thermal images are contained in Figure 9-2. Heartbeat occurrences and respiration cycles are clearly visible, along with the beginning of a motion-artifact-corrupted segment that is confirmed in the thermal images. The child moves from laying down, close to supine, to slightly sitting up, looking over the side of the bed.

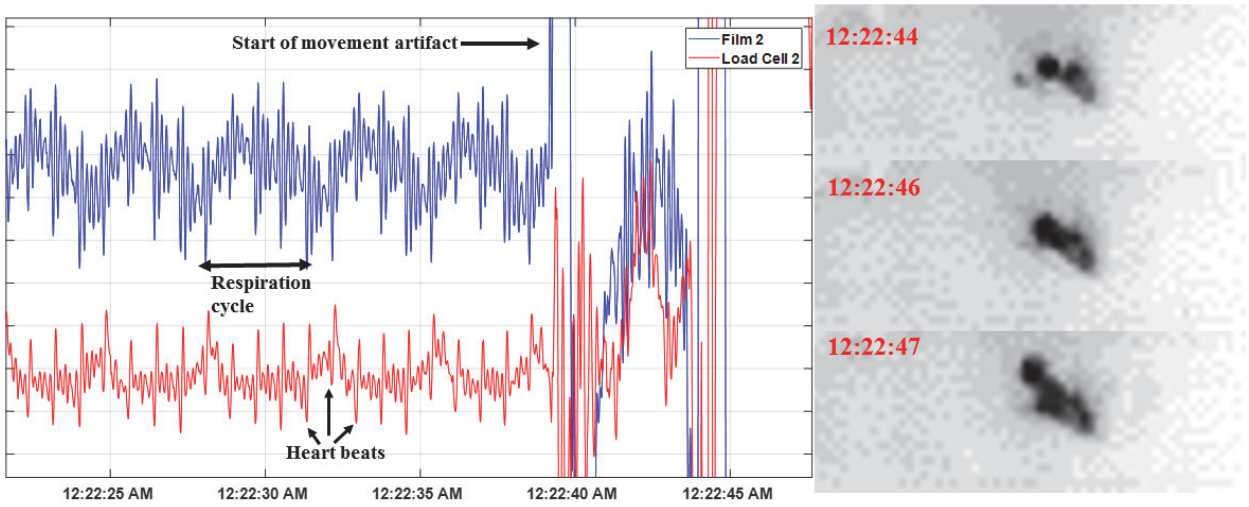

Figure 9-2. Representative data from bed system 1: BCG/respiration composite data from film 2 and load cell 2 (left) and corresponding thermal imagery (color inverted) (right).

In addition to the week-long datasets, two nights of representative data are selected for COP analysis – the night of June 7th-8th and August 10th-11th for bed system 1. COP estimates are computed for each LVM file, where approximately 168 LVM files are generated per night. These data are displayed in Figure 9-3 for two nights, where the child using bed system 1 stayed more towards the center of the bed for the night of August 10th-11th but was closer to the top for June 7th-8th. The team was unable to produce COP plots for bed system 2 since three of the load cell acquisition channels were working improperly.

During the installation of the bed systems, it was soon realized that an Ethernet access point was not easily accessible in either room. At first, the team decided to utilize commercial PowerLine networking devices, where the data are transmitted over the power line between two PowerLine hubs, and the second hub that receives these data is connected to the network. However, the PowerLine devices caused regular spikes in the supply voltage for the load cells.

Once this was discovered, the PowerLine devices were replaced with the Wi-Fi data acquisition systems discussed in Chapter 4. Unfortunately, the voltage spiking due to the PowerLine devices caused some of the load cell acquisition channels on the NI analog input module to malfunction. Having a spare NI 9220 analog module available made it possible to begin gathering COP data for bed system 1. However, the NI 9220 module for bed system 2 was not repaired within the timeframe of the study, so the team decided to let the system run with the channels that were still functional as opposed to losing days of BCG data due to the entire system being down. Even with this setback, vast amounts of high-quality data were collected with both systems.

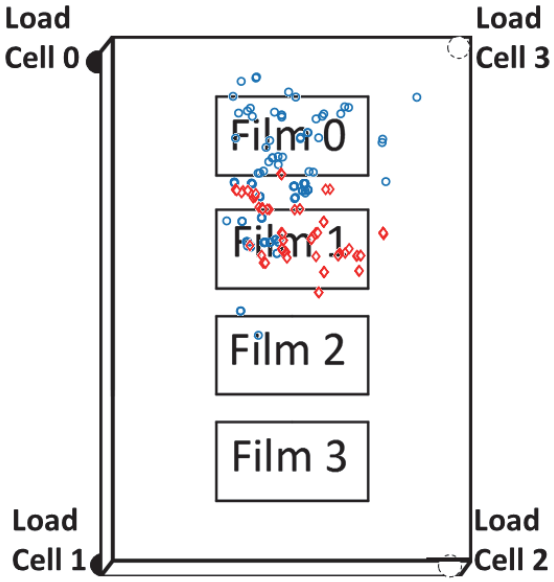

Figure 9-3. Center of position throughout the night for bed system 1: June 7th-8th (blue circles, 145 points) and August 10th-11th (red diamonds, 133 points). Each point is the median *x* and *y* position per saved LVM file.

BCG Signal Quality

The BCG signals were segmented into one-minute intervals, and the BCG signal quality index (see Chapter 7) was calculated for each one-minute window of BCG data for each sensor and bed system for the entire week worth of data. Note that the analysis window was restricted from 8 p.m. to 7 a.m. the next morning for each night. In total, 4,655 signal quality values on an average of 665 one-minute data segments per night were calculated for each bed system for the entire week. Table 9-1 and Table 9-2 depict the amount of intervals that each sensor had the highest signal quality for bed system 1 and bed system 2, respectively.

Table 9-1. Number of times each sensor had the highest signal quality index for seven nights of data (June 7/8 to June 13/14) – Bed system 1.

Sensor	Number of Times Best	Number of Times Best (percentage)	Total Intervals
			4,655
Film 0	702	15.1%	
Film 1	1188	25.5%	
Film 2	378	8.1%	
Film 3	471	10.1%	
Load Cell 0	800	17.2%	
Load Cell 1	880	18.9%	
Load Cell 2	143	3.1%	
Load Cell 3	93	2.0%	

Table 9-2. Number of times each sensor had the highest signal quality index for seven nights of data (August 10/11 to August 17/18) – Bed system 2.

Sensor	Number of Times Best	Number of Times Best (percentage)	Total Intervals
			4,655
Film 0	1319	28.3%	
Film 1	968	20.8%	
Film 2	502	10.8%	
Film 3	1122	24.1%	
Load Cell 0	0	0%	
Load Cell 1	582	12.5%	
Load Cell 2	1	0%	
Load Cell 3	161	3.5%	

Heartbeat Interval Estimation

Heartbeat interval estimates were extracted from the BCG signal with the highest quality index. Boxplots displaying the median (red line), 25th and 75th percentiles of the estimated HBIs are illustrated for each bed system in Figure 9-4, where the red '+' symbols represent outliers beyond the maximum whisker length of 1.0 times the interquartile range (25th to 75th percentile).

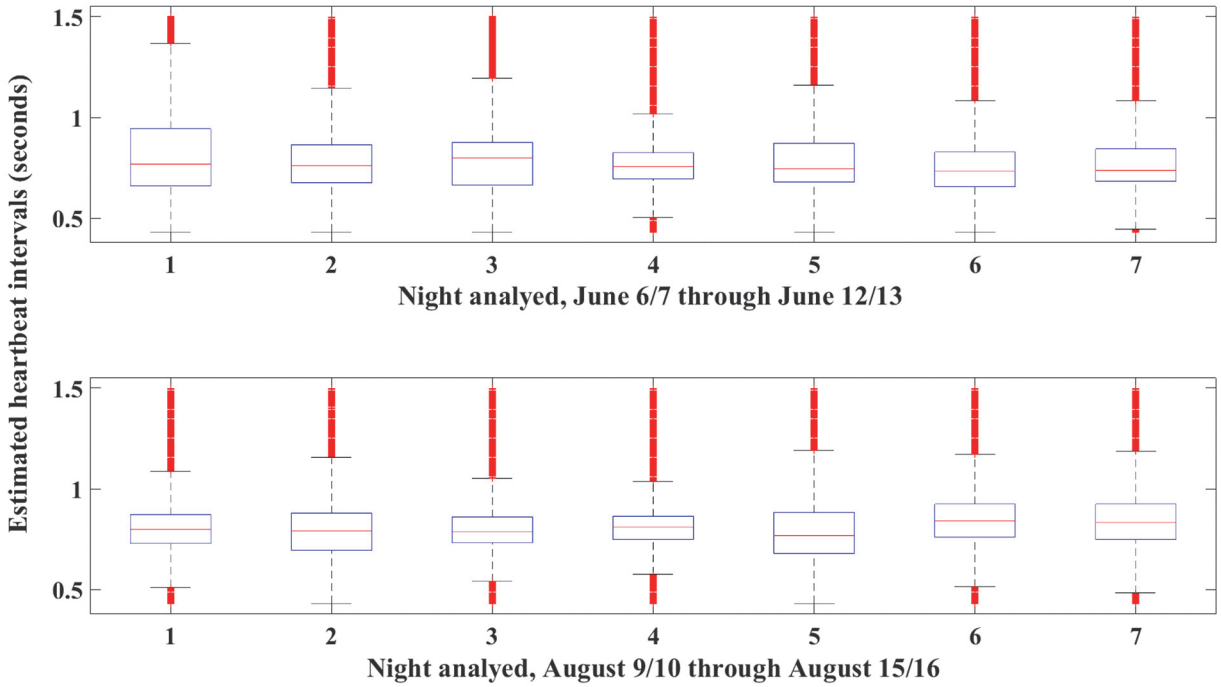

Figure 9-4. Boxplots of estimated heartbeat intervals (HBIs) over seven consecutive days for both bed systems.

Respiration Rate Estimation

For each night, collected data are separated into one-minute segments. For each segment, the respiration component is separated from the BCG components, the DC offset is removed, and the maximum value of the single-sided spectrum in the frequency domain is identified. The frequency corresponding to the maximum provides the respiration rate. Similar boxplots for estimated respiration rates per night for both bed systems are contained in Figure 9-5.

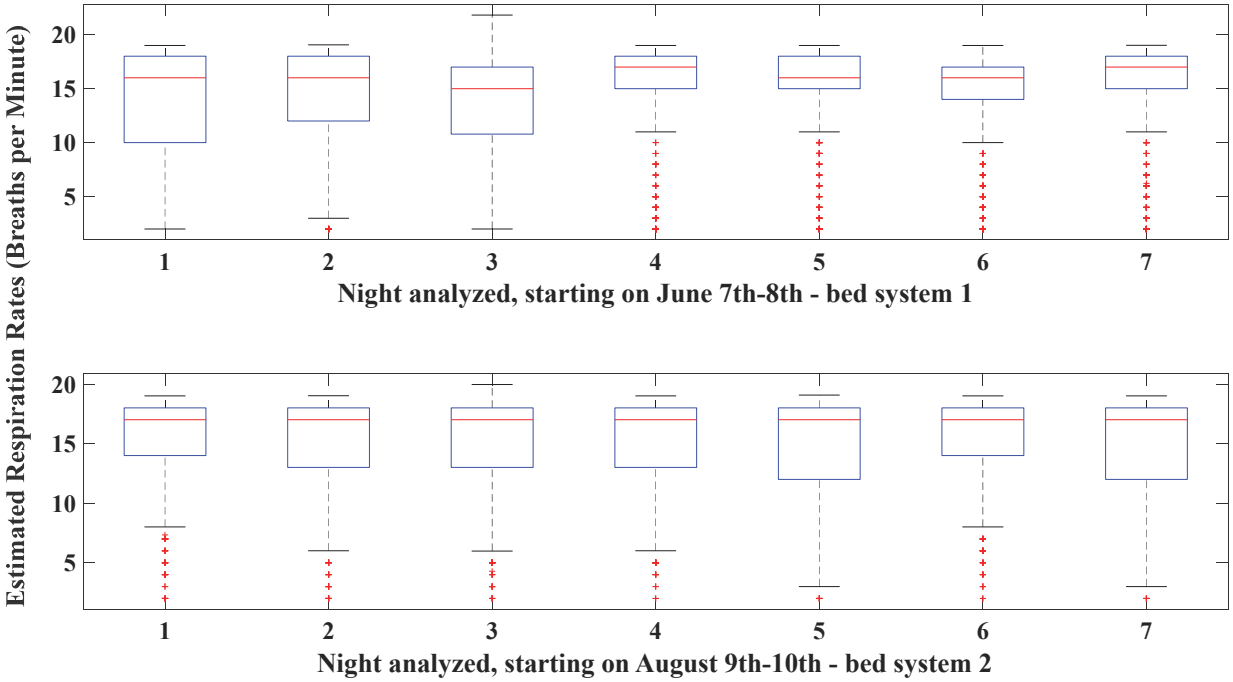

Figure 9-5. Boxplots of estimated respiration rates over seven consecutive days for both bed systems.

One night of estimated HBIs after a 21st order median filter was applied are illustrated in Figure 9-6.

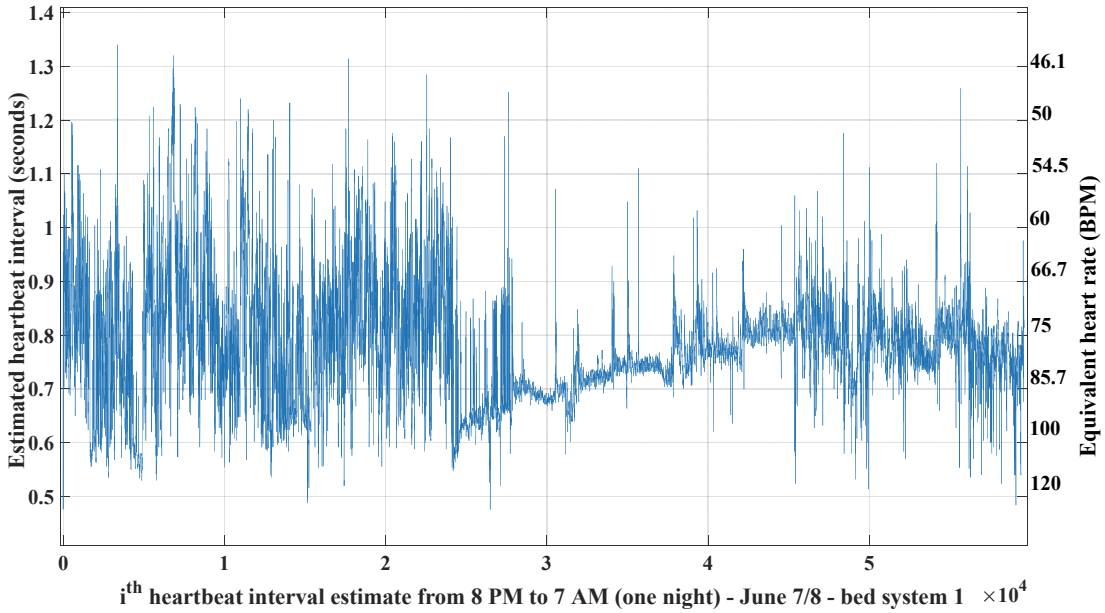

Figure 9-6. Estimated heartbeat intervals for bed system 1, night 1 (June 7th-8th). The plot presents results from applying a 21-point median filter to the estimates.

The above data/plots, which are representative of any night while the bed systems are functional, illustrate the ability of these systems to collect data over long time periods. These data also demonstrate that these multi-sensor systems are useful for estimating heartbeat intervals. For both children, and for each night, the median heartbeat interval stayed below 1 second, or in other words, stayed above 60 beats per minute. It is worth noting that these children are not large individuals – it speaks well of the sensitive bed system that it is able to record such data consistently.

Discussion/Lessons Learned

Issues with Individual Beds

The two children were two different ages/sizes and had different demographics, but each system still worked well when it was properly integrated into the respective child's room. These systems require power and must be plugged into wall outlets – they are not battery operated. For bed system 2, the layout of the child's room made it difficult to hide the power cable running from the wall to the acquisition hardware stored under the bed. This was not an issue for the first month or so, but after he became aware of the power cord, it became a common habit to unplug the cable. The team attempted to move the bed in order to cover the outlet but was unsuccessful in deterring him from finding a way to unplug the system. This habit eventually led to a behavior incident in which he not only unplugged the bed, but he also pulled on the cord connected to the hardware and disabled the system. After this incident, the team decided to take down system 2, emphasizing the need to develop unobtrusive systems for this population. The room housing bed system 1 had a better layout. From the start of the study, the power cord stayed hidden behind the head of the bed and never became an issue.

Broader Thoughts

Currently, the best option to assess the nighttime sleep quality of this population is with manual periodic bed checks [39]. While this study only involved two children, the work has demonstrated that a sensor-based bed system has the capability to monitor the physiological signals of children with severe disabilities and autism unobtrusively and reliably over the course of months as an arguably superior alternative to manual bed checks.

One major lesson learned from this study was that children are very curious and they will interact/play with anything that appears out of the ordinary. Once subject two (bed system 2)

became aware of the power cord running from his bed to the wall, it became a consistent habit for him to unplug the system. Even after our team was able to securely hide the cable, it was too late – the behavior had been developed, and it did not take long before the system was unplugged again. This issue was never encountered with the other child (bed system 1), as the power cord was successfully hidden behind the bed for the entire duration of the study.

Another major lesson learned is that communication is extremely important. Heartspring has a day school, several residential group homes, a gym, a cafeteria, and other facilities on their campus – they have quite a large staff to keep everything running smoothly. When the KSU team did not effectively communicate to the group home 3 staff that bed system 2 was moved on purpose to prevent another unplugging event, a staff member pushed the bed back to its original location, breaking the connection from the wall, leading to a loss of data for several nights. At first, the team believed this was another behavior incident, but after viewing the thermal images the next day, the cause of the power outage was clear.

Chapter 10 - Conclusion

This dissertation presented a bed-based nighttime monitoring toolset capable of acquiring physiological signals unobtrusively and autonomously. Such a system can be utilized in numerous applications (e.g., personalized healthcare, preventative care systems, or the monitoring of sensitive populations). The driving motivation for the creation of this monitoring toolset was the need to quantify the sleep of children with low-functioning autism. Therefore, the system platform was designed to appear to be, and feel no different from, a normal bed. This is an important design detail, as the acceptance of monitoring platforms and medical devices is vital to their success in long-term monitoring applications.

A review of ballistocardiography instrumentation techniques, including the originally proposed methods from the dawn of the field in the 1940s to modern-day techniques was provided, making it possible to understand how the forces generated by the heart are coupled to the instrumentation device and how waveform morphology can be affected. The system platform, sensor set, custom conditioning hardware, and National Instruments data acquisition hardware and software that comprise the bed system were described in detail in Chapters 3 and 4. Results and lessons learned from gathering nighttime data from children at Heartspring was the focus of Chapters 6 and 9. Innovative BCG signal processing techniques were presented in Chapters 7 and 8 – both of which add promise to the realization of a longer-term robust monitoring system.

The review in Chapter 2 presented a model for how the forces due to each heartbeat are coupled to the sensing device, and this model helps to describe the instrumentation effects in terms of signal changes that occur in all forms of ballistocardiography. Ideal cases based on original system designs were discussed to understand how different systems provide BCGs of varying morphology. The models can be further used to understand instrumentation effects due to modern measurement systems, where the more popular techniques were discussed. The approach presented in the review can be applied to innovative BCG acquisition systems, making it possible to compare recorded waveforms between systems.

The bed-based system was tested in the environments of three different children with severe disabilities and low-functioning autism, demonstrating that it can function well for long periods of time and monitor the physiological signals of this underserved, sensitive population.

The system proved to be capable of unobtrusively recording 1) the BCG, which can be used to estimate instantaneous heart rate, 2) respiration, and 3) motion without causing any disturbance to a children's environment, when implemented properly. These investigations open the door to better understanding how sleep quality relates to daytime cognitive ability for children with autism and physical disabilities. Future studies can seek to collect more data on numerous children to better understand this relationship for this underserved population.

Further, BCG signal processing techniques to characterize BCG signal quality, plus a preprocessing inverse filter, were presented, and their effectiveness was quantified. The team found that the EMFi or load cell sensor which provides the highest SNR seems to depend on the location of the sensor relative to the subject; neither sensing modality proved to be superior (Chapter 6).

The BCG signal makes it possible to assess cardiac health and track physiological parameters unobtrusively. Often, an ECG is collected simultaneously with a BCG to assess BCG-based HBI estimation algorithms, but in real-world applications, ECG data will not always be available. To that end, Chapter 7 presented a modified signal quality index that can be used to assess BCG HBI estimates and demonstrated that a close relationship exists between the quality index and the FAR.

Estimating the heartbeat intervals from BCG signals is not a trivial problem, especially when working with multi-sensor systems. The work presented in Chapter 8 demonstrated that this bed-based system is capable of accurately tracking HBIs regardless of sleeping position (an important aspect when working with severely disabled autistic children) and mattress type. While this study had a limited number of subjects, the team was still able to gather 400, 100-second data segments for analysis.

The link between sleep quality and daytime behaviors for children with severe disabilities and low-functioning autism is still not well understood. With this underserved population, the standard technique for monitoring sleep quality (PSG) is simply not a viable option. Unobtrusive techniques such as ballistocardiography offer the ability to quantify sleep quality by monitoring the micro-movements caused by each heartbeat. Chapter 9 presented the results from a six-month long study conducted at Heartspring, where data were collected on two children with severe autism. The long duration study tested the bed system's capability to operate in such an environment for a prolonged period of time. Heartbeat intervals, respiration rates, and motion

activity were tracked each night for the duration of study. The success with running the bed system remotely for this study indicates that the bed system can be utilized for even longer studies and greater numbers of children – studies which will be needed to fully develop the relationship between sleep quality and daytime functionality for this population.

References

[1] U. E. Bauer, P. A. Briss, R. A. Goodman, and B. A. Bowman, "Prevention of chronic disease in the 21st century: elimination of the leading preventable causes of premature death and disability in the USA," *The Lancet*, vol. 384, no. 9937, pp. 45–52, Jul. 2014.

[2] "Population Clock." [Online]. Available: https://www.census.gov/popclock/. [Accessed: 05-Mar-2019].

[3] T. M. Dall, P. D. Gallo, R. Chakrabarti, T. West, A. P. Semilla, and M. V. Storm, "An aging population and growing disease burden will require a large and specialized health care workforce by 2025," *Health Aff. Proj. Hope*, vol. 32, no. 11, pp. 2013–2020, Nov. 2013.

[4] D. J. Pallin, C. A. Camargo, J. A. Espinola, and D. J. Pallin, "US population aging and demand for inpatient services," *J. Hosp. Med.*, vol. 9, no. 3, Mar. 2014.

[5] R. A. Cohen and W. K. Kirzinger, "Financial burden of medical care: a family perspective," *NCHS Data Brief*, no. 142, pp. 1–8, Jan. 2014.

[6] T. Coughlin, "ICCE Tricorder Session Explores the Future of Home Health Care [Conference Review]," *IEEE Consum. Electron. Mag.*, vol. 2, no. 3, pp. 49–51, Jul. 2013.

[7] B. E. Lewis, "Narrative Medicine and Healthcare Reform," *J. Med. Humanit.*, vol. 32, no. 1, pp. 9–20, Mar. 2011.

[8] S. Adeyemi, E. Demir, and T. Chaussalet, "Towards an evidence-based decision making healthcare system management: Modelling patient pathways to improve clinical outcomes," *Decis. Support Syst.*, vol. 55, no. 1, pp. 117–125, Apr. 2013.

[9] M. Pavel *et al.*, "The Role of Technology and Engineering Models in Transforming Healthcare," *IEEE Rev. Biomed. Eng.*, vol. 6, pp. 156–177, 2013.

[10] A. P. Dhawan, "Collaborative Paradigm of Preventive, Personalized, and Precision Medicine With Point-of-Care Technologies," *IEEE J. Transl. Eng. Health Med.*, vol. 4, pp. 1–8, 2016.

[11] M. Harris and J. Habetha, "The MyHeart project: A framework for personal health care applications," in *2007 Computers in Cardiology*, 2007, pp. 137–140.

[12] J. Yoon, C. Davtyan, and M. van der Schaar, "Discovery and Clinical Decision Support for Personalized Healthcare," *IEEE J. Biomed. Health Inform.*, vol. 21, no. 4, pp. 1133–1145, Jul. 2017.

[13] N. V. Chawla and D. A. Davis, "Bringing Big Data to Personalized Healthcare: A Patient-Centered Framework," *J. Gen. Intern. Med.*, vol. 28, no. 3, pp. 660–665, Sep. 2013.

[14] J. Kim, N. Liu, H. Tan, and C. Chu, "Unobtrusive Monitoring to Detect Depression for Elderly With Chronic Illnesses," *IEEE Sens. J.*, vol. 17, no. 17, pp. 5694–5704, Sep. 2017.

[15] Y. Zheng *et al.*, "Unobtrusive Sensing and Wearable Devices for Health Informatics," *IEEE Trans. Biomed. Eng.*, vol. 61, no. 5, pp. 1538–1554, May 2014.

[16] L. Samy, M. Huang, J. J. Liu, W. Xu, and M. Sarrafzadeh, "Unobtrusive Sleep Stage Identification Using a Pressure-Sensitive Bed Sheet," *IEEE Sens. J.*, vol. 14, no. 7, pp. 2092–2101, Jul. 2014.

[17] "EMFIT Sleep Tracking & Monitoring with Heart-Rate-Variability," *EMFIT*. [Online]. Available: https://www.emfit.com. [Accessed: 05-Mar-2019].

[18] "QS+ACTIVE^{TM} – contact free health and sleep tracker with heart-rate-var," *Emfit Ltd · Webshop EU*. [Online]. Available: https://shop-eu.emfit.com/products/emfit-qs. [Accessed: 05-Mar-2019].
[19] "Beddit Sleep Monitor." [Online]. Available: https://www.beddit.com/. [Accessed: 05-Mar-2019].
[20] J. W. Gordon, "Certain Molar Movements of the Human Body produced by the Circulation of the Blood," *J Anat Physiol*, vol. 11, pp. 533–536, 1877.
[21] W. Dock and F. Taubman, "Some technics for recording the ballistocardiogram directly from the body," *Am. J. Med.*, vol. 7, no. 6, pp. 751–755, Dec. 1949.
[22] Issac Starr, A. J. Rawson, H. Schroeder, and N. R. Joseph, "Studies on the estimation of cardiac output in man, and of abnormalities in cardiac function, from the heart's recoil and the blood's impacts; the ballistocardiogram," *Amer J Phys*, vol. 127, pp. 1–28, 1939.
[23] H. W. Lewis, D. H. Smith, and M. R. Lewis, "Ballistocardiographic Instrumentation," *Rev. Sci. Instrum.*, vol. 27, no. 10, pp. 835–837, Oct. 1956.
[24] I. Starr and A. Noordergraaf, *Ballistocardiography in cardiovascular research: Physical aspects of the circulation in health and disease.* Philadelphia, PA: Lippincott, 1967.
[25] L. Giovangrandi, O. T. Inan, R. M. Wiard, M. Etemadi, and G. T. A. Kovacs, "Ballistocardiography - A method worth revisiting," in *2011 Annual International Conference of the IEEE Engineering in Medicine and Biology Society*, Boston, MA, 2011, pp. 4279–4282.
[26] O. T. Inan *et al.*, "Ballistocardiography and Seismocardiography: A Review of Recent Advances," *IEEE J. Biomed. Health Inform.*, vol. 19, no. 4, pp. 1414–1427, Jul. 2015.
[27] "Heartspring." [Online]. Available: https://www.heartspring.org/. [Accessed: 17-Mar-2019].
[28] J. F. Dewald, A. M. Meijer, F. J. Oort, G. A. Kerkhof, and S. M. Bögels, "The influence of sleep quality, sleep duration and sleepiness on school performance in children and adolescents: A meta-analytic review," *Sleep Med. Rev.*, vol. 14, no. 3, pp. 179–189, Jun. 2010.
[29] S. Cohen, R. Conduit, S. W. Lockley, S. M. Rajaratnam, and K. M. Cornish, "The relationship between sleep and behavior in autism spectrum disorder (ASD): a review," *J. Neurodev. Disord.*, vol. 6, no. 1, p. 44, 2014.
[30] A. L. Richdale, "Autism and Other Developmental Disabilities," in *Oxford Handbook of Infant, Child, and Adolescent Sleep and Behavior*, A. Wolfson and H. Montgomery-Downs, Eds., 2013, pp. 471–494.
[31] Y. Lin *et al.*, "0321 Wearable Device ECG and G-Sensor-based Sleep Stage Evaluation using PSG-based Learning Signal," *Sleep*, vol. 41, no. suppl_1, pp. A123–A123, Apr. 2018.
[32] D. J. Buysse, C. F. Reynolds, T. H. Monk, Hoch, A. L. Yeager, and D. J. Kupfer, "Quantification of Subjective Sleep Quality in Healthy Elderly Men and Women Using the Pittsburgh Sleep Quality Index (PSQI)," *Sleep*, vol. 14, no. 4, pp. 331–338, Jul. 1991.
[33] C. R. Johnson *et al.*, "Exploring sleep quality of young children with autism spectrum disorder and disruptive behaviors," *Sleep Med.*, vol. 44, pp. 61–66, Apr. 2018.
[34] A. Lambert, S. Tessier, A.-C. Rochette, P. Scherzer, L. Mottron, and R. Godbout, "Poor sleep affects daytime functioning in typically developing and autistic children not complaining of sleep problems: A questionnaire-based and polysomnographic study," *Res. Autism Spectr. Disord.*, vol. 23, pp. 94–106, Mar. 2016.

[35] A. J. Esbensen, E. K. Hoffman, E. Stansberry, and R. Shaffer, “Convergent validity of actigraphy with polysomnography and parent reports when measuring sleep in children with Down syndrome,” *J. Intellect. Disabil. Res. JIDR*, vol. 62, no. 4, pp. 281–291, Apr. 2018.

[36] B. A. Malow, M. L. Marzec, S. G. McGrew, L. Wang, L. M. Henderson, and W. L. Stone, “Characterizing sleep in children with autism spectrum disorders: a multidimensional approach,” *Sleep*, vol. 29, no. 12, pp. 1563–1571, Dec. 2006.

[37] Y. Tatsumi, I. Mohri, S. Shimizu, M. Tachibana, Y. Ohno, and M. Taniike, “Daytime physical activity and sleep in preschoolers with developmental disorders,” *J. Paediatr. Child Health*, vol. 51, no. 4, pp. 396–402, Apr. 2015.

[38] C. R. Johnson, K. S. Turner, E. Foldes, M. M. Brooks, R. Kronk, and L. Wiggs, “Behavioral parent training to address sleep disturbances in young children with autism spectrum disorder: a pilot trial,” *Sleep Med.*, vol. 14, no. 10, pp. 995–1004, Oct. 2013.

[39] “CentrePoint Insight Watch | ActiGraph.” [Online]. Available: https://www.actigraphcorp.com/cpiw/. [Accessed: 01-Apr-2019].

[40] “Philips - Actiwatch 2 Activity monitor,” *Philips*. [Online]. Available: https://www.usa.philips.com/healthcare/product/HC1044809/actiwatch-2-activity-monitor. [Accessed: 01-Apr-2019].

[41] S. Cohen *et al.*, “Sleep patterns predictive of daytime challenging behavior in individuals with low-functioning autism,” *Autism Res.*, vol. 11, no. 2, pp. 391–403, 2018.

[42] O. T. Inan, M. Etemadi, R. M. Wiard, L. Giovangrandi, and G. T. A. Kovacs, “Robust ballistocardiogram acquisition for home monitoring,” *Physiol. Meas.*, vol. 30, no. 2, pp. 169–185, Feb. 2009.

[43] A. D. Wiens, M. Etemadi, S. Roy, L. Klein, and O. T. Inan, “Toward Continuous, Noninvasive Assessment of Ventricular Function and Hemodynamics: Wearable Ballistocardiography,” *IEEE J. Biomed. Health Inform.*, vol. 19, no. 4, pp. 1435–1442, Jul. 2015.

[44] D. Shao, F. Tsow, C. Liu, Y. Yang, and N. Tao, “Simultaneous Monitoring of Ballistocardiogram and Photoplethysmogram Using a Camera,” *IEEE Trans. Biomed. Eng.*, vol. 64, no. 5, pp. 1003–1010, May 2017.

[45] C.-S. Kim *et al.*, “Ballistocardiogram: Mechanism and Potential for Unobtrusive Cardiovascular Health Monitoring,” *Sci. Rep.*, vol. 6, no. 1, Nov. 2016.

[46] C. Carlson *et al.*, “Bed-based instrumentation for unobtrusive sleep quality assessment in severely disabled autistic children,” in *2016 38th Annual International Conference of the IEEE Engineering in Medicine and Biology Society (EMBC)*, 2016, pp. 4909–4912.

[47] P. Fonseca, X. Long, M. Radha, R. Haakma, R. M. Aarts, and J. Rolink, “Sleep stage classification with ECG and respiratory effort,” *Physiol. Meas.*, vol. 36, no. 10, pp. 2027–2040, Oct. 2015.

[48] S. J. Redmond, P. de Chazal, C. O’Brien, S. Ryan, W. T. McNicholas, and C. Heneghan, “Sleep staging using cardiorespiratory signals,” *Somnologie - Schlafforschung Schlafmed.*, vol. 11, no. 4, pp. 245–256, Dec. 2007.

[49] J. M. Kortelainen, M. O. Mendez, A. M. Bianchi, M. Matteucci, and S. Cerutti, “Sleep Staging Based on Signals Acquired Through Bed Sensor,” *IEEE Trans. Inf. Technol. Biomed.*, vol. 14, no. 3, pp. 776–785, May 2010.

[50] C. Kuo, Y. Liu, D. Chang, C. Young, F. Shaw, and S. Liang, “Development and Evaluation of a Wearable Device for Sleep Quality Assessment,” *IEEE Trans. Biomed. Eng.*, vol. 64, no. 7, pp. 1547–1557, Jul. 2017.
[51] X. Long, P. Fonseca, J. Foussier, R. Haakma, and R. M. Aarts, “Sleep and Wake Classification With Actigraphy and Respiratory Effort Using Dynamic Warping,” *IEEE J. Biomed. Health Inform.*, vol. 18, no. 4, pp. 1272–1284, Jul. 2014.
[52] A. Alivar *et al.*, “Motion Detection in Bed-Based Ballistocardiogram to Quantify Sleep Quality,” in *GLOBECOM 2017 - 2017 IEEE Global Communications Conference*, 2017, pp. 1–6.
[53] C. Bruser, J. M. Kortelainen, S. Winter, M. Tenhunen, J. Parkka, and S. Leonhardt, “Improvement of force-sensor-based heart rate estimation using multichannel data fusion,” *IEEE J. Biomed. Health Inform.*, vol. 19, no. 1, pp. 227–235, Jan. 2015.
[54] B. H. Choi, G. S. Chung, J.-S. Lee, D.-U. Jeong, and K. S. Park, “Slow-wave sleep estimation on a load-cell-installed bed: a non-constrained method,” *Physiol. Meas.*, vol. 30, no. 11, pp. 1163–1170, Nov. 2009.
[55] A. O. Bicen, D. Whittingslow, and O. Inan, “Template-Based Statistical Modeling and Synthesis for Noise Analysis of Ballistocardiogram Signals: A Cycle-Averaged Approach,” *IEEE J. Biomed. Health Inform.*, pp. 1–1, 2018.
[56] I. Starr and H. A. Schroeder, “Ballistocardiogram. II. normal standards, abnormalities commonly found in diseases of the heart and circulation, and their significance,” *J. Clin. Invest.*, vol. 19, no. 3, pp. 437–450, May 1940.
[57] Y. Henderson, “The mass movements of the circulation as shown by a recoil curve,” *Amer J Phys*, vol. 14, pp. 287–298, 1905.
[58] S. L.-O. Martin *et al.*, “Weighing Scale-Based Pulse Transit Time is a Superior Marker of Blood Pressure than Conventional Pulse Arrival Time,” *Sci. Rep.*, vol. 6, no. 1, Dec. 2016.
[59] A. Q. Javaid, I. S. Chang, and A. Mihailidis, “Ballistocardiogram Based Identity Recognition: Towards Zero-Effort Health Monitoring in an Internet-of-Things (IoT) Environment,” in *2018 40th Annual International Conference of the IEEE Engineering in Medicine and Biology Society (EMBC)*, 2018, pp. 3326–3329.
[60] B. J. M. van Rooij, K. Tavakolian, S. Arzanpour, A. P. Blaber, and C. A. D. Leguy, “Non-invasive estimation of cardiovascular parameters using ballistocardiography,” in *2015 37th Annual International Conference of the IEEE Engineering in Medicine and Biology Society (EMBC)*, Milan, 2015, pp. 1247–1250.
[61] M. Takano and A. Ueno, “Noncontact In-Bed Measurements of Physiological and Behavioral Signals Using an Integrated Fabric-Sheet Sensing Scheme,” *IEEE J. Biomed. Health Inform.*, pp. 1–1, 2018.
[62] A. Martín-Yebra *et al.*, “Studying heart rate variability from ballistocardiography acquired by force platform: Comparison with conventional ECG,” in *2015 Computing in Cardiology Conference (CinC)*, 2015, pp. 929–932.
[63] A. Eblen-Zajjur, “A SIMPLE BALLISTOCARDIOGRAPHIC SYSTEM FOR A MEDICAL CARDIOVASCULAR PHYSIOLOGY COURSE,” *Adv. Physiol. Educ.*, vol. 27, no. 4, pp. 224–229, Dec. 2003.
[64] A. D. Wiens and O. T. Inan, “Accelerometer body sensor network improves systolic time interval assessment with wearable ballistocardiography,” in *2015 37th Annual*

International Conference of the IEEE Engineering in Medicine and Biology Society (EMBC), 2015, pp. 1833–1836.

[65] and W. Jianqi, Y. Yu, and J. Xijing, "Study of the Ballistocardiogram signal in life detection system based on radar," in *2007 29th Annual International Conference of the IEEE Engineering in Medicine and Biology Society*, 2007, pp. 2191–2194.

[66] G. Fierro, F. Silveira, and R. Armentano, "Low group delay signal conditioning for wearable central blood pressure monitoring device," in *2017 39th Annual International Conference of the IEEE Engineering in Medicine and Biology Society (EMBC)*, 2017, pp. 3285–3288.

[67] J. M. Kortelainen and J. Virkkala, "FFT averaging of multichannel BCG signals from bed mattress sensor to improve estimation of heart beat interval," *Conf. Proc. Annu. Int. Conf. IEEE Eng. Med. Biol. Soc. IEEE Eng. Med. Biol. Soc. Annu. Conf.*, vol. 2007, pp. 6686–6689, 2007.

[68] H. Ashouri and O. T. Inan, "Improving the accuracy of proximal timing detection from ballistocardiogram signals using a high bandwidth force plate," in *2016 IEEE-EMBS International Conference on Biomedical and Health Informatics (BHI)*, 2016, pp. 553–556.

[69] C. Brüser, S. Winter, and S. Leonhardt, "Robust inter-beat interval estimation in cardiac vibration signals," *Physiol. Meas.*, vol. 34, no. 2, pp. 123–138, Feb. 2013.

[70] C. Carlson *et al.*, "A Pilot Study of an Unobtrusive Bed-Based Sleep Quality Monitor for Severely Disabled Autistic Children*," in *2018 40th Annual International Conference of the IEEE Engineering in Medicine and Biology Society (EMBC)*, 2018, pp. 4343–4346.

[71] W. Jia, Y. Li, Y. Bai, Z. Mao, M. Sun, and Q. Zhao, "Estimation of heart rate from a chest-worn inertial measurement unit," in *2015 International Symposium on Bioelectronics and Bioinformatics (ISBB)*, 2015, pp. 148–151.

[72] A. D. Wiens and O. T. Inan, "A Novel System Identification Technique for Improved Wearable Hemodynamics Assessment," *IEEE Trans. Biomed. Eng.*, vol. 62, no. 5, pp. 1345–1354, May 2015.

[73] H. J. Baek, G. S. Chung, K. K. Kim, and K. S. Park, "A Smart Health Monitoring Chair for Nonintrusive Measurement of Biological Signals," *IEEE Trans. Inf. Technol. Biomed.*, vol. 16, no. 1, pp. 150–158, Jan. 2012.

[74] E. J. Pino, C. Larsen, J. Chavez, and P. Aqueveque, "Non-invasive BCG monitoring for non-traditional settings," in *2016 38th Annual International Conference of the IEEE Engineering in Medicine and Biology Society (EMBC)*, 2016, pp. 4776–4779.

[75] W. R. Scarborough *et al.*, "Proposals for Ballistocardiographic Nomenclature and Conventions: Revised and Extended: Report of Committee on Ballistocardiographic Terminology," *Circulation*, vol. 14, no. 3, pp. 435–450, Sep. 1956.

[76] I. Starr *et al.*, "First Report of the Committee on Ballisto- cardiographic Terminology," *Circulation*, vol. VII, pp. 929–931, Jun. 1953.

[77] Talbot Samuel A. and Harrison W. Kirby, "Dynamic Comparison of Current Ballistocardiographic Methods," *Circulation*, vol. 12, no. 4, pp. 577–587, Oct. 1955.

[78] Talbot Samuel A. and Harrison W. Kirby, "Dynamic Comparison of Current Ballistocardiographic Methods," *Circulation*, vol. 12, no. 5, pp. 845–857, Nov. 1955.

[79] Talbot S. A. and Harrison W. K., "Dynamic Comparison of Current Ballistocardiographic Methods," *Circulation*, vol. 12, no. 6, pp. 1022–1033, Dec. 1955.

[80] H. C. Burger, A. Noordergraaf, and H. J. L. Kamps, “Physical Basis of Ballistocardiography. V: The distortion of the ballistocardiogram caused by the movement of the heart inside the body.,” *Am. Heart J.*, vol. 53, no. 6, pp. 907–921, Jun. 1957.
[81] S. A. Talbot, D. C. Deuchar, F. W. Davis, and W. R. Scarborough, “The aperiodic ballistocardiograph,” *Bull. Johns Hopkins Hosp.*, vol. 94, no. 1, pp. 27–33, Jan. 1954.
[82] W. K. Harrison and S. A. Talbot, “Two new forms of ultra-low frequency ballistocardiograph,” *Bibl. Cardiol.*, no. 19, pp. 13–18, 1967.
[83] W. R. Scarborough and D. H. Smith, “1. The ballistocardiograph research society: a history of its first decade and remarks on progress in research, 1956-1967,” *Bibl. Cardiol.*, vol. 20, pp. 129–165, 1968.
[84] J. L. Nickerson and H. J. Curtis, “The design of the ballistocardiograph,” p. 11.
[85] C. Ambrosi and I. Starr, “High-frequency shin-bar ballistocardiograms, a method of greatly improving simple shin-bar records,” *Am. Heart J.*, vol. 68, no. 4, pp. 500–507, Oct. 1964.
[86] S. R. Arbeit and N. Lindner, “A new full-frequency range calibrated ballistocardiograph. I. Recording the body ballistics in displacement, velocity, and acceleration,” *Am. Heart J.*, vol. 45, no. 1, pp. 52–59, Jan. 1953.
[87] P. S. Luna and R. Pallas, “Automatic Concealed Heart Rate Detection from the BCG in Seated Position,” *IEEE Lat. Am. Trans.*, vol. 13, no. 3, pp. 583–588, Mar. 2015.
[88] Y. Yao *et al.*, “Mitigation of Instrument-Dependent Variability in Ballistocardiogram Morphology: Case Study on Force Plate and Customized Weighing Scale,” *IEEE J. Biomed. Health Inform.*, pp. 1–1, 2019.
[89] A. Q. Javaid, A. D. Wiens, N. F. Fesmire, M. A. Weitnauer, and O. T. Inan, “Quantifying and Reducing Posture-Dependent Distortion in Ballistocardiogram Measurements,” *IEEE J. Biomed. Health Inform.*, vol. 19, no. 5, pp. 1549–1556, Sep. 2015.
[90] T. Koivistoinen, S. Junnila, A. Varri, and T. Koobi, “A new method for measuring the ballistocardiogram using EMFi sensors in a normal chair,” in *The 26th Annual International Conference of the IEEE Engineering in Medicine and Biology Society*, 2004, vol. 1, pp. 2026–2029.
[91] J. L. Nickerson, “Studies on the natural frequency and damping of internal organs in relation to the origin of the whole body ballistocardiogram,” *Am. J. Cardiol.*, vol. 12, no. 4, p. 580, Oct. 1963.
[92] I. Hoffman, M. Kissin, and M. M. Schwarzschild, “Oscillation-Free Ballistocardiography: A Simple Technic and a Demonstration of Its Validity,” *Circulation*, vol. 13, no. 6, pp. 905–908, Jun. 1956.
[93] M. Tobin, J. N. Edson, R. Dickes, G. H. Flamm, and L. Deutsch, “The elimination of body resonance distortion from the direct-body ballistocardiogram,” *Circulation*, vol. 12, no. 1, pp. 108–113, Jul. 1955.
[94] K. Lydon *et al.*, “Robust heartbeat detection from in-home ballistocardiogram signals of older adults using a bed sensor,” in *2015 37th Annual International Conference of the IEEE Engineering in Medicine and Biology Society (EMBC)*, 2015, pp. 7175–7179.
[95] D. D. He, E. S. Winokur, and C. G. Sodini, “A continuous, wearable, and wireless heart monitor using head ballistocardiogram (BCG) and head electrocardiogram (ECG),” in *2011 Annual International Conference of the IEEE Engineering in Medicine and Biology Society*, 2011, pp. 4729–4732.

[96] W. C. Hixson and D. E. Beischer, “Biotelemetry of the triaxial ballistocardiogram and electrocardiogram in a weightless envrionment. Monograph No. 10,” *Res. Rep. Nav. Sch. Aviat. Med. US*, pp. 1–112, Sep. 1964.
[97] G. K. Prisk, S. Verhaeghe, D. Padeken, H. Hamacher, and M. Paiva, “Three-dimensional ballistocardiography and respiratory motion in sustained microgravity,” *Aviat. Space Environ. Med.*, vol. 72, no. 12, pp. 1067–1074, Dec. 2001.
[98] G. K. Prisk and P. Migeotte, “Physiological insights from gravity-free ballistocardiography,” in *2013 35th Annual International Conference of the IEEE Engineering in Medicine and Biology Society (EMBC)*, 2013, pp. 7282–7285.
[99] V. G. Koutkias, I. Chouvarda, A. Triantafyllidis, A. Malousi, G. D. Giaglis, and N. Maglaveras, “A Personalized Framework for Medication Treatment Management in Chronic Care,” *IEEE Trans. Inf. Technol. Biomed.*, vol. 14, no. 2, pp. 464–472, Mar. 2010.
[100] K. K. Venkatasubramanian, A. Banerjee, and S. K. S. Gupta, “PSKA: Usable and Secure Key Agreement Scheme for Body Area Networks,” *IEEE Trans. Inf. Technol. Biomed.*, vol. 14, no. 1, pp. 60–68, Jan. 2010.
[101] S. T. Ali, V. Sivaraman, D. Ostry, G. Tsudik, and S. Jha, “Securing First-Hop Data Provenance for Bodyworn Devices Using Wireless Link Fingerprints,” *IEEE Trans. Inf. Forensics Secur.*, vol. 9, no. 12, pp. 2193–2204, Dec. 2014.
[102] E. A. McGlynn *et al.*, “The Quality of Health Care Delivered to Adults in the United States,” *N. Engl. J. Med.*, vol. 348, no. 26, pp. 2635–2645, Jun. 2003.
[103] A. Akl, B. Taati, and A. Mihailidis, “Autonomous Unobtrusive Detection of Mild Cognitive Impairment in Older Adults,” *IEEE Trans. Biomed. Eng.*, vol. 62, no. 5, pp. 1383–1394, May 2015.
[104] S. Majumder, L. Chen, O. Marinov, C. Chen, T. Mondal, and M. J. Deen, “Noncontact Wearable Wireless ECG Systems for Long-Term Monitoring,” *IEEE Rev. Biomed. Eng.*, vol. 11, pp. 306–321, 2018.
[105] J. Sakuma, D. Anzai, and J. Wang, “Performance of human body communication-based wearable ECG with capacitive coupling electrodes,” *Healthc. Technol. Lett.*, vol. 3, no. 3, pp. 222–225, 2016.
[106] J. Wannenburg, R. Malekian, and G. P. Hancke, “Wireless Capacitive-Based ECG Sensing for Feature Extraction and Mobile Health Monitoring,” *IEEE Sens. J.*, vol. 18, no. 14, pp. 6023–6032, Jul. 2018.
[107] “Automated Test and Automated Measurement Systems - National Instruments.” [Online]. Available: http://www.ni.com/en-us.html. [Accessed: 01-Apr-2019].
[108] R. P. Foundation, “Raspberry Pi — Teach, Learn, and Make with Raspberry Pi,” *Raspberry Pi*. [Online]. Available: https://www.raspberrypi.org. [Accessed: 21-Jan-2019].
[109] “Specification for the LabVIEW Measurement File (.lvm) - National Instruments.” [Online]. Available: http://www.ni.com/tutorial/4139/en/. [Accessed: 01-Apr-2019].
[110] S. Rajala and J. Lekkala, “Film-Type Sensor Materials PVDF and EMFi in Measurement of Cardiorespiratory Signals— A Review,” *IEEE Sens. J.*, vol. 12, no. 3, pp. 439–446, Mar. 2012.
[111] J. Gomez-Clapers, A. Serra-Rocamora, R. Casanella, and R. Pallas-Areny, “Uncertainty factors in time-interval measurements in ballistocardiography,” p. 5, 2013.

[112] K. Watanabe, T. Watanabe, H. Watanabe, H. Ando, T. Ishikawa, and K. Kobayashi, "Noninvasive measurement of heartbeat, respiration, snoring and body movements of a subject in bed via a pneumatic method," *IEEE Trans. Biomed. Eng.*, vol. 52, no. 12, pp. 2100–2107, Dec. 2005.
[113] J. H. Shin, B. H. Choi, Y. G. Lim, D. U. Jeong, and K. S. Park, "Automatic ballistocardiogram (BCG) beat detection using a template matching approach," in *2008 30th Annual International Conference of the IEEE Engineering in Medicine and Biology Society*, 2008, pp. 1144–1146.
[114] J. Pan and W. J. Tompkins, "A Real-Time QRS Detection Algorithm," *IEEE Trans. Biomed. Eng.*, vol. BME-32, no. 3, pp. 230–236, Mar. 1985.
[115] J. Alametsä, A. Palomäki, and J. Viik, "Local ballistocardiographic spectrum studies from signals obtained from limbs and carotid artery with an EMFi sensor induced with a tilt table," *Conf. Proc. Annu. Int. Conf. IEEE Eng. Med. Biol. Soc. IEEE Eng. Med. Biol. Soc. Annu. Conf.*, vol. 2013, pp. 7008–7011, 2013.
[116] C. McCall *et al.*, "Standing ballistocardiography measurements in microgravity," in *2014 36th Annual International Conference of the IEEE Engineering in Medicine and Biology Society*, 2014, pp. 5180–5183.
[117] N. Bershad and A. Rockmore, "On estimating signal-to-noise ratio using the sample correlation coefficient (Corresp.)," *IEEE Trans. Inf. Theory*, vol. 20, no. 1, pp. 112–113, Jan. 1974.
[118] G. Singleton, S. Warren, and W. Piersel, "Clinical overview of the need for technologies for around-the-clock monitoring of the health status of severely disabled autistic children," in *2014 36th Annual International Conference of the IEEE Engineering in Medicine and Biology Society*, 2014, pp. 789–791.
[119] A. Suliman, C. Carlson, S. Warren, and D. Thompson, "Performance Evaluation of Processing Methods for Ballistocardiogram Peak Detection," in *2018 40th Annual International Conference of the IEEE Engineering in Medicine and Biology Society (EMBC)*, 2018, pp. 502–505.
[120] O. T. Inan, M. Etemadi, R. M. Wiard, G. T. A. Kovacs, and L. Giovangrandi, "Non-invasive measurement of Valsalva-induced hemodynamic changes on a bathroom scale ballistocardiograph," *Conf. Proc. Annu. Int. Conf. IEEE Eng. Med. Biol. Soc. IEEE Eng. Med. Biol. Soc. Annu. Conf.*, vol. 2008, pp. 674–677, 2008.
[121] C.-S. Kim, A. M. Carek, R. Mukkamala, O. T. Inan, and J.-O. Hahn, "Ballistocardiogram as Proximal Timing Reference for Pulse Transit Time Measurement: Potential for Cuffless Blood Pressure Monitoring," *IEEE Trans. Biomed. Eng.*, vol. 62, no. 11, pp. 2657–2664, Nov. 2015.
[122] I. Sadek, J. Biswas, B. Abdulrazak, Z. Haihong, and M. Mokhtari, "Continuous and unconstrained vital signs monitoring with ballistocardiogram sensors in headrest position," in *2017 IEEE EMBS International Conference on Biomedical Health Informatics (BHI)*, 2017, pp. 289–292.
[123] A. Alivar *et al.*, "Motion Artifact Detection and Reduction in Bed-Based Ballistocardiogram," *IEEE Access*, vol. 7, pp. 13693–13703, 2019.
[124] S. Junnila, A. Akhbardeh, A. Varri, and T. Koivistoinen, "An EMFi-film sensor based ballistocardiographic chair: performance and cycle extraction method," in *IEEE Workshop on Signal Processing Systems Design and Implementation, 2005.*, 2005, pp. 373–377.

[125] J. Paalasmaa, H. Toivonen, and M. Partinen, “Adaptive Heartbeat Modeling for Beat-to-Beat Heart Rate Measurement in Ballistocardiograms,” *IEEE J. Biomed. Health Inform.*, vol. 19, no. 6, pp. 1945–1952, Nov. 2015.
[126] C. Bruser, K. Stadlthanner, S. de Waele, and S. Leonhardt, “Adaptive Beat-to-Beat Heart Rate Estimation in Ballistocardiograms,” *IEEE Trans. Inf. Technol. Biomed.*, vol. 15, no. 5, pp. 778–786, Sep. 2011.
[127] D. O’Shaughnessy, “Linear predictive coding,” *IEEE Potentials*, vol. 7, no. 1, pp. 29–32, Feb. 1988.
[128] “One-sample and paired-sample t-test - MATLAB ttest.” [Online]. Available: https://www.mathworks.com/help/stats/ttest.html. [Accessed: 04-Apr-2019].
[129] “One-sample Kolmogorov-Smirnov test - MATLAB kstest.” [Online]. Available: https://www.mathworks.com/help/stats/kstest.html. [Accessed: 04-Apr-2019].
[130] R. Harder *et al.*, “Heart rate variability during sleep in children with autism spectrum disorder,” *Clin. Auton. Res. Off. J. Clin. Auton. Res. Soc.*, vol. 26, no. 6, pp. 423–432, Dec. 2016.

Appendix A - Robust Heartbeat Interval Estimation and Fusion Technique

The complete algorithm from [69] has two main sections: a basic algorithm and an extended algorithm. In the basic algorithm, the following approach is used to detect continuous heartbeat intervals using an overlapping sliding window with a small step size.

Basic Algorithm. The basic algorithm provides HBI estimates:

1. Within the windowed data, calculate three functions (a-c) that are lag-dependent.
    a. Modified autocorrelation.
    b. Modified average magnitude difference.
    c. Maximum amplitude pairs.
2. Interpreting the three estimates as posterior probability density functions, combine the three estimates into a joint probability density function.
3. Find the maximum point in the joint PDF. This is the estimated local interval length.
4. Shift the window by a small constant Δt and repeat steps 1 through 3.

Given the small window shift, several estimates will correspond to the same HBI. Thus, an extended algorithm is needed to reduce the number of estimates to one for each HBI.

Extended Algorithm. The extended algorithm reduces duplicate HBI estimates to one HBI:

1. For each segment of windowed data, find the set of peaks in the right half of the analysis window.
2. Using the estimated local interval length, N_i, determine the right boundary peak (P_i), as

$$P_i = n_i + arg\max_{m \epsilon M_i}(w_i[m] + w_i[m - N_i]). \quad (30)$$

    where w_i is the current window of data under analysis, M_i is the set of peaks within the right half of the analysis window, and n_i is the center of the analysis window. The extended algorithm determines anchor points in each analysis window that can be used to combine similar heartbeat estimates.
3. Find the set of unique peaks among the set of estimated right boundary points.
4. Group the local interval lengths together that correspond to unique right boundary peaks (a.k.a., anchor points).

    Calculate the median local interval length for each set as the final HBI estimate.

The algorithm outputs the estimated HBIs along with a corresponding estimated peak location. For the fusion approach, instead of combining three lag-dependent functions, there are three functions for each sensor. Thus, for the bed-based system comprised of eight sensors, 24 posterior probability density functions are combined into one joint probability density function. The local beat intervals are computed in the same fashion as the outlined Basic Algorithm.

For the Extended Algorithm, a single waveform is needed to determine the right boundary points. A simple technique to create the single waveform can be implemented by computing the average across time for all of the signals. However, with the bed system being comprised of multiple sensors having a large distance between them, BCGs recorded by the various sensors are often out of phase with each other. To help mitigate this, a single sensor's BCG (typically Film sensor 0) is used as a reference, and the other BCG waveforms are corrected if they are out of phase. To accomplish this, the correlation coefficient is computed between the reference BCG and every other recorded BCG. If the correlation coefficient is negative, the BCG under question is inverted. After the single, time-averaged waveform is calculated, the Extended Algorithm is computed in the same manner as the single-channel approach.

Appendix B - Custom Hardware Printed Circuit Board Design

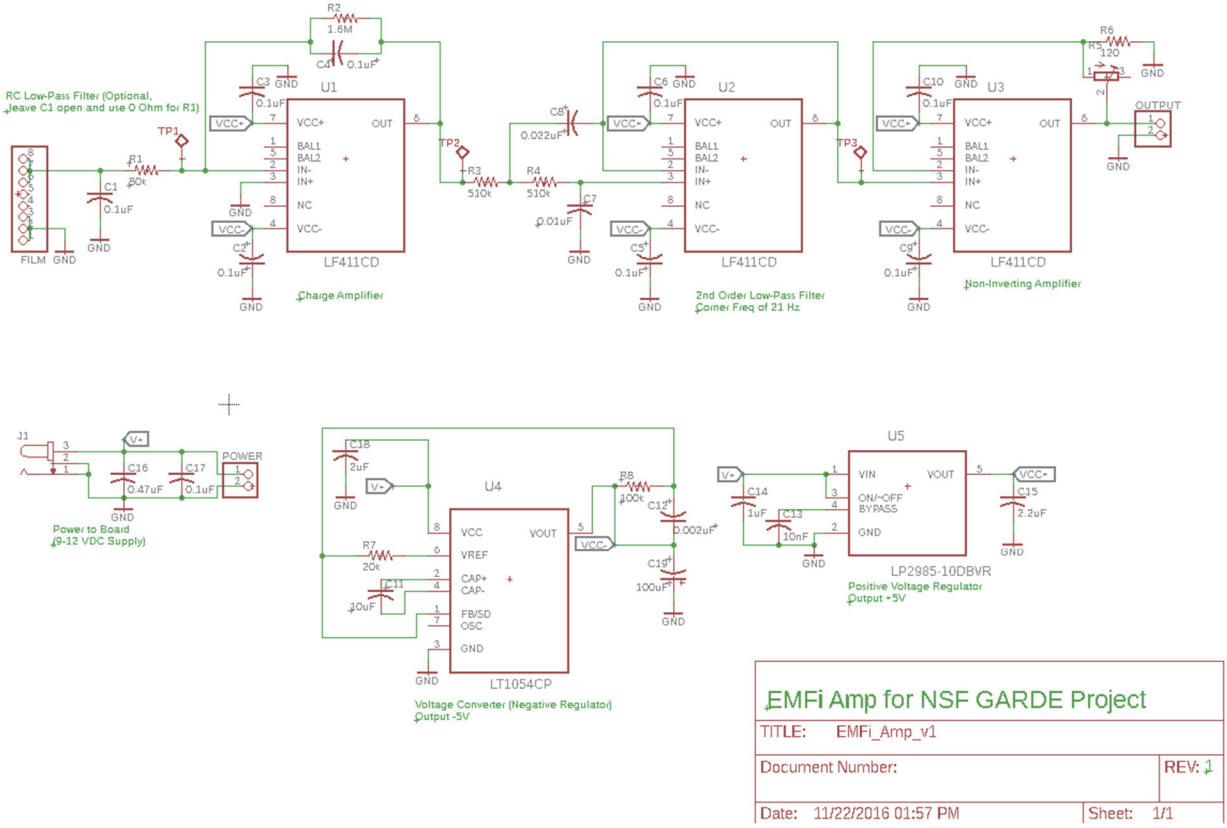

Figure B-1. Circuit board schematic version 1.

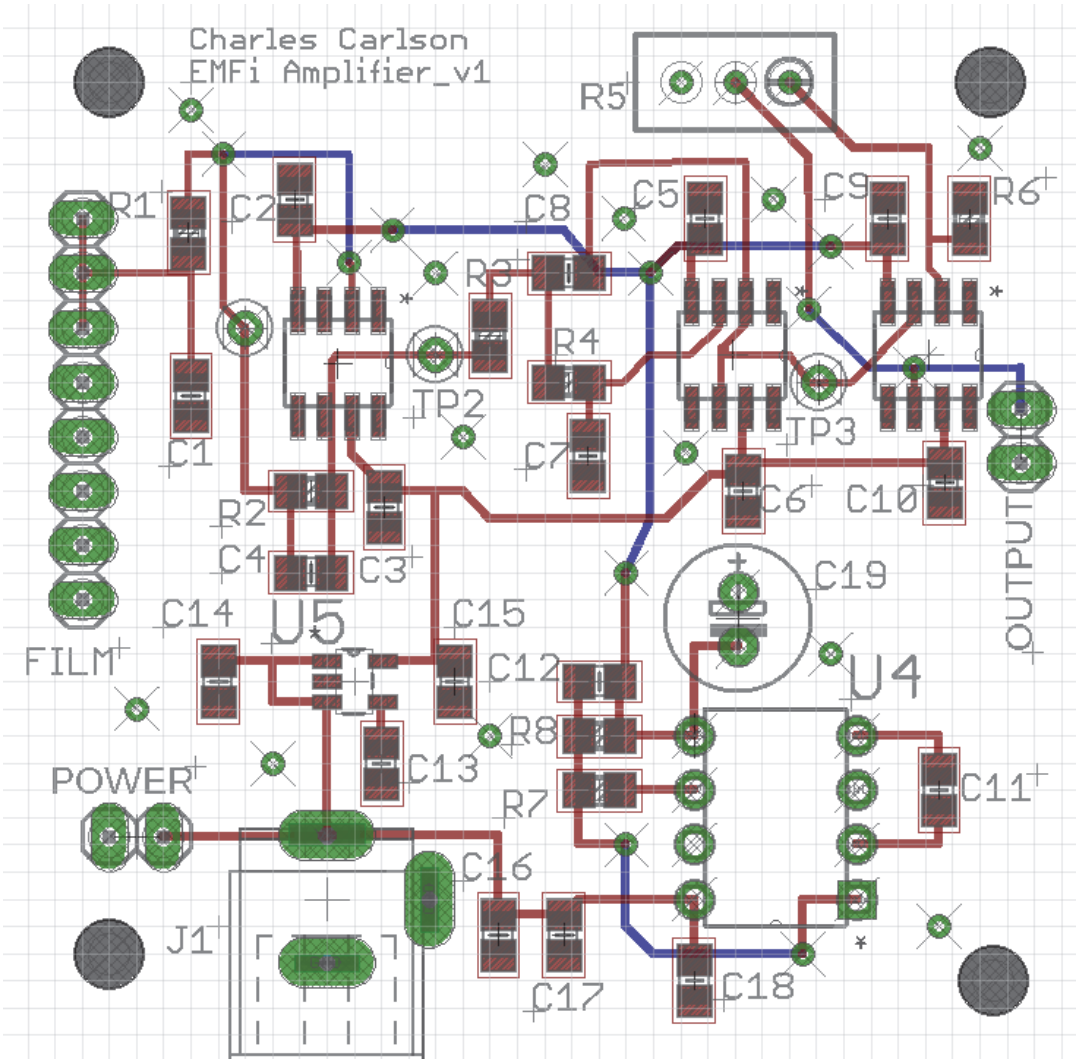

Figure B-2. Circuit board layout version 1.

Table B-1. Bill of materials version 1.

Part	Value	Device	Package	Description
C1	0.1uF	C-USC0805	C0805	CAPACITOR
C2	0.1uF	C-USC0805	C0805	CAPACITOR
C3	0.1uF	C-USC0805	C0805	CAPACITOR
C4	0.1uF	C-USC0805	C0805	CAPACITOR
C5	0.1uF	C-USC0805	C0805	CAPACITOR
C6	0.1uF	C-USC0805	C0805	CAPACITOR
C7	0.01uF	C-USC0805	C0805	CAPACITOR
C8	0.022uF	C-USC0805	C0805	CAPACITOR
C9	0.1uF	C-USC0805	C0805	CAPACITOR
C10	0.1uF	C-USC0805	C0805	CAPACITOR
C11	10uF	C-USC0805	C0805	CAPACITOR
C12	0.002uF	C-USC0805	C0805	CAPACITOR

C13	10nF	(0.01u)	C-USC0805	CAPACITOR
C14	1uF	C-USC0805	C0805	CAPACITOR
C15	2.2uF	C-USC0805	C0805	CAPACITOR
C16	0.47uF	C-USC0805	C0805	CAPACITOR
C17	0.1uF	C-USC0805	C0805	CAPACITOR
C18	2uF	C-USC0805	C0805	CAPACITOR
C19	100uF	CPOL-USE2.5-7	E2,5-7	POLARIZED
FILM	PINHD-1X8	1X08	PIN	HEADER
J1	JACK-PLUG0	SPC4077	DC	POWER
OUTPUT	PINHD-1X2	1X02	PIN	HEADER
POWER	PINHD-1X2	1X02	PIN	HEADER
R1	80k	R-US_R0805	R0805	RESISTOR
R2	10M	R-US_R0805	R0805	RESISTOR
R3	510k	R-US_R0805	R0805	RESISTOR
R4	510k	R-US_R0805	R0805	RESISTOR
R5	POTENTIOMETER	PT-SPIN	Potentiometer	
R6	500	R-US_R0805	R0805	RESISTOR
R7	20k	R-US_R0805	R0805	RESISTOR
R8	100k	R-US_R0805	R0805	RESISTOR
TP1	TPTP5001	TPTP5001	TP5000OR5001	
TP2	TPTP5001	TPTP5001	TP5000OR5001	
TP3	TPTP5001	TPTP5001	TP5000OR5001	
U1	LF411CD	LF411CD	SOIC127P600X175-8N	JFET-INPUT
U2	LF411CD	LF411CD	SOIC127P600X175-8N	JFET-INPUT
U3	LF411CD	LF411CD	SOIC127P600X175-8N	JFET-INPUT
U4	LT1054CP	LT1054CP	DIP254P762X508-8	VOLTAGE
U5	LP2985A-18DBVJ	LP2985A-18DBVJ	SOT95P280X145-5N	150-mA

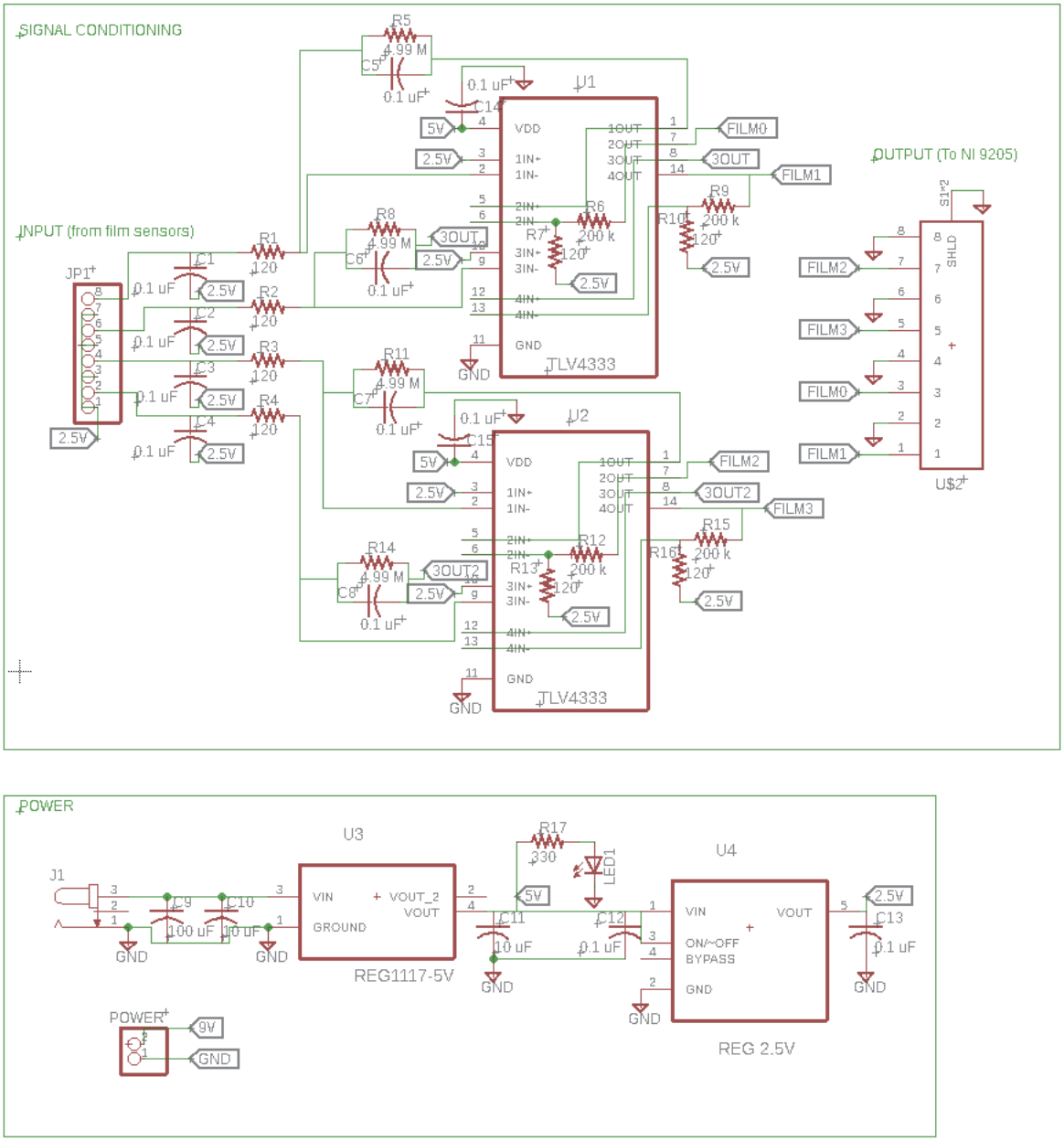

Figure B-3. Circuit board schematic version 2.

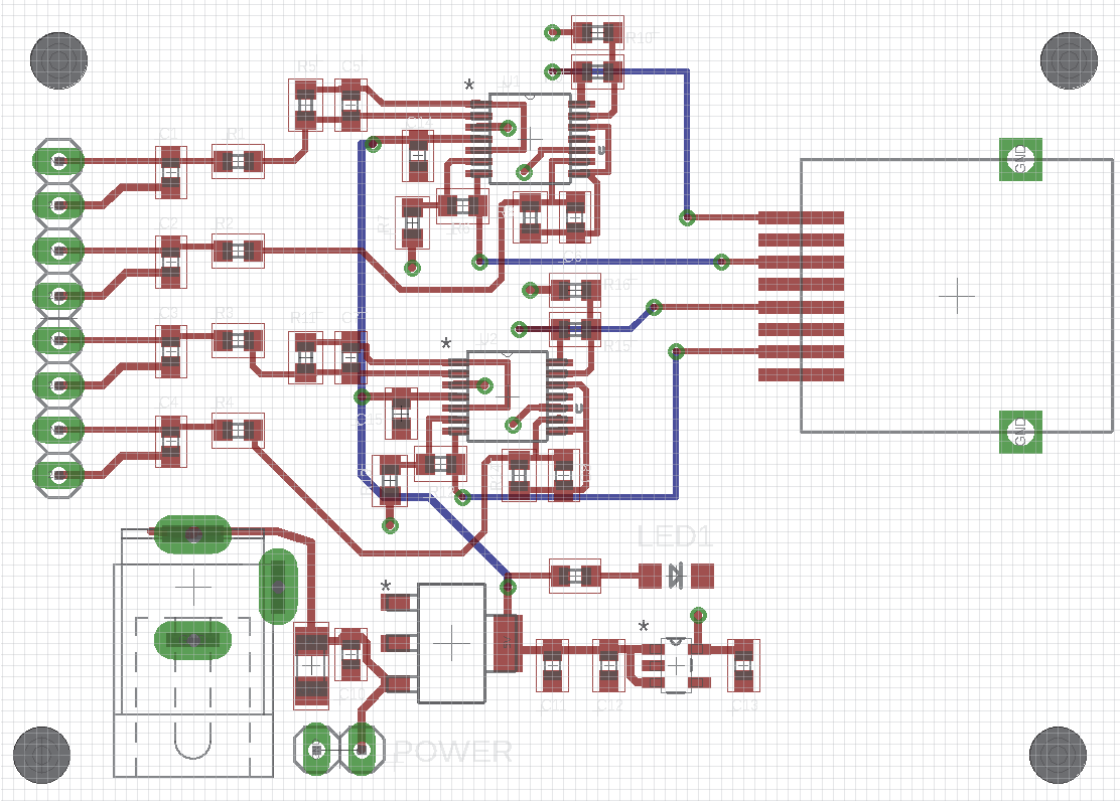

Figure B-4. Circuit board layout version 2.

Table B-2. Bill of materials version 2.

Part	Value	Device	Package	Description
C1	0.1 uF	C-SMD0603	603	CAPACITOR
C2	0.1 uF	C-SMD0603	603	CAPACITOR
C3	0.1 uF	C-SMD0603	603	CAPACITOR
C4	0.1 uF	C-SMD0603	603	CAPACITOR
C5	0.1 uF	C-SMD0603	603	CAPACITOR
C6	0.1 uF	C-SMD0603	603	CAPACITOR
C7	0.1 uF	C-SMD0603	603	CAPACITOR
C8	0.1 uF	C-SMD0603	603	CAPACITOR
C9	100 uF	C-USC1206	C1206	CAPACITOR
C10	10 uF	C-SMD0603	603	CAPACITOR
C11	10 uF	C-SMD0603	603	CAPACITOR
C12	0.1 uF	C-SMD0603	603	CAPACITOR
C13	0.1 uF	C-SMD0603	603	CAPACITOR
C14	0.1 uF	C-SMD0603	603	CAPACITOR
C15	0.1 uF	C-SMD0603	603	CAPACITOR
J1		JACK-PLUG0	SPC4077	DC POWER JACK
JP1		PINHD-1X8	1X08	PIN HEADER
LED1		LED1206	LED-1206	LEDs

POWER		PINHD-1X2	1X02	PIN HEADER
R1	120	R-US_R0603	R0603	RESISTOR
R2	120	R-US_R0603	R0603	RESISTOR
R3	120	R-US_R0603	R0603	RESISTOR
R4	120	R-US_R0603	R0603	RESISTOR
R5	4.99 M	R-US_R0603	R0603	RESISTOR
R6	200 k	R-US_R0603	R0603	RESISTOR
R7	120	R-US_R0603	R0603	RESISTOR
R8	4.99 M	R-US_R0603	R0603	RESISTOR
R9	200 k	R-US_R0603	R0603	RESISTOR
R10	120	R-US_R0603	R0603	RESISTOR
R11	4.99 M	R-US_R0603	R0603	RESISTOR
R12	200 k	R-US_R0603	R0603	RESISTOR
R13	120	R-US_R0603	R0603	RESISTOR
R14	4.99 M	R-US_R0603	R0603	RESISTOR
R15	200 k	R-US_R0603	R0603	RESISTOR
R16	120	R-US_R0603	R0603	RESISTOR
R17	330	R-US_R0603	R0603	RESISTOR
U$2	RJLSE4238101T	RJLSE4238101T	RJLSE4238101T	
U1	TLV4333	TLV274CPW	SOP65P640X120-14N	OPERATIONAL AMPLIFIERS
U2	TLV4333	TLV274CPW	SOP65P640X120-14N	OPERATIONAL AMPLIFIERS
U3	REG1117-5V	REG1117-3.3	SOT230P700X180-4N	Low Dropout Positive Regulator
U4	REG 2.5V	LP2985A-18DBVJ	SOT95P280X145-5N	150-mA LOW-NOISE LOW-DROPOUT REGULATOR

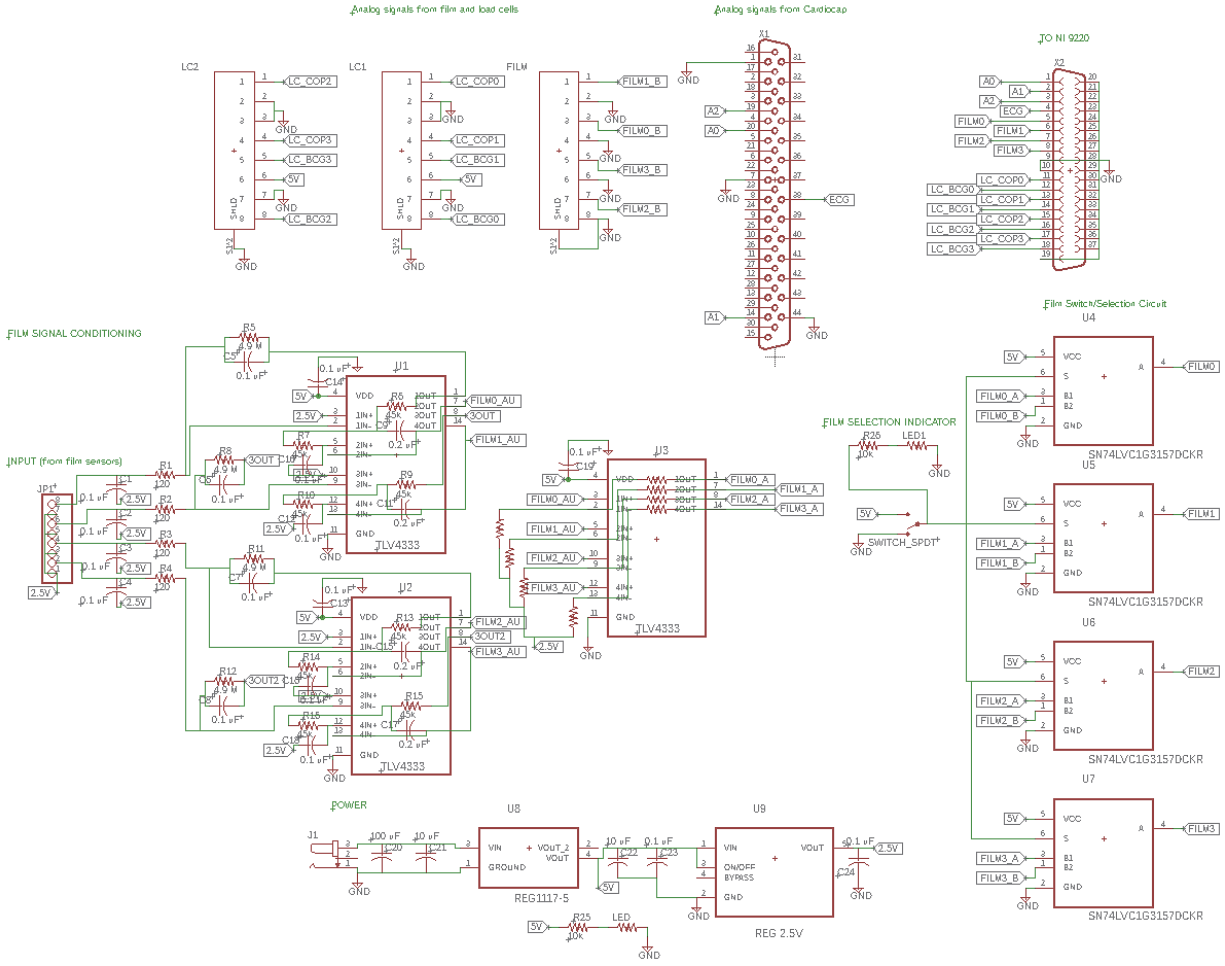

Figure B-5. Circuit board schematic version 3.

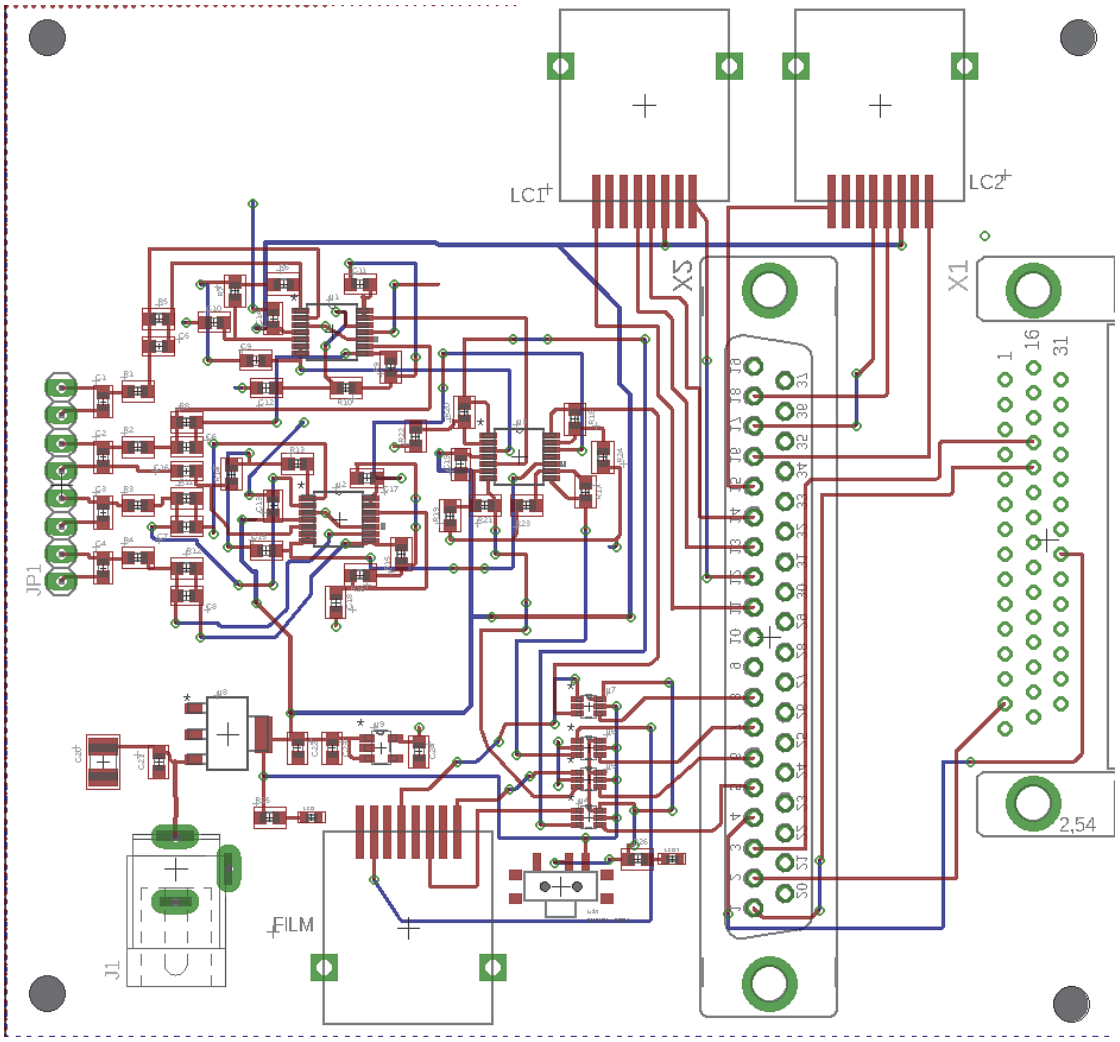

Figure B-6. Circuit board layout version 3.

Table B-3. Bill of materials version 3.

Part	Value	Device	Package	Description
C1	0.1 uF	C-SMD0603	603	CAPACITOR
C2	0.1 uF	C-SMD0603	603	CAPACITOR
C3	0.1 uF	C-SMD0603	603	CAPACITOR
C4	0.1 uF	C-SMD0603	603	CAPACITOR
C5	0.1 uF	C-SMD0603	603	CAPACITOR
C6	0.1 uF	C-SMD0603	603	CAPACITOR
C7	0.1 uF	C-SMD0603	603	CAPACITOR
C8	0.1 uF	C-SMD0603	603	CAPACITOR
C9	0.2 uF	C-SMD0603	603	CAPACITOR
C10	0.1 uF	C-SMD0603	603	CAPACITOR
C11	0.2 uF	C-SMD0603	603	CAPACITOR
C12	0.1 uF	C-SMD0603	603	CAPACITOR

C13	0.1 uF	C-SMD0603	603	CAPACITOR
C14	0.1 uF	C-SMD0603	603	CAPACITOR
C15	0.2 uF	C-SMD0603	603	CAPACITOR
C16	0.1 uF	C-SMD0603	603	CAPACITOR
C17	0.2 uF	C-SMD0603	603	CAPACITOR
C18	0.1 uF	C-SMD0603	603	CAPACITOR
C19	0.1 uF	C-SMD0603	603	CAPACITOR
C20	100 uF	C-USC1210	C1210	CAPACITOR
C21	10 uF	C-SMD0603	603	CAPACITOR
C22	10 uF	C-SMD0603	603	CAPACITOR
C23	0.1 uF	C-SMD0603	603	CAPACITOR
C24	0.1 uF	C-SMD0603	603	CAPACITOR
FILM	RJLSE4238101T	RJLSE4238101T	RJLSE4238101T	
J1		JACK-PLUG0	SPC4077	DC POWER JACK
JP1		PINHD-1X8	1X08	PIN HEADER
LC1	RJLSE4238101T	RJLSE4238101T	RJLSE4238101T	
LC2	RJLSE4238101T	RJLSE4238101T	RJLSE4238101T	
LED		R-SMD0402	402	RESISTOR
LED1		R-SMD0402	402	RESISTOR
R1	120	R-US_R0603	R0603	RESISTOR
R2	120	R-US_R0603	R0603	RESISTOR
R3	120	R-US_R0603	R0603	RESISTOR
R4	120	R-US_R0603	R0603	RESISTOR
R5	4.9 M	R-US_R0603	R0603	RESISTOR
R6	45k	R-US_R0603	R0603	RESISTOR
R7	45k	R-US_R0603	R0603	RESISTOR
R8	4.9 M	R-US_R0603	R0603	RESISTOR
R9	45k	R-US_R0603	R0603	RESISTOR
R10	45k	R-US_R0603	R0603	RESISTOR
R11	4.9 M	R-US_R0603	R0603	RESISTOR
R12	4.9 M	R-US_R0603	R0603	RESISTOR
R13	45k	R-US_R0603	R0603	RESISTOR
R14	45k	R-US_R0603	R0603	RESISTOR
R15	45k	R-US_R0603	R0603	RESISTOR
R16	45k	R-US_R0603	R0603	RESISTOR
R17	45k	R-US_R0603	R0603	RESISTOR
R18	45k	R-US_R0603	R0603	RESISTOR
R19	45k	R-US_R0603	R0603	RESISTOR
R20	45k	R-US_R0603	R0603	RESISTOR

R21	45k	R-US_R0603	R0603	RESISTOR
R22	45k	R-US_R0603	R0603	RESISTOR
R23	45k	R-US_R0603	R0603	RESISTOR
R24	45k	R-US_R0603	R0603	RESISTOR
R25	10k	R-US_R0603	R0603	RESISTOR
R26	10k	R-US_R0603	R0603	RESISTOR
U$1	SWITCH_SPDT	SWITCH_SPDT	KPS-1290	SWCH-10651
U1	TLV4333	TLV274CPW	SOP65P640X120-14N	OPERATIONAL AMPLIFIERS
U2	TLV4333	TLV274CPW	SOP65P640X120-14N	OPERATIONAL AMPLIFIERS
U3	TLV4333	TLV274CPW	SOP65P640X120-14N	OPERATIONAL AMPLIFIERS
U4	SN74LVC1G3157DCKR	SN74LVC1G3157DCKR	SOT65P210X110-6N	SPDT ANALOG SWITCH
U5	SN74LVC1G3157DCKR	SN74LVC1G3157DCKR	SOT65P210X110-6N	SPDT ANALOG SWITCH
U6	SN74LVC1G3157DCKR	SN74LVC1G3157DCKR	SOT65P210X110-6N	SPDT ANALOG SWITCH
U7	SN74LVC1G3157DCKR	SN74LVC1G3157DCKR	SOT65P210X110-6N	SPDT ANALOG SWITCH
U8	REG1117-5	REG1117-3.3	SOT230P700X180-4N	Low Dropout Positive Regulator
U9	REG 2.5V	LP2985-28DBVTE4	SOT95P280X145-5N	LOW-NOISE LOW-DROPOUT REGULATOR WITH SHUTDOWN
X1		HF44HN	HDF44HN	SUB-D
X2		F37VP	F37VP	SUB-D

Appendix C - LabVIEW Measurement File Structure

The LabVIEW measurement (LVM) file structure was configured within the virtual instrument using the Write to Measurement File subvi. The settings for the subvi are shown below. Only one header segment and no x values (time column) were included to save space. The data were saved to a series of LVM files, where a new file was generated every five minutes. Therefore, if any of the data were corrupted, only a segment of data would be lost.

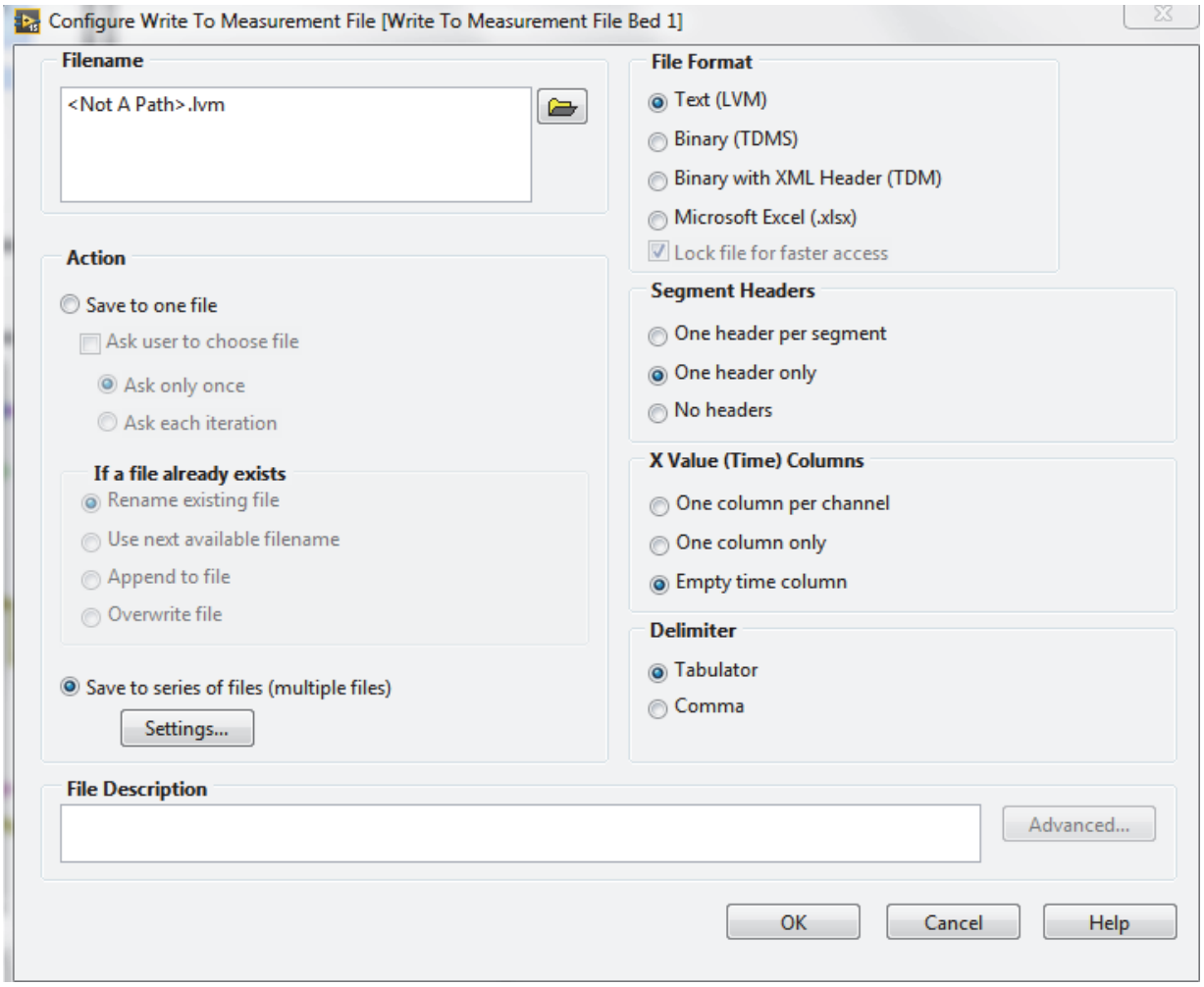

Figure C-1. LabVIEW measurement file structure.

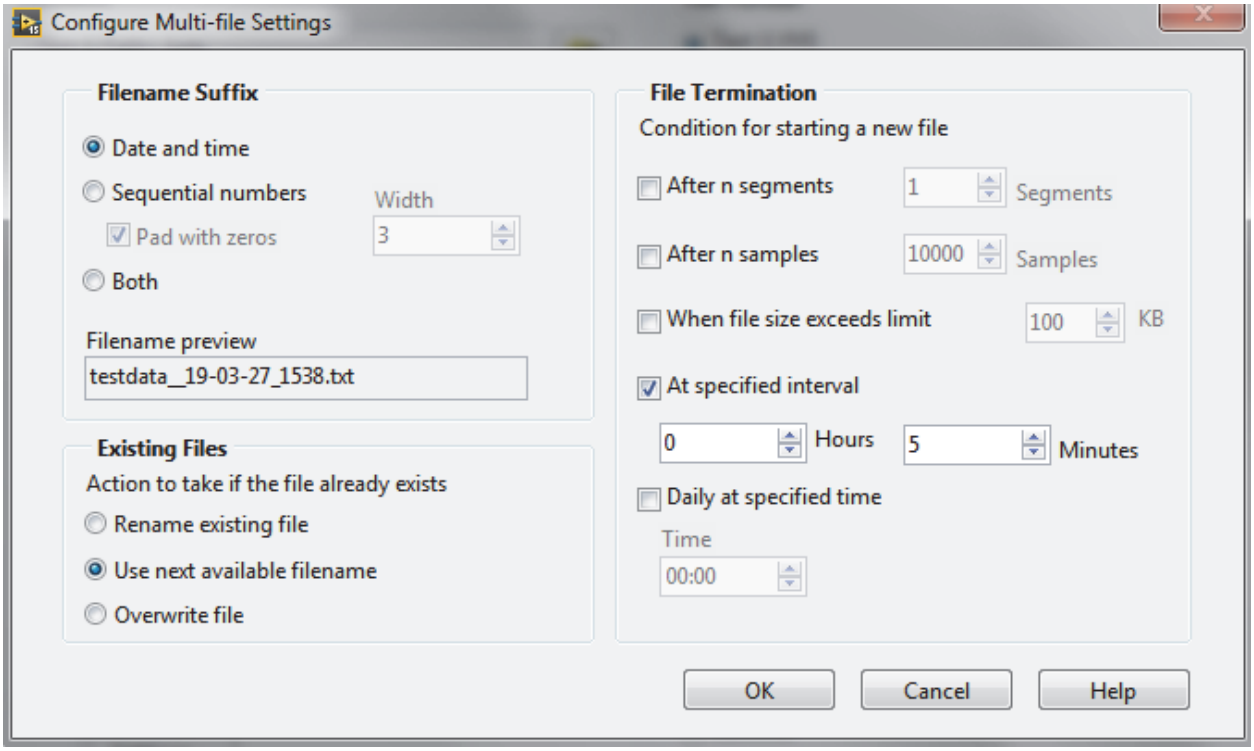

Figure C-2. LabVIEW multi-file settings.

Appendix D - Conditioned Analog Channels and NI 9220 Inputs Interface

NI 9220 pinout and connection to conditioned EMFi and LC signals

AI 4 (pin 5) - Film0

AI 5 (pin 6) - Film1

AI 6 (pin 7) - Film2

AI 7 (pin 8) - Film3

AI 8 (pin 11) - LC_COP0

AI 9 (pin 12) - LC_BCG0

AI 10 (pin 13) - LC_COP1

AI 11 (pin 14) - LC_BCG1

AI 12 (pin 15) - LC_COP2

AI 13 (pin 16) - LC_BCG2

AI 14 (pin 17) - LC_COP3

AI 15 (pin 18) - LC_BCG3

NI cDAQ chassis info

NI cDAQ-9184 "Bed_1_Wood"

NI cDAQ-9174 "Bed_2_Plastic"

Appendix E - Reuse Permission Grants

Dear Charles Carlson,

Thank you for your email. As to your request, I am pleased to inform you that permission is granted hereby to to use Figure 1 and Figure 2 from

Bibliotheca Cardiologica, No. 19
Editor(s): Noordergraaf, A. (Philadelphia, PA)
Pollack, G.H. (Philadelphia, PA)
Ballistocardiography and Cardiac Performance
11th Annual Meeting, Atlantic City, N.J., April 1966
ISBN: 978-3-8055-0026-5

to be reproduced in your thesis as well as in your article in 'Critical Reviews™ in Biomedical Engineering', provided that proper credit will be given to the original source and that S. Karger AG, Basel will be mentioned.

Please note that this is a non-exclusive permission, hence any further use, edition, translation or distribution, either in print or electronically, requires written permission again as this permission is valid for the above mentioned purpose only.

This permission applies only to copyrighted content that S. Karger AG owns, and not to copyrighted content from other sources. If any material in our work appears with credit to another source, you must also obtain permission from the original source cited in our work. All content reproduced from copyrighted material owned by S. Karger AG remains the sole and exclusive property of S. Karger AG. The right to grant permission to a third party is reserved solely by S. Karger AG.

Thank you for your understanding and cooperation.

Hopefully, I have been of assistance to you with the above.

Best regards,

Erika Brunner
Manager ePartners, Rights & Permissions
t +41 61 306 12 48
e.brunner@karger.com

KARGER

S. Karger AG | Medical and Scientific Publishers| Allschwilerstrasse 10 | 4009 Basel | Switzerland
t +41 61 306 11 11 | f +41 61 306 12 34 | www.karger.com

This Agreement between Kansas State University -- Charles Carlson ("You") and The American Physiological Society ("The American Physiological Society") consists of your license details and the terms and conditions provided by The American Physiological Society and Copyright Clearance Center.

License Number	4553800371700
License date	Mar 21, 2019
Licensed Content Publisher	The American Physiological Society
Licensed Content Publication	American Journal of Physiology, Consolidated
Licensed Content Title	THE DESIGN OF THE BALLISTOCARDIOGRAPH
Licensed Content Author	John L. Nickerson, Howard J. Curtis
Licensed Content Date	Aug 1, 1944
Licensed Content Volume	142
Licensed Content Issue	1
Type of Use	Thesis/Dissertation
Requestor type	non-profit academic/educational
Readers being charged a fee for this work	No
Format	electronic
Portion	figures/tables/images
Number of figures/tables/images	1
Will you be translating?	no
World Rights	no
Order reference number	
Title	Development of a Bed-based Nighttime Monitoring Toolset - Dissertation
Institution name	Kansas State University
Expected presentation date	Apr 2019
Portions	Figure 2. Illustrates two views of the bed and a detailed drawing of damping device. On page 4.
Requestor Location	Kansas State University 1854 Claflin Rd Apt 06 MANHATTAN, KS 66502 United States Attn: Kansas State University
Billing Type	Invoice
Billing Address	Kansas State University 1854 Claflin Rd Apt 06 MANHATTAN, KS 66502 United States Attn: Kansas State University
Total	0.00 USD

This Agreement between Kansas State University -- Charles Carlson ("You") and The American Physiological Society ("The American Physiological Society") consists of your license details and the terms and conditions provided by The American Physiological Society and Copyright Clearance Center.

License Number	4553800667082
License date	Mar 21, 2019
Licensed Content Publisher	The American Physiological Society
Licensed Content Publication	American Journal of Physiology, Consolidated
Licensed Content Title	STUDIES ON THE ESTIMATION OF CARDIAC OUPTUT IN MAN, AND OF ABNORMALITIES IN CARDIAC FUNCTION, FROM THE HEART'S RECOIL AND THE BLOOD'S IMPACTS; THE BALLISTOCARDIOGRAM
Licensed Content Author	Isaac Starr, A. J. Rawson, H. A. Schroeder, et al
Licensed Content Date	Jul 31, 1939
Licensed Content Volume	127
Licensed Content Issue	1
Type of Use	Thesis/Dissertation
Requestor type	non-profit academic/educational
Readers being charged a fee for this work	No
Format	electronic
Portion	figures/tables/images
Number of figures/tables/images	1
Will you be translating?	no
World Rights	no
Order reference number	
Title	Development of a Bed-based Nighttime Monitoring Toolset - Dissertation
Institution name	Kansas State University
Expected presentation date	Apr 2019
Portions	Figure 1 on page 3.
Requestor Location	Kansas State University 1854 Claflin Rd Apt 06 MANHATTAN, KS 66502 United States Attn: Kansas State University
Billing Type	Invoice
Billing Address	Kansas State University 1854 Claflin Rd Apt 06 MANHATTAN, KS 66502 United States Attn: Kansas State University
Total	0.00 USD

This Agreement between Kansas State University -- Charles Carlson ("You") and Elsevier ("Elsevier") consists of your license details and the terms and conditions provided by Elsevier and Copyright Clearance Center.

License Number	4542550287897
License date	Mar 05, 2019
Licensed Content Publisher	Elsevier
Licensed Content Publication	American Heart Journal
Licensed Content Title	A new full-frequency range calibrated ballistocardiograph. I Recording the body ballistics in displacement, velocity, and accelleration
Licensed Content Author	Sidney R. Arbeit,Norman Lindner
Licensed Content Date	Jan 1, 1953
Licensed Content Volume	45
Licensed Content Issue	1
Licensed Content Pages	8
Start Page	52
End Page	59
Type of Use	reuse in a journal/magazine
Requestor type	academic/educational institute
Intended publisher of new work	Begell House
Portion	figures/tables/illustrations
Number of figures/tables/illustrations	1
Format	both print and electronic
Are you the author of this Elsevier article?	No
Will you be translating?	No
Original figure numbers	Figure 2.
Title of the article	Ballistocardiography Instrumentation: A Review
Publication new article is in	Critical Reviews™ in Biomedical Engineering
Publisher of the new article	Begell House
Author of new article	Charles Carlson
Expected publication date	Jan 2020
Estimated size of new article (number of pages)	20
Requestor Location	Kansas State University 1854 Claflin Rd Apt 06 MANHATTAN, KS 66502 United States Attn: Kansas State University
Publisher Tax ID	98-0397604
Total	0.00 USD